TR-EE68-1
NASA Grant No. NsG-553
PRF 4695

PURDUE UNIVERSITY
SCHOOL OF ELECTRICAL ENGINEERING

PERFORMANCE OF SELF-BIT SYNCHRONIZATION SYSTEMS

by

P. A. Wintz

and

E. J. Luecke

January 1968
Lafayette, Indiana

Supported by
National Aeronautics and Space Administration

PURDUE UNIVERSITY

SCHOOL OF ELECTRICAL ENGINEERING

PERFORMANCE OF SELF BIT SYNCHRONIZERS FOR THE DETECTION OF ANTICORRELATED BINARY SIGNALS

by

P. A. Wintz

E. J. Luecke

June, 1968

Lafayette, Indiana

Supported By:

NATIONAL AERONAUTICS AND SPACE ADMINISTRATION

Under

Grant NsG-553

TABLE OF CONTENTS

Page

LIST OF TABLES

LIST OF FIGURES

ABSTRACT

In a digital communication system, it is necessary to properly synchronize the receiver time base so that the digital time symbols can be properly detected. This research is concerned with optimum and suboptimum ways of providing self synchronization for binary anticorrelated signaling.

Expected absolute error, as determined from the probability density function of synchronizing error, is used as the performance measure when no detector is specified. Degradation of effective signal to noise ratio is used as the performance measure for operation with a correlation detector.

A maximum likelihood synchronizer is derived and its performance evaluated by Monte Carlo techniques. The structure of the optimum synchronizer is complex but it leads to a suboptimum system composed of a cascade of a low pass filter, square law nonlinearity, and a band pass filter centered at the symbol rate. This system is analyzed and its performance as function of its parameters is presented and compared with the optimum synchronizer. Finally, a system for testing prototype synchronizers is described and experimental results for the suboptimum synchronizer and several other prototype systems is presented.

The following are the most significant results. Both the optimum and suboptimum systems perform better when the signaling symbol waveform is a half sine pulse or a raised cosine pulse rather than the commonly

used square pulse. Using the amount of memory time necessary to achieve a fixed level of degradation of signal to noise ratio as a measure of comparison, the suboptimum system with the half sine or raised cosine pulses requires only twice as much memory time as the optimum system. Signaling with square pulses requires 15 times more memory time with the suboptimum system.

If square pulses are not used, the degradation in performance with a suboptimum system is not great enough to warrant potential use of the optimum system. The results also show that the reduction of signal to noise ratio below .05 - .1 db requires excessive increases in memory time and should not be attempted.

I. INTRODUCTION

1.1 Synchronization

A digital communication system may be described as a process in which a set of symbols of predetermined duration and predetermined form, representing some form of message are conveyed from one point in space to a second. In this process, the form of the symbols may be altered, the time base may be lengthened or shortened, and the character of the process further changed by various additive and multiplicative disturbances. It is the function of the receiver to process these distorted symbols in such a manner that the original set of symbols may be recovered or detected.

The problem of optimally detecting these digital symbols has been investigated under many various conditions of disturbances. The problem of additive gaussian noise gives rise to the so-called matched filter or correlation detector. Fading, multipath, and intersymbol interference effects have also been considered and optimum receivers have been derived for certain cases of such disturbances. In all of these studies it is assumed that the receiver has a proper time base, i.e., it knows the epoch and duration of each symbol.

In a great many of the applications of digital communication systems the information to be transmitted appears serially in a time multiplexed form. The information content is arranged in groupings of individual symbols which may be called words; groupings of words which might be called frames; and further groupings of frames which might be called sequences.

The actual naming of these groupings is not particularly important and great variation of names exists in the literature. For the receiver to properly process this received information it is necessary that the receiver be able to identify the beginning and duration of each symbol, word, frame, and sequence. This on-going identification is generally called synchronization of the receiver.

Synchronization techniques can roughly be divided into two types: (1) stable clocks, and (2) correlation. Often, both are used in the same receiver, depending on the level of synchronization (bit, frames, etc.). Briefly, clock techniques employ, both at the receiver and at the transmitter, oscillators that operate at the same frequency. The receiver oscillator provides the timing signals for the detection of the individual symbols. Periodically in the sequence of symbols a special symbol is inserted. The receiver recognizes this symbol and compares the phase of the local clock and the epoch of this special symbol and resets the clock phase to agree with the epoch of the special symbol.

Correlation techniques rely primarily on the choice of a code symbol which has high correlation with a stored replica at the receiver when the two are "in-phase" and very low correlation when the two are "out-of-phase". The "in-phase" indication is used to provide timing to a receiver clock which is usually coupled back to the correlator in a closed loop system.

Consider the constraints placed on the designer of a digital system. He has power, bandwidth, and total transmission time as independent parameters. He has a given quantity of information (bits) to be transmitted at a given error rate or probability of error. After assigning values to the cost factors associated with the parameters of power, bandwidth and time, the

designer who wishes to design an "optimum" system must in some way minimize the volume of the power-bandwidth-time space. One obvious undesirable component of the available space is due to synchronization. It conveys no message information, yet it takes up either time, power, or bandwidth, or some of each. Any technique which economically reduces the space required for synchronization is obviously desirable.

1.2 The Problem

This research investigates the process of self bit synchronization as it applies to anticorrelated digital low pass signals. Self synchronization is defined as the process by which the necessary timing for the detection of the binary data is extracted directly from the information bearing signals. No separate channels for synchronization are used and the information bearing signals are constrained to have no added energy solely for synchronization purposes. The signal bandwidth is kept to the same order of magnitude as it would have if external synchronization methods were used. As a result, little or none of the time-power-bandwidth space is used for bit synchronization.

Little attention has been given to this problem in the literature. Since the problem reduces to estimating epoch of a received signal, there is a conceptual similarity to the problem of detecting the epoch of a radar echo. The vast store of techniques available for the solution of the radar problem does not carry over to the digital data problem, however, because symbols occur immediately before and after the symbol for which an estimate is being made. Another area in which the estimation of the phase of an incoming signal is carried out is in pulse systems on telephone and telegraph. Here, however, the signal to noise ratio is high and the

techniques are based on detecting the zero crossings of the signal. The problem as treated in this work considers the low signal to noise ratio case where zero crossings are of no value in detecting epoch.

Wintz and Hancock[1] consider the problem of determining the performance of an epoch estimator-correlation detector system for an M-ary alphabet. The phase of the carrier is assumed known and no specific form is given for the epoch estimator. Probability of detection error is computed for binary signalling with a prescribed signal autocorrelation function. Van Horn[2] presents a correlation strategy for self bit synchronization which uses a bank of correlators similar to the detection system used in some radars. No claims are made about the optimality of this system or about its practicality. Finally, Stiffler[3] proposes a maximum likelihood procedure for estimation of synchronization position which requires the knowledge of the infinite past or at least enough of the past so that truncation errors are negligible.

The problem is closely related to the problem of obtaining the required reference signal for coherent detection of PSK signals. Van Trees[4] proposed a "synchronizer" which consisted of transmitted reference carrier and a squaring loop for the self generation of a reference signal. He showed that optimum performance occurred when the carrier power was decreased to zero and only the self synchronizer was used. Lindsey[5] has evaluated the error probability for such a system with the assumption that the necessary bit timing was available for the correlation detector.

1.3 Content and Contributions

A synchronizer which is optimum in the maximum likelihood sense is derived in Chapter II. Unlike that of Stiffler, this likelihood procedure is good for any memory time which is a finite integral number of symbol periods. Its only lack of generality lies in the fact that the period of the received symbol sequence is assumed to be known or accurately estimated.

The form of the optimum synchronizer does not lend itself to easy implementation. There are a number of possible suboptimum solutions which can easily and economically be built. Chapter III presents one such system which is composed of a lowpass filter followed by a square law device and a bandpass filter. The solution for the periodic signal power and noise spectral density at the input to the bandpass filter is derived for lowpass signalling waveforms over a wide range of input filter cutoff frequencies.

In order to compare synchronizers, some common performance measure must be used. In Chapter IV, measures are proposed for comparing synchronizers without reference to the detector which they are driving, and for comparing the overall system performance when the synchronizer is driving a correlation detector. These measures clearly show the role of symbol waveshape on system performance.

The description of the experimental system which was used to test the performance of several suboptimum synchronizers is presented in Chapter V. Experimental work was desirable in order to verify the results predicted by the analytical solution, to verify the assumptions made concerning the probability density function of the phase of the output of the bandpass filter, and, most importantly, to obtain and compare the performance of other suboptimum systems which are not readily analyzed

by the methods of Chapter IV.

Chapter VI presents the results of the Monte Carlo simulation of the optimum synchronizer and of the analytical and experimental performance of the suboptimum systems. Assumptions made in the analytical solution are verified and an overall model is completed. The optimum and suboptimum performances are compared for the case of the synchronizer driving a correlation detector.

A resumé of the conclusions that are drawn from this work is presented in Chapter VII.

II. OPTIMUM SOLUTION

The basic problem in obtaining self bit synchronization is that of finding, at the receiver, the epoch of each symbol. Although it may not always be easily put into a mathematical formulation of the received signals, this epoch is one of the several parameters which describe the received random process. As such, it is possible to use the techniques of maximum likelihood parameter estimation to derive an optimum self bit synchronizer. This chapter presents such a derivation and the resulting structure of the self synchronizer.

2.1 Basic Assumptions

The signal that is available at the synchronizer is a binary sequence of anticorrelated symbols. The basic symbol has a duration of T seconds and is defined by $S(t)$ during this duration. It is assumed that both the functional form of $S(t)$ and its duration T are known at the synchronizer. This exact knowledge of T may not be a realistic assumption for the typical situation. However, T is usually known to within a narrow range of values and good estimates can be made by relatively simple methods. The joint estimation of T and epoch is a considerably more difficult problem than that of estimating epoch alone.

It is further assumed that exactly KT seconds of received signal are available to the self synchronizer for processing. This record, even though it is exactly K symbol durations long, contains parts of K + 1 symbols since the last ϵT seconds of one symbol are included at the start of the record and the first $(1 - \epsilon)T$ seconds of a symbol are included at the end of the record. Fig. 2.1 summarizes the assumed form of the received signal.

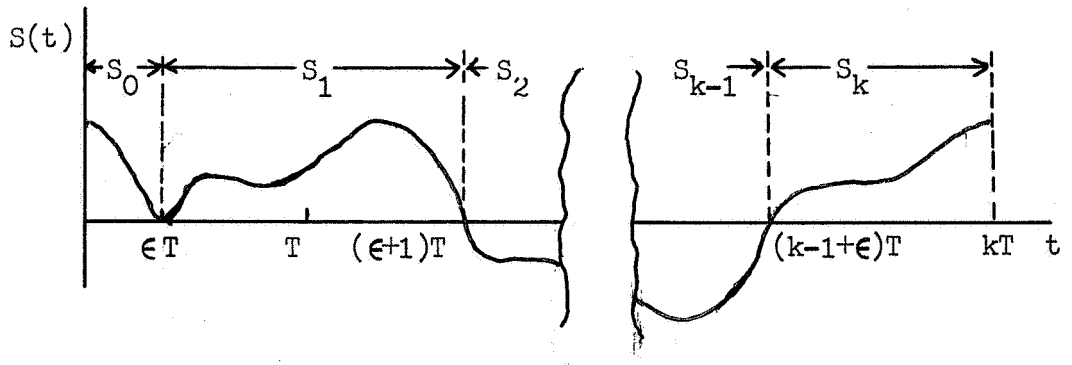

Fig. 2.1 Assumed Form of Typical Received Signal

Here, the notation S_j is used to indicate the symbol received during the jth interval and does not implicitly specify the functional form of the symbol.

The received signal is perturbed by an additive noise, n(t), that is assumed to be a sample function from a zero-mean gaussian random process of known autocorrelation function. The total input to the synchronizer is the sum of the signal and noise and is given by

$$x(t) = s(t) + n(t) \qquad 0 \leq t < K\,T \qquad 2.1$$

Now, it is assumed that a set of weighted orthonormal basis functions can be chosen to represent the time functions s(t) and n(t) during each of the K+1 intervals. If this is done, it is possible to represent the time functions in each of the K+1 intervals by a column vector made up of the weighting coefficients. Hence, during each interval

$$\overline{X}_j = \overline{S}_j + \overline{N}_j \qquad j = 0, 1, \ldots K \qquad 2.2$$

where $\overline{S}_j$ and $\overline{N}_j$ are the column vectors representing the received signal and noise during the j-th interval.

Some comment concerning the structure of the noise vectors is

necessary. If the sample function of noise during the j-th interval is gaussian, then the linear operations defined by the orthonormal expansion insure that each of the components of N_j is a gaussian random variable. For the two cases of general interest, these components can be made to be uncorrelated. If the noise is white, any choice of basis functions produces uncorrelated components. It will be assumed that the noise is white so that $\overline{N_j N_j^T} = \sigma^2 I$, where $\bar{I}$ is the identity matrix. Because the components are gaussian and uncorrelated, they are also independent. Finally, it is apparent that, because the components of each vector are statistically independent, the vectors $\bar{N}_i$ and $\bar{N}_j$ are also independent.

Finally, it is necessary to assume that each binary symbol has an a priori probability of occurance of 1/2. Since anticorrelated signaling is assumed, this means that

$$\text{Prob } \{S_j = + S(t)\} = \text{Prob } \{S_j = - S(t)\} = 1/2 \qquad 2.3$$

2.2 Derivation of Optimum Synchronizer

As seen in Fig. 2.1, ϵ is that fractional part of one symbol duration before the first complete symbol is processed by the synchronizer. This parameter will be used as the measure of the epoch of the received symbols. The received data during the entire interval KT is given by the partitioned vector $\bar{X} = (\bar{X}_o, \bar{X}_1 \ldots \bar{X}_K)$.

In order to obtain the maximum likelihood solution, the a posteriori probability density function $p(\epsilon/\bar{X})$ is required. It can be found by applying Bayes' rule to the joint density function $p(\bar{X}, \epsilon)$. However, care must be taken in the formulation of $p(\bar{X}, \bar{\epsilon})$ since there is, in reality, a third random variable that is operating in this problem.

This random variable is the sequence of symbols that is transmitted during the observation interval KT. Let $\overline{Q} = (Q_o, Q_1, Q_2 \cdots Q_K)$ be a vector whose components Q_j are the random variables which determine which of the two symbols are transmitted during each interval j. When a positive symbol is transmitted, $Q_j = +1$ and when a negative symbol is transmittted, $Q_j = -1$. The joint density function of $\overline{X}$, ϵ, and $\overline{Q}$ is

$$P(\overline{X}, \epsilon, \overline{Q}) = P(\overline{X}/\epsilon, \overline{Q})\, P(\epsilon, \overline{Q}) \tag{2.4}$$

But,

$$\int_Q P(\overline{X}, \epsilon, \overline{Q})\, d\overline{Q} = P(\overline{X}, \epsilon) = P(\overline{X}/\epsilon)\, P(\epsilon) \tag{2.5}$$

Now, the epoch and the symbol sequence are statistically independent, so that

$$P(\epsilon, \overline{Q}) = P(\epsilon)\, P(\overline{Q}) \tag{2.6}$$

and

$$P(\overline{X}/\epsilon)\, P(\epsilon) = \int_Q P(\overline{X}/\epsilon, \overline{Q})\, P(\epsilon)\, P(\overline{Q})\, dQ \tag{2.7}$$

Finally,

$$P(\epsilon/\overline{X})\, P(\overline{X}) = P(\overline{X}/\epsilon)\, P(\epsilon) \tag{2.8}$$

so that the desired a posteriori density function is

$$P(\epsilon/\overline{X}) = \frac{P(\epsilon)}{P(\overline{X})} \int_Q P(\overline{X}/\epsilon, \overline{Q})\, P(\overline{Q})\, d\overline{Q} \tag{2.9}$$

This may be considerably simplified because of the following conditions: (1) The transmitted symbols are assumed to be independent so that the random variables $Q_j (j=0,1,\ldots K)$ are independent; (2) The noise vectors

$\bar{N}_j (j=0,1,\ldots K)$ are independent (See Sec. 2.1); (3) The signal and the noise random processes are also independent. These conditions insure that the observations X_j are conditionally independent so that

$$P(\bar{X}/\epsilon, \bar{Q})\, P(\bar{Q}) = \left\{ \prod_{j=0}^{K} P(\bar{X}_j/\epsilon, Q_j) \right\} \left\{ \prod_{j=0}^{K} P(Q_j) \right\}$$

$$= \prod_{j=0}^{K} P(\bar{X}_j/\epsilon, Q_j)\, P(Q_j) \qquad 2.10$$

The conditional density function in 2.10 is k variate gaussian with covariance matrix $\Phi_j = \sigma^2 \bar{I}$ and mean $Q_j \bar{S}_j(\epsilon)$ and is written as

$$P(\bar{X}_j/\epsilon, Q_j) = \frac{1}{(2\pi)^{k/2}\,\sigma} \left(\exp\left\{ -\frac{1}{2\sigma^2} \left(\bar{X}_j - Q_j \bar{S}_j(\epsilon)\right)^T \left(\bar{X}_j - Q_j \bar{S}_j(\epsilon)\right) \right\} \right)$$

$$= \left(\frac{\exp\left\{ -\frac{1}{2\sigma^2} \left(\bar{X}_j^T \bar{X}_j + \bar{S}_j^T(\epsilon) \bar{S}_j(\epsilon) \right) \right\}}{(2\pi)^{k/2}\,\sigma} \right) \left(\exp\left\{ \left(\frac{1}{\sigma^2}\right) Q_j \bar{X}_j^T \bar{S}_j(\epsilon) \right\} \right)$$

2.11

For simplicity, the argument of S_j will be dropped in the following equations.

Returning now to 2.9, because of independence, summing over all Q is reduced to summing over the two values of Q_j for each symbol so that

$$\int_Q P(\bar{X}, \epsilon, \bar{Q})\, P(\bar{Q})\, d\bar{Q} = \prod_{j=0}^{K} \int_{Q_j} P(\bar{X}_j/\epsilon, Q_j)\, P(Q_j)\, d(Q_j)$$

$$= \prod_{j=0}^{K} \left\{ \frac{\exp\left\{ \frac{-1}{2\sigma^2} \left(\bar{X}_j^T \bar{X}_j + \bar{S}_j^T \bar{S}_j \right) \right\}}{(2\pi)^{k/2}\,\sigma} \right\} \left\{ \frac{1}{2} \left(\exp\left[\frac{\bar{X}_j^T \bar{S}_j}{\sigma^2} \right] + \exp\left[-\frac{\bar{X}_j^T \bar{S}_j}{\sigma^2} \right] \right) \right\}$$

$$= \prod_{j=0}^{K} \left\{ \quad \cdot \quad \right\} \left\{ \cosh\left(\frac{\bar{X}_j^T \bar{S}_j}{\sigma^2} \right) \right\}$$

$$= \left\{ \frac{\exp\left[-\frac{1}{2\sigma^2}\sum_{j=0}^{K}\overline{X}_j^T\overline{X}_j\right]\exp\left[-\frac{1}{2\sigma^2}\sum_{j=1}^{K-1}\overline{S}_j^T\overline{S}_j\right]}{(2\pi)^{\frac{k(K+1)}{2}}\sigma^{(k+1)}} \right\} \left\{ \exp\left[-\frac{1}{2\sigma^2}(\overline{S}_o^T\overline{S}_o + \overline{S}_k^T\overline{S}_k)\right] \right\} \left\{ \prod_{j=0}^{K}\cosh\left(\frac{\overline{X}_j^T\overline{S}_j}{\sigma^2}\right) \right\} \qquad 2.12$$

The factoring in the last line is done this way because the products $\overline{S}_j^T\overline{S}_j$ for all "interior" symbols are independent of ϵ but those products produced by the first and last symbols depend on ϵ. However, if it is remembered that $\overline{S}_o$ represents the "tail" of a symbol and $\overline{S}_k$ represents the corresponding "head", then it is seen that $\overline{S}_o^T\overline{S}_o + \overline{S}_k^T\overline{S}_k$ is always equal to the energy of one complete symbol and hence is a constant. The first two bracketed terms may now be replaced by a constant C since they are not functions of ϵ and will not enter into the maximizing process. 2.9 now becomes

$$P(\epsilon/\overline{X}) = g(\epsilon) = \left(\frac{P(\epsilon)}{P(\overline{X})}\right)(C)\prod_{j=0}^{K}\cosh\left(\frac{\overline{X}_j^T\overline{S}_j}{\sigma^2}\right) \qquad 2.13$$

It is reasonable to assume that all values of ϵ between 0 and T are equally likely so that $p(\epsilon) = 1/T$. Since $p(\overline{X})$ does not depend on ϵ, the maximum likelihood estimator of ϵ is the value that maximizes

$$g'(\epsilon) = \prod_{j=0}^{K}\cosh\left(\frac{\overline{X}_j^T\overline{S}_j(\epsilon)}{\sigma^2}\right) \qquad 2.14$$

The ϵ has been reinserted here to emphasize the dependence of $\overline{S}_j$ on ϵ.

Since $L(\epsilon) = \log g'(\epsilon)$ has extrema at the same values of ϵ as $g'(\epsilon)$ does, $L(\epsilon)$ can also be used for the maximum likelihood estimator.

$$L(\epsilon) = \log_{\epsilon}\left[\prod_{j=0}^{K} \cosh\left(\frac{\bar{X}_j^T \bar{S}_j(\epsilon)}{\sigma^2}\right)\right] = \sum_{j=0}^{K} \log_{\epsilon} \cosh\left(\frac{\bar{X}_j^T \bar{S}_j(\epsilon)}{\sigma^2}\right)$$

2.15

2.3 Synchronizer Structure

The following interpretation can be given to 2.15. To obtain the statistic for a given value of ϵ in order to find the maximum, the following procedure is used. Correlate the first ϵT seconds of the received record of KT seconds duration with the last ϵT seconds of the basic symbol waveform. Compute the log hyperbolic cosine of this and store the result. Next, take the portion of the received record from $t=\epsilon T$ to $t=(\epsilon+1)T$ and correlate this with the symbol waveform. Again, take the log hyperbolic cosine of the correlator output and add this result to the one for the first ϵT seconds.

Continue in this manner except that the last $(1-\epsilon)T$ seconds of the record is correlated with the first $(1-\epsilon)T$ seconds of the basic symbol. At the end of KT seconds, the output statistics in each accumulator are tested and the value of ϵ associated with the largest statistic is announced as the estimate of correct synchronizing position.

III. SUBOPTIMUM SYNCHRONIZER

The optimum synchronizer that was derived in Chapter II is difficult to implement without the aid of a special purpose digital computer. Its essential features, however, are included in a suboptimum synchronizer that is extremely simple. This chapter presents, in detail, the analysis of the performance of the system shown in Fig. 3-1.

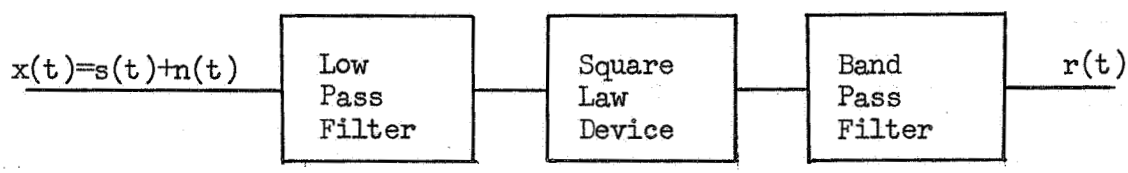

Fig. 3.1 Block Diagram of Suboptimum Synchronizer

3.1 Introduction

The input to the system, x(t), is the sum of a random signal process s(t) and additive white gaussian noise, n(t). As in Chapter II, s(t) is a first order Markov process of anticorrelated symbols +S(t) and -S(t) which have duration T. The output, r(t), is a sine wave at the symbol rate frequency which is perturbed by additive narrowband noise. The positive zero crossing of this sine wave, properly phase shifted to account for the phase shift in the low pass filter, is taken as the estimate of the epoch of each symbol.

Two different approaches can be used as a guide to why this particular suboptimum system is chosen. As one possible approach, consider the optimum synchronizer derived in Chapter II. The first operation there is one of correlating the received wave form with a stored

replica of the basic symbol waveform. As used in the optimum synchronizer, the output of the correlator is identical to that of a matched filter and such a matched filter could be substituted for the correlator. For most low pass symbol waveshapes, the low pass filter acts as a reasonable approximation to the matched filter for these waveshapes. Hence, in a general way, the low pass filter is a suboptimum approximation to the correlator in the optimum solution. The square law nonlinearity in the suboptimum solution is a reasonable approximation to the log-cosh operation. At low input levels, the log-cosh function is essentially square law. Fig. 3.2 compares the log-cosh and square law functions. Finally, the band pass filter performs the memory or summing function. In the optimum synchronizer, all previous symbol periods are weighted equally. However, the band pass filter performs an exponential weighting into the past.

A second approach to the choice of the suboptimum synchronizer appeals to an ad hoc solution. The thinking is as follows: The received signal is a series of positive and negative symbol pulses occuring in a random sequence. If these pulses are filtered by an even function nonlinear filter, the output will be a periodic function with period T. The square law device which has been chosen yields analytic simplifications. An absolute value nonlinearity would probably be easier to implement in practice. With no filtering at the input, the output of the square law device is a periodic function that has as its basic waveshape the square of the waveform of the input symbols. A bandpass filter, tuned to the symbol rate, will extract the fundamental component of this periodic function. The phase of this fundamental

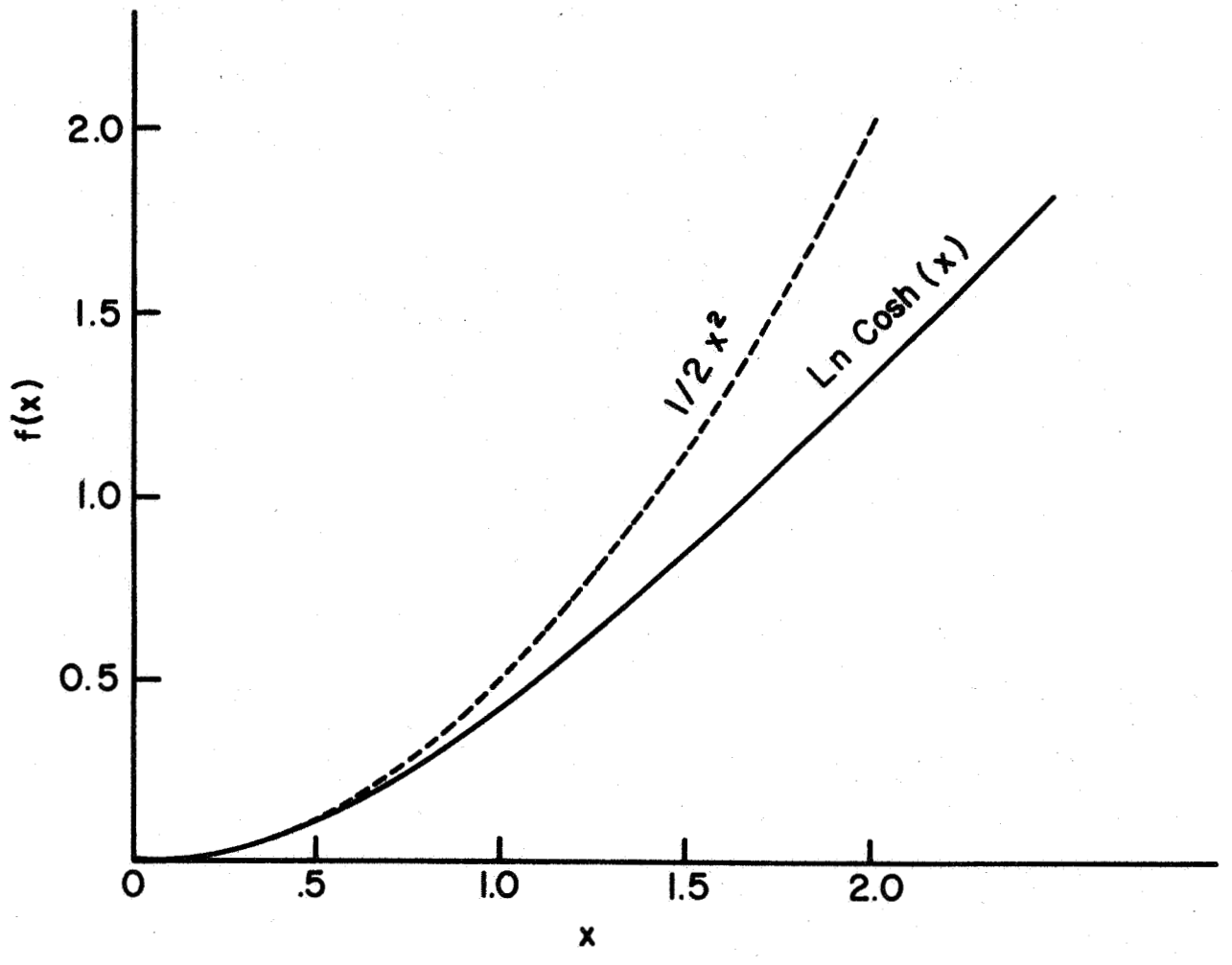

Fig. 3.2 Graph of Log Cosh(X) and 1/2 X^2

component is the required estimate of the start of each symbol. Because the input signal included wideband noise, it seems reasonable to provide some low pass filtering at the input.

3.2 Outline of Analysis

The analysis of the suboptimum synchronizer performance is somewhat complex. In this section, an overview is given of the general problems involved in the analysis and the particular section of the chapter in which their solution is presented.

The input to the system is the sum of two random processes, which after low pass filtering, are passed through a square law device and then band pass filtered. The statistics of phase at the output of the bandpass filter cannot generally be found in an analytic form, since the noise input to the filter is non-gaussian. Furthermore, the phase and gain characteristics of the filter contribute to the random phase process in an unknown way. For the same given noise equivalent-bandwidth two filters with different gain-phase characteristics will have different random phase density functions. However, it is reasonable to expect that the probability density function will be similar to that which applies when narrow band gaussian noise is added to a sine wave. In this density function the only parameter is a sine wave signal power to noise ratio. For the suboptimum system, such a ratio can be computed. Experimental results given in Appendix B and Chapter VI show that such a density function does fit the observed random phase process.

Hence, it is necessary to compute this signal to noise ratio. It is evaluated by finding the discrete component of the power spectrum

at the symbol repetition frequency and by assuming that the continuous portion in the range of the bandwidth of the bandpass filter is flat so that its value at the symbol repetition frequency may be used to calculate the noise power. The final form of this signal to noise ratio, in terms of the input signal to noise ratio, is presented in Sec. 3-7.

To compute the power spectrum at the output of the square law device, the direct method for the solution of non-linear devices is used. If the spectral densities of the input processes to the square law device are known, then the contribution due to the signal-cross-noise and the noise-cross-noise are computed by the direct convolution of the input spectral densities. The contribution due to the signal-cross-signal, however, must be computed by a special technique. These calculations are presented in Sec. 3.6.

Finally, in order to complete these calculations, the spectrum of the signal process must be known. The derivation necessary to compute the spectrum of the anticorrelated symbols used in the system is presented in Sec. 3.3.

3.3 Spectrum of Pulse Trains

In this section, the basic spectral relationships for digital signals are reviewed and the results for the special case of anti-correlated signaling are derived. It is assumed that the digital process, i.e. the Markov process of advancing from one digital symbol to the next, is first order Markov. This assumption may not be good enough for some classes of coded signals with error correction redundancy. However, to treat such a problem is very difficult, and

it is doubtful that such a solution would be very different from that obtained with a first order assumption. On the other hand, it could be argued that the first order assumption is too strong for a very simple digital system. However, there is a useful set of theory that has been developed for this case and it is easy to specialize these results to the case where each symbol is independent of the last.

The work of Huggins[6], Zadeh[7], and Barnard[8] is drawn upon heavily in the derivations that follow. The results given are due initially to Huggins. Using the formulation due to Barnard, the power spectral density of a Markov pulse train is

$$S_{xx}(f) = \lim_{\alpha \to 0} \sum_i \sum_j G_i(\bar{S}) G_j(S) \left\{ p_i \left[\frac{F_{ij}(S)}{1-F_{jj}(S)} + \delta_{ij} \right] + p_j \left[\frac{F_{ji}(\bar{S})}{1-F_{ii}(\bar{S})} \right] \right\} \tag{3.1}$$

where $S=\alpha+j\omega$ is complex frequency, $\bar{S}=\alpha-j\omega$, $G_i(s)$ is the Laplace transform of the i-th pulse waveform, p_i is the steady state expectation of the i-th pulse waveform, and $F_{ij}(s)$ is the Laplace transformation of the probability of the first occurance of state j when state i occurred at time = 0. $F_{ii}(s)$ is the Laplace transformation of the probability of the first return to state i. δ_{ij} is the Kroneker Delta. Huggins defines the factors like

$$\frac{F_{jj}(s)}{1-F_{jj}(s)} + \delta_{ij} \tag{3.2}$$

as the expectation of the occurence of state j following the known occurence of state i.

Signal flow graph methods for the calculation of the terms $F_{ij}(s)$ are presented by Huggins. Following his methods, the signal random

process is described by the flow graph of Fig. 3.3.

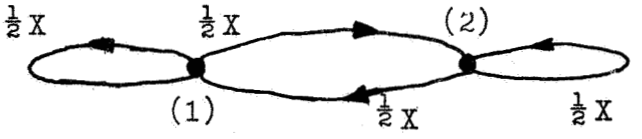

Fig. 3.3 Signal Flow Graph for Assumed Signal Random Process

State (1) is the occurence of a positive symbol and state (2) is the negative symbol. For equiprobable symbols, the conditional probability density function of a transition form (1) to (2) is $P_{12}=1/2\ \delta(t-T)$. This shows the fact that until time T no transition can take place. In a similar manner, $p_{11}=p_{22}=_{21}=p_{12}$. The Laplace transformation of $p_{ij}(t)$ is

$$\mathcal{L}\{1/2\ \delta(t-T)\} = \frac{1}{2}e^{-sT} = \frac{1}{2}X \qquad 3.3$$

These functions are shown in Fig. 3.3.

To compute $F_{12}(s)$, state (2) becomes a sink and the signal flow graph that results is shown in Fig. 3.4.

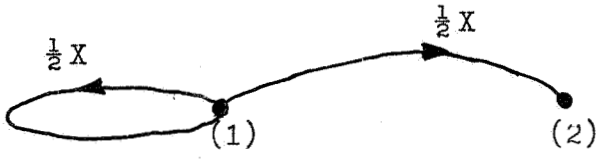

Fig. 3.4 Signal Flow Graph for Computation of $F_{12}(S)$

By signal flow methods, the average transmission from node (1) to (2) is

$$F_{12} = \frac{(1/2)X}{1-(1/2)X} \qquad 3.4$$

For the first return to state (1) the graph is shown in Fig. 3.5.

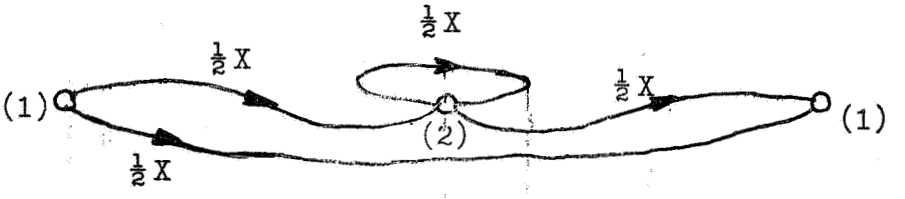

Fig. 3.5 Signal Flow Graph for Computation of $F_{11}(S)$

and

$$F_{11} = (1/2)X + \frac{(1/2)\,(X)\,(1/2)\,(X)}{1 - (1/2)\,X} = \frac{(1/2)X}{1-(1/2)X} \qquad 3.5$$

By symmetry, $F_{21}=F_{12}$ and $F_{22}=F_{11}$. These expressions must now be substituted into 3.1. For anticorrelated signaling, there are only two different symbols $G_1(s)$ and $G_2(s)$. $G_2(s)$ is equal to the negative of $G_1(s)$. Returning to 3.1 and performing the indicated summation results in

$$\begin{aligned} S_{xx}(f) = \lim_{\alpha\to 0}\Big\{ & G_1(\bar{s})G_1(s)\Big[p_1\Big(\frac{F_{11}(s)}{1-F_{11}(s)} + 1\Big) + p_1\Big(\frac{F_{11}(\bar{s})}{1-F_{11}(\bar{s})}\Big)\Big] \\ & + G_1(\bar{s})G_2(s)\Big[p_1\Big(\frac{F_{12}(s)}{1-F_{22}(s)}\Big) + p_2\Big(\frac{F_{21}(\bar{s})}{1-F_{11}(\bar{s})}\Big)\Big] \\ & + G_2(\bar{s})G_1(s)\Big[p_2\Big(\frac{F_{21}(s)}{1-F_{11}(s)}\Big) + p_1\Big(\frac{F_{12}(\bar{s})}{1-F_{22}(\bar{s})}\Big)\Big] \\ & + G_2(\bar{s})G_2(s)\Big[p_2\Big(\frac{F_{22}(s)}{1-F_{22}(s)} + 1\Big) + p_2\Big(\frac{F_{22}(\bar{s})}{1-F_{22}(\bar{s})}\Big)\Big]\Big\} \end{aligned} \qquad 3.6$$

At this point the assumption that each symbol is equiprobable is made. This means that $p_1=p_2=1/2$. Furthermore, it is noted that $F_{11}(s)=F_{22}(s)$ and that $F_{12}(s)=F_{21}(s)$. Making these substitutions in 3.6 yields

$$\begin{aligned} S_{xx}(f) = \lim_{\alpha\to 0}\Big\{ & \tfrac{1}{2}\Big[G_1(\bar{s})G_1(s)+G_2(\bar{s})\,G_2(s)\Big]\Big[\frac{F_{11}(s)}{1-F_{11}(s)} + \frac{F_{11}(\bar{s})}{1-F_{11}(\bar{s})} + 1\Big] \\ & + \tfrac{1}{2}\Big[G_1(\bar{s})G_2(s)+G_2(\bar{s})G_1(s)\Big]\Big[\frac{F_{12}(s)}{1-F_{11}(s)} + \frac{F_{12}(\bar{s})}{1-F_{11}(\bar{s})}\Big]\Big\} \end{aligned} \qquad 3.7$$

Now, the first term in the first set of braces is

$$\frac{F_{11}(s)}{1-F_{11}(s)} = \frac{(x/2)(1-x/2)}{1-(x/2)(1-x/2)} = \frac{x/2}{1-x} = (1/2)[\exp(-sT)/1-\exp(-sT)] \qquad 3.8$$

As α approaches 0, $\bar{s}$ goes to -s and the full quantity in the first set of braces becomes

$$\left\{\frac{1}{2}\left[e^{-sT}/1-e^{-sT}\right]+\frac{1}{2}\left[e^{+sT}/1+e^{+sT}\right]+1\right\} = \left\{1+\frac{1}{2}\left[\frac{e^{-sT}-1+e^{+sT}-1}{1-e^{-sT}-e^{+sT}+1}\right]\right\} = \frac{1}{2} \qquad 3.9$$

Similarly, the term in the second set of braces is -(1/2). The final result is

$$S_{xx}(f) = \frac{1}{4}\{S_{11}(f)+S_{22}(f)-S_{12}(f)-S_{21}(f)\} \qquad 3.10$$

where

$$S_{ij}(f) = G_i(j2\pi f)\, G_j(-j2\pi f) \qquad 3.11$$

For the special case of anticorrelated signaling, $S_{11}(f) = S_{22}(f)$ and $S_{12}(f) = -S_{21}(f) = -S_{11}(f)$. Hence,

$$S_{xx}(f) = S_{11}(f) \qquad 3.12$$

This interesting result shows that the spectrum of an equiprobable anticorrelated pulse train is identical to the spectrum of the basic symbol pulse.

3.4 Discrete Components of the Spectrum

The results, due to Barnard, for the discrete spectrum are

$$S^{d}_{xx}(f) = \left(\sum_{i}\sum_{j} p_i p_j G_i(j2\pi f) G_j(-j2\pi f)\right) \sum_{n=-\infty}^{+\infty} \delta(f-n/T) \qquad 3.13$$

For the special case being considered, this reduces to

$$S^{d}_{xx}(f) = \left([p_1-p_2]^2 S_{11}(f)\right) \sum_{n=-\infty}^{+\infty} \delta(f-n/T) \qquad 3.14$$

Note that when each symbol is equiprobable, there is no power in the discrete frequency components of the pulse train. Some symbol shapes, such as the square pulse, have nulls in their spectrum at those frequencies for which discrete components are possible. For such pulses, there is no power in the discrete components for any probability of occurence of symbols.

3.5 Low Pass Filter Response

It is assumed in the derivations that follow that the input signal to the synchronizer is an anticorrelated binary signal train composed of a basic symbol waveform s(t) of duration T as in Fig. 3.6.

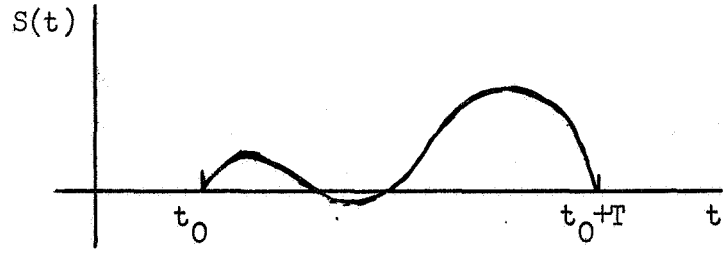

Fig. 3.6 Typical Symbol Waveform

Using the procedure of Sec. 3.3, the Laplace transform of s(t) is G(s) and the corresponding continuous spectral density is

$$S_{ss}(f) = G(j\,2\,\pi\,f)\,G(-j\,2\,\pi\,f) \tag{3.15}$$

At the output of the single pole low pass filter the new power spectrum is

$$S'_{ss}(f) = S_{ss}(f)\,H(j\,2\,\pi\,f)\,H(-j\,2\,\pi\,f) = S_{ss}(f)/[1+(f/f_c)^2] \tag{3.16}$$

where $H(j2\pi f)$ is the impulse response of the filter and f_c is the half power cutoff frequency of the low pass filter.

The noise component is computed with the assumption that the noise spectral density at the output of the filter is

$$S'_{nn}(f) = (N_o/2)/[1 + (f/f_c)^2] \tag{3.17}$$

In the time domain, the effect of low pass filtering the signal random process is to produce a new random process in which the pulse that is transmitted in one period is stretched out into the subsequent period. This stretching is usually called intersymbol interference. For low pass filter cutoff frequencies greater than 1/4 of the symbol rate, it can be assumed with negligible error that the intersymbol

interference lasts for only one symbol duration. This assumption corresponds to the condition of the impulse response of the filter decaying to $\exp(-\pi)$ of its original value in two symbol periods. This assumption leads to the formulation of the problem which is summarized in Fig. 3.7.

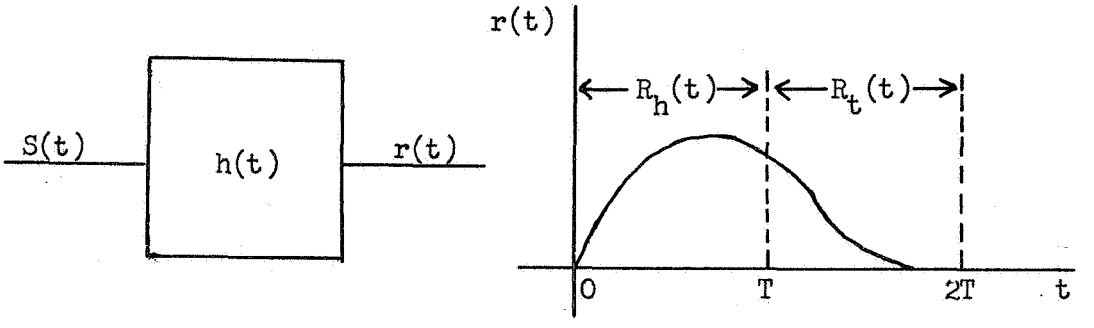

Fig. 3.7 Typical Low Pass Filter Response

Here, the response of the low pass filter to the input pulse has been divided into the "head" response and the "tail" response. When the input to the low pass filter is a pulse train of positive and negative pulses, the response during any interval is composed of four possible wave shapes. Let the response of the filter to a positive symbol be $R_h(t) + R_t(t)$ where $R_h(t)$ describes the output during $0 < t < T$ and is 0 for $t > T$. $R_t(t)$ is the output during $T < t < 2T$ and is 0 for $t < T$. The four resulting possible pulses during the interval $0 < t < T$ are

(1) $+R_h(t) + R_t(t+T)$

(2) $+R_h(t) - R_t(t+T)$

(3) $-R_h(t) + R_t(t+T)$

(4) $-R_h(t) - R_t(t+T)$

3.6 Square Law Device Response

In order to calculate the signal to noise ratio at the input to the bandpass filter, it is necessary to calculate both the "signal" power and the noise power spectrums at the output of the square law device in the frequency band of the narrow band bandpass filter. To do this, we make use of the direct method for the computation of the output spectrum of a square law device with random signal and noise input process. For reference, see for instance, Davenport and Root (9). A brief resume' of the results is presented here.

Let $x(t) = s(t) + n(t)$ where both $s(t)$ and $n(t)$ are sample functions from independent random processes with zero means and variances σ_s^2 and σ_n^2. The square law device is described by $y = a(x)^2$. The autocorrelation function of the random process is

$$R_y(\tau) = a^2\left[R_s^2(\tau) + 4R_s(\tau)\, R_n(\tau) + R_n^2(\tau) + 2\,\sigma_s^2\,\sigma_n^2\right] \qquad (3.19)$$

After making the assumption that the noise process is gaussian, the power spectral density, which is the inverse Fourier transform of $R_y(t)$, can be reduced to

$$S_y(f) = a^2\Big\{\mathcal{F}^{-1}\Big(R_s^2(\tau) + 4\int_{-\infty}^{+\infty} S_n(\lambda)\, S_s(f-\lambda)\, d\lambda$$

$$+ 2\int_{-\infty}^{+\infty} S_n(\lambda)\, S_n(f-\lambda)\, d\lambda + \left[2(\sigma_s^2\sigma_n^2) + \sigma_n^4\right]\delta(f)\Big\} \qquad (3.20)$$

where $S_n(x)$ and $S_s(x)$ are the spectral densities of the input signal and input noise processes. The gaussian noise assumption is necessary in order to reduce the inverse Fourier transform of the squared noise process to a convolution of spectral densities.

The term $\mathcal{F}^{-1}(R_s 2(\tau))$ represents the spectral density of the square of the signal random process. Because the input signal is not gaussian, the result of the squaring cannot be reduced to a convolution of the input process.

At this point it is useful to pause to consider the steps which must be taken to achieve a solution. First, the spectral density of the signal random process at the input to the square law device must be computed and convolved with the noise spectrum. Next, the noise spectrum must be convolved with itself. Last of all, the discrete and continuous portions of the square of the signal process must be computed.

Using the results from Sec. 3.5, the convolution integrals to be evaluated are

$$S_{sxn}(f) = \int_{-\infty}^{+\infty} \frac{(N_o/2)\, S_{ss}(f-\lambda)}{[1-(\lambda/f_c)^2]\,[1-[(f-\lambda)/f_c]^2]}\, d\lambda \qquad (3.21)$$

and

$$S_{nxn}(f) = \int_{-\infty}^{+\infty} \frac{(N_o/2)^2}{[1-(\lambda/f_c)^2]\,[1-[(f-\lambda)/f_c]^2]}\, d\lambda \qquad (3.22)$$

In general, these integrals are not easily evaluated. But because only the value at one particular frequency, the symbol repetition frequency, is really needed, these integrals can be evaluated by simple numerical integration.

The discrete and continuous portions of the spectrum due to the signal-cross-signal component are computed by squaring the random signal process at the output of the low pass filter and using the results of Sec. 3.3 and 3.4. On squaring the random symbol sequence made up of the

four pulses in 3.18 only two symbols will result. These are

$$(1)\quad \left\lfloor (R_h(t))^2 + (R_t(t+T))^2 \right\rfloor \quad + \quad \left\lfloor 2\, R_h(t)\, R_t(t+T) \right\rfloor$$

$$(2)\quad \left\lfloor (R_h(t))^2 + (R_t(t+T))^2 \right\rfloor \quad - \quad \left\lfloor 2\, R_h(t)\, R_t(t+T) \right\rfloor \qquad 3.23$$

Now, let

$$H_1(S) = \mathcal{L}\{(R_h(t))^2 + (R_t(t+T))^2\}$$

$$H_2(S) = \mathcal{L}\{2\, R_h(t)\, R_t(t+T)\} \qquad 3.24$$

Using the results of 3.10 the power spectrum is

$$\begin{aligned} S_{ss}(f) &= 1/4\{2\, H_1(j2\pi f)\, H_1(-j2\pi f) + 2\, H_2(j2\pi f)\, H_2(-j2\pi f) \\ &\quad - 2\, H_1(j2\pi f)\, H_1(-j2\pi f) + 2\, H_2(j2\pi f)\, H_2(-j2\pi f)\} \\ &= H_2(j2\pi f)\, H_2(-j2\pi f) \end{aligned} \qquad 3.25$$

This result indicates that the continuous component of the spectral density is given by the spectrum of a pulse which is determined by the product of the "head" waveshape and the "tail" waveshape. Note how the continuous spectral density goes to zero as the tail is reduced to zero. This happens when the input filter is removed and is to be expected, since squaring the input signal, with no filtering, gives a completely periodic output.

The discrete component of the output of the filter is now easily handled using the results of 3.13.

$$\begin{aligned} S^{d}_{ss}(f) = 1/4\{ &\left\lfloor H_1(j2\pi f)+H_2(j2\pi f) \right\rfloor \left\lfloor H_1(-j2\pi f)+H_2(-j2\pi f) \right\rfloor \\ &+\left\lfloor H_1(j2\pi f)+H_2(j2\pi f) \right\rfloor \left\lfloor H_1(-j2\pi f)-H_2(-j2\pi f) \right\rfloor \\ &\left\lfloor H_1(j2\pi f)-H_2(j2\pi f) \right\rfloor \left\lfloor H_1(-j2\pi f)+H_2(-j2\pi f) \right\rfloor \\ &\left\lfloor H_1(j2\pi f)-H_2(j2\pi f) \right\rfloor \left\lfloor H_1(-j2\pi f)-H_2(-j2\pi f) \right\rfloor \} \sum_{n=-\infty}^{+\infty} \delta(f-n/T) \end{aligned}$$

3.26

This reduces, after much manipulation, to

$$S_{ss}^{d}(f) = \left\{H_1(j2\pi f)\ H_1(-j2\pi f)\right\} \sum_{n=-\infty}^{+\infty} \delta(f-n/T) \qquad 3.27$$

Inspection of the form of this solution as the input filter is removed shows that $H_1(s)$ reduces to

$$H_1(s) = \mathcal{L}\left[(R_h(t))^2\right] \qquad 3.28$$

$(R_h(t))^2$ is identical to the square of the basic symbol waveshape. This result is seen to be equivalent to the well known result in linear system theory that the Fourier coefficients of a periodic pulse train are equal to the values of the Fourier transform of the pulse evaluated at the frequencies n/T.[10]

3.7 Signal to Noise Ratio at the Bandpass Filter

The derivation of the preceding sections have been carried out in order that the signal to noise ratio, R_M, in the pass band of the bandpass filter may be calculated. This discrete component of the spectrum at the symbol rate is taken as the signal. The noise power is computed by taking the product of the sum of the continuous components of the spectrum with the noise equivalent bandwidth of the filter.

The assumed density function for the phase at the filter output is

$$p(\Theta) = e^{-R_d}\left\{1+(\sqrt{\pi R_d}\cos\theta)(e^{-[\sqrt{R_d}\cos\theta]^2})(1+\mathrm{erf}(\sqrt{R_d}\cos\theta))\right\} \qquad 3.29$$

This density results when narrowband gaussian noise is added to a sine wave. It is assumed that the signal to noise ratio, R_M, that is computed is linearly related to the parameter R_d in the density function.

In order to bring together the work in this and previous section into one expression useful for the calculation of R_M, the following definitions are made. Let s(t) be the elementary functional form defining the symbol pulse. The received symbol has amplitude A.

$$S(t) = As(t) \tag{3.30}$$

The spectral density of the symbol pulse is $T_{SS}(f)$. The spectral density of the received symbol sequence is

$$S_{ss}(f) = A^2 T_{ss}(f) \tag{3.31}$$

The energy in the received pulse is

$$E = \int_o^T [As(t)]^2 dt = A^2 E_s \tag{3.32}$$

The noise equivalent bandwidth of the filter, normalized to the symbol rate, is Δ f.

By letting f=1/T (n=1) in 3.26, the signal power in the pass band is computed. If the low pass filtered symbol waveform is used to calculate $S^d_{ss}(1/T)$, the resultant power at the bandpass filter is

$$2 a^2 A^4 S^d_{ss}(1/T) \tag{3.33}$$

The contribution to the noise due to the signal-cross-signal term is found by evaluating 3.25 at f=1/T. Using the low pass filtered

waveform again for the calculation results in

$$S_{ss}(1/T) = H_2(j[2\pi/T])\ H_2(-j(2\pi/T)) = S'_{sxs} \qquad 3.34$$

The received single sided spectral density at the center of the bandpass is then

$$2\,a^2\,A^4\,S'_{sxs} \qquad 3.35$$

For computation purposes, 3.21 is written as

$$S_{sxn} = N_o/2 \int_{-\infty}^{+\infty} \frac{S_s(f-\lambda)\,d\lambda}{[1-(\lambda/f_c)^2][1-[(f-\lambda)/f_c]^2]} = (N_o/2)\,S'_{sxn} \qquad 3.36$$

Similarly, 3.22 becomes

$$S_{nxn} = N_o^2/4 \int_{-\infty}^{+\infty} \frac{1\,d\lambda}{[1-(\lambda/f_c)^2]\,[1-(f-\lambda)]} = (N_o^2/4)\,S'_{nxn} \qquad 3.37$$

The signal to noise ratio at the bandpass filter is then

$$R_M = \frac{2\,a^2\,A^4\,S^d_{ss}(1/T)}{[2\,a^2A^4\,S'_{sxs} + \frac{(2)(4)\,A^2N_o}{2}\,S'_{sxn} + \frac{(2)(2)N_o^2}{4}\,S'_{nxn}]\ \Delta f} \qquad 3.38$$

At this point, the result can be written in terms of an input signal to noise ratio $(S/N) = 2E/N_o$ where $A^2=E/E_s$.

$$R_M = \frac{S^d_{ss}\,(1/T)}{[S'_{sxs} + \frac{4\,E_s}{(S/N)}\,S'_{sxn} + \frac{2\,E_s^2}{(S/N)^2}\,S'_{nxn}]\ \Delta f} \qquad 3.39$$

The factor E_s and the spectral densities must be evaluated for each symbol waveshape and degree of low pass filtering.

IV. MEASURES OF PERFORMANCE

There are no commonly accepted performance measures for bit synchronizing systems. Designers have tended to build systems which are relatively precise and hence they have avoided asking the question "How well does it work?" This chapter first presents a useful measure of bit synchronizer performance for the general case where no detector has been specified. It then concludes with a solution for the probability of detection error for a correlation detector that operates with non-perfect synchronization.

4.1 Performance Without Detector Specified

The situation that exists in a bit synchronizer that has been perturbed by noise is indicated in Fig. 4.1. Here, correct synchronizing pulses should occur every T seconds but noise in the synchronizing system causes the pulses to be displaced ahead and behind the correct position. This displacement is often called jitter. The jitter is indicated here by the times ϵT where ϵ is the fractional synchronization error.

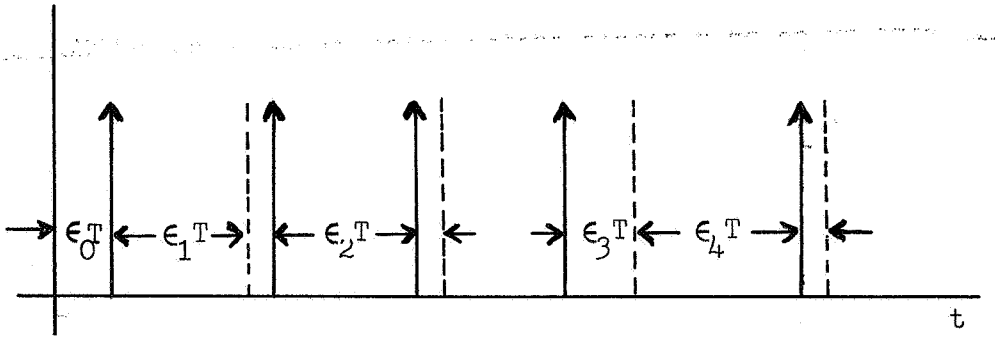

Fig. 4.1 Typical Sequence of Synchronizing Pulses

There are two types of detection errors which are caused by these jittery timing pulses. If $|\epsilon| < 1/2$, detection errors are caused by "looking" at the detector output at the wrong instant of time. For example, in a PAM system, "looking" at the wrong time results in obtaining a lower sampled value than the correct one. In a correlation detector, the output is sampled at some time other than the time that the signal component of the output is a maximum and hence the equivalent signal to noise ratio is reduced. The second type of error occurs when $|\epsilon| > 1/2$. Here the number of decisions made by the detector is more or less than the number of symbols that has been transmitted. These insertions or deletions have a tendency to cause a whole word or frame in a telemetry format to be incorrectly interpreted. This type of error is commonly referred to as bit slippage. Only errors of the first type are considered in this chapter. The probability of bit slippage is assumed to be negligible.

If, for the case of $|\epsilon| < 1/2$, the mechanism that is causing the timing errors is random, then there exists a corresponding probability density function on ϵ which is defined over the interval $-1/2 < \epsilon < +1/2$. If no particular detector is specified, this density function becomes the basis for the most reasonable way to describe and specify the synchronizer performance. Generally, it is desirable to be able to describe performance in terms of the fewest possible numbers--preferably one. At first glance, the variance or RMS error seems to be a good choice. However, in the work which follows, a less common parameter, the mean absolute error $|\overline{\epsilon}|$, has been chosen. This has been done because of the ease with which it can be measured in a prototype system. In Chapter 5, the details of how this is easily done are given.

For unimodal density functions this moment is closely related to the RMS error or standard deviation. For the density function that was assumed for the suboptimum system analyzed in Chapter 3, $|\overline{\epsilon}|$ is about .8 of the value of σ over a very wide range of the input signal to noise ratio parameter. See Appendix B for a more complete comparison of these two moments for typical density functions.

4.2 Synchronizing a Correlation Detector

The most meaningful measure of performance of a symbol synchronizer is the degradation which it causes in the probability of detection error. To determine this performance, however, it is necessary to specify a particular detector. Since correlation detection is optimum for known signals, the performance of such a detector with jittery synchronization is derived in this and the following sections.

The situation that is assumed at the correlation detector is as follows. The input to the correlator is a signal $S_s(t)$ and additive white gaussian noise $n(t)$. $S_s(t)$ represents a sequence of anticorrelated symbols of duration T and basic waveform $S(t)$. $S(t) = f(t)$ for $0 < t \leq T$ and is zero elsewhere. $S_s(t)$ may be written as

$$S_s(t) = \sum_{n=-\infty}^{+\infty} (-1)^j \, S(t-mT) \qquad 4.1$$

where j is a random variable that takes on values of ± 1 during each symbol interval.

Ideally, during each interval $nT < t \leq (n+1)T$, the received signal is correlated with a stored replica, $S_r(t-nT)$, of $S(t)$. Because of non-ideal synchronizer operation, an error ϵ exists during the desired detection interval and the correlation operation begins at $t = nT + \epsilon T$

instead of nT. The output of the detector at $(n+1)T + \epsilon T$ is made up of two components. M is the result of the correlation of the signal with the reference and Δ results from the correlation of the input noise with the reference. This is summarized in Fig. 4.2

$$M = \int_{(\epsilon+n)T}^{(\epsilon+n+1)T} S_s(t)\, S_x(t-[n+\epsilon]T)dt \qquad 4.2$$

$$\Delta = \int_{(\epsilon+n)T}^{(\epsilon+n+1)T} n(t)\, S_x(t-[n+\epsilon]T)dt \qquad 4.3$$

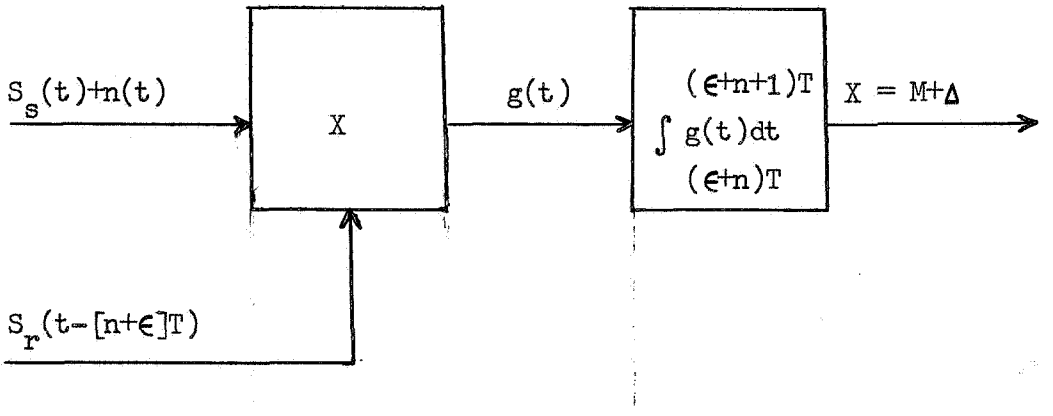

Fig. 4.2 Block Diagram of Correlation Detector

If the noise is gaussian, X is a gaussian random variable whose variance depends on the spectrum of the input noise and the waveshape of S(t) but not on ϵ or the received signal sequence. The mean of X is a function of ϵ and the signal sequence.

Let Q represent the particular sequence of symbols that occurs during the detection interval $[(n-1)T, (n+2)T]$. This interval is three symbols long and must be chosen because ϵ may be positive or negative and hence correlation may begin during the (n-1)th symbol or carry into

the (n+1)the symbol. The joint density function for the three random variables X, ϵ, and Q is

$$p(X/\epsilon,Q) = p(X/\epsilon,Q)\ p(\epsilon,Q) = p(X/\epsilon,Q)\ p(\epsilon)\ P(Q) \qquad 4.4$$

The last statement in 4.4 is possible since ϵ and Q are independent. The conditional density function for X is

$$p(X/\epsilon,Q) = \frac{1}{\sqrt{2\pi}\,\sigma} \exp\left[\frac{-1}{2\sigma^2}\,(X - m(\epsilon,Q))^2\right] \qquad 4.5$$

where $\sigma^2 = \overline{\Delta^2}$ and $m(\epsilon,Q)$ is the value computed by 4.2 for a given ϵ and Q.

The detection rule that is assumed for the detector is the one that would be used if synchronization were perfect. This rule is: choose +S if $X \geq 0$ and -S if $X < 0$. The events

$$\{X < 0/ + S\}$$

and

$$\{X \geq 0/ - S\}$$

are errors and the probability of these events determines the resulting probability of detection error. This probability of detection error

$$\begin{aligned} P_{d.e.} &= P\{X < 0/ + S\}\ P\{+S\} + P\{X \geq 0/ - S\}\ P\{-S\} \\ &= P(+S) \int_{-\infty}^{0} p(X/+ S)dx + P(-S) \int_{0}^{\infty} p(X/- S)dx \end{aligned} \qquad 4.6$$

where $p(X/+ S)$ is the probability density function for the condition that +S was transmitted during the intended detection interval and $p(X/- S)$ applies when -S was transmitted.

The evaluation of the two integrals proceeds as follows. When +S is transmitted during the intended detection interval $[nT,(n+1)T]$

there are four possible sequences that can be involved in the correlation. Using the notation of Fig. 4.3, these are tabulated in Fig. 4.4. Similarly when -S is transmitted, four other sequences are involved and these are also tabulated in Fig. 4.4

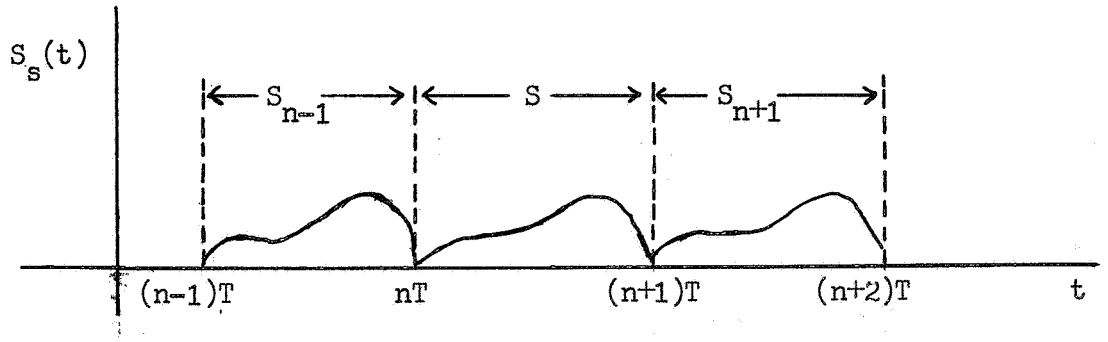

Fig. 4.3 Notation for Received Symbol Sequence

S_{n-1}	S_n	S_{n+1}	Q
+S	+S	+S	Q_1
-S	+S	+S	Q_2
+S	+S	-S	Q_3
-S	+S	-S	Q_4
+S	-S	+S	Q_5
-S	-S	+S	Q_6
+S	-S	-S	Q_7
-S	-S	-S	Q_8

Fig. 4.4 Eight Possible Symbol Sequences

For these events when +S is transmitted

$$p(X/+S) = \int_{\epsilon} \int_{Q} p(X/\epsilon,Q)\ p(\epsilon)\ p(Q)d\epsilon dQ \qquad 4.7$$

where the summation over Q is for those sequences where S_n is positive. For p(X/-S) the summation is over those Q that have negative symbols for S_n. Let $m_i(\epsilon)$ be the mean that is computed for a given value of ϵ and sequence Qi. Using this notation.

$$P(X/+S) = \int_{\epsilon} p(\epsilon) \left(\sum_{i=1}^{4} \frac{1}{\sqrt{2\pi}\ \sigma} \exp\left[\frac{-1}{2\sigma^2}(X-m_i(\epsilon))\right]\right)d\epsilon \qquad 4.8$$

$$P(X/-S) = \int_{\epsilon} p(\epsilon) \left(\sum_{i=5}^{8} \frac{1}{\sqrt{2\pi}\ \sigma} \exp\left[\frac{-1}{2\sigma^2}(X-m_i(\epsilon))\right]\right)d\epsilon$$

If it is assumed that each symbol is equally likely, then P(+S) = P(-S) = 1/2 and P(Qi) = 1/4. It is now possible to write 4.6 as

$$P_{d.e.} = \frac{1}{2} \int_{-\infty}^{0} 1/4 \int_{\epsilon} p(\epsilon) \sum_{i=1}^{4} \frac{1}{\sqrt{2\pi}\ \sigma} \exp\left(\frac{-1}{2\sigma^2}(X-m_i(\epsilon)\right)d\epsilon dX \qquad 4.9$$

$$+ 1/2 \int_{0}^{\infty} \frac{1}{4} \int_{\epsilon} p(\epsilon) \sum_{i=5}^{8} \frac{1}{\sqrt{2\pi}\ \sigma} \exp\left(\frac{-1}{2\sigma^2}(X-m_i(\epsilon))\right)d\epsilon dX$$

After interchanging the order of integration and using the definition

$$\Phi(X) = \int_{-\infty}^{X} \frac{1}{\sqrt{2\pi}\ \sigma} \exp(-X^2/2)dX$$

4.9 becomes

$$P_{d.e.} = 1/8 \int_{\epsilon} p(\epsilon)\left[\sum_{i=1}^{4} \Phi\left(\frac{-m_i(\epsilon)}{\sigma}\right) + \sum_{i=5}^{8} \left[1-\Phi\left(\frac{-m_i(\epsilon)}{\sigma}\right)\right]\right]d\epsilon \qquad 4.10$$

$$= 1/8 \int_{\epsilon} p(\epsilon)\left[\sum_{i=1}^{4} \Phi\left(\frac{-m_i(\epsilon)}{\sigma}\right) + \sum_{i=5}^{8} \Phi\left(\frac{+m_i(\epsilon)}{\sigma}\right)\right]d\epsilon$$

In order to continue further, the particular values of $m_i(t)$ need to be calculated so that further simplification can be obtained. It is recalled from 4.2 that

$$m_i(t) = \int_{(\epsilon+n)T}^{(\epsilon+n+1)T} S_{si}(t)\, S_r(t - [n+\epsilon]T)dt$$

where $S_{si}(t)$ is used to indicate a received signal that has the sequence Q_i during the detection interval. What this integral involves is shown in Fig. 4.5.

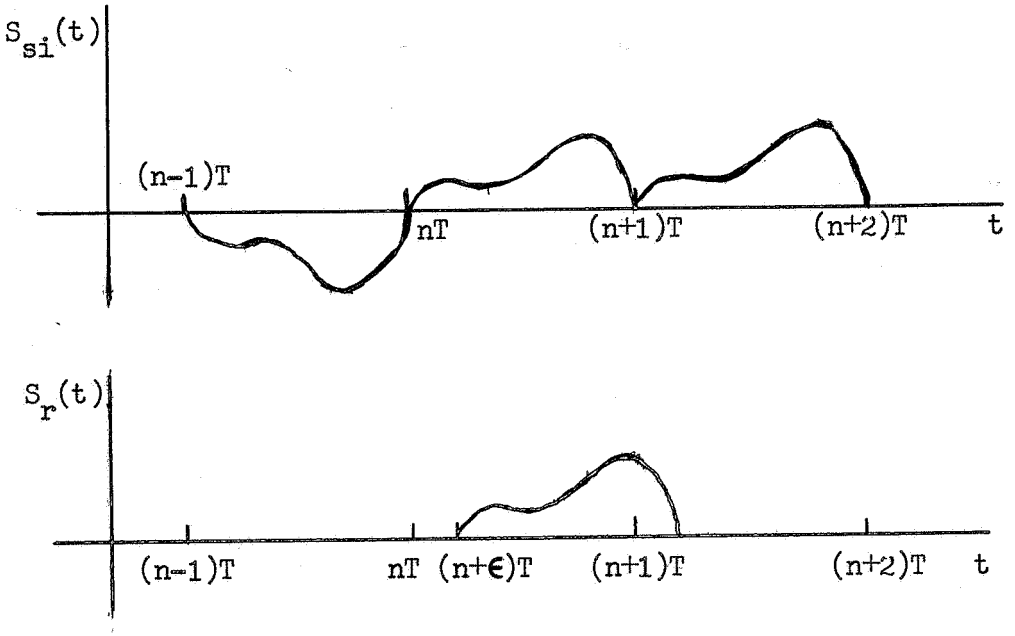

Fig. 4.5 Waveshapes Involved in Correlator Detector

For $\epsilon > 0$, as shown in Fig. 4.5

$$m_i(\epsilon) = \int_{nT+\epsilon T}^{(n+1)T} S_n(t-nT)\, S_r(t-[n+\epsilon]T)dt$$

$$+ \int_{(n+1)T}^{(n+1+\epsilon)} S_{n+1}(t-(n+1)T)\, S_r(t-(n+\epsilon)T)dt \qquad 4.11$$

$$= \int_0^{T-\epsilon} S_n(y+\epsilon)S_r(y)dy + \int_0^{\epsilon} S_{n+1}(y)S_r(y+[T-\epsilon])dy$$

Now, if

$$R_{ss}(\epsilon) = \int_{-\infty}^{+\infty} S(X)S(X+\epsilon)dX = \int_{0}^{T-\epsilon} S(X)S(X+\epsilon)dX \qquad 4.12$$

since $S(X) = 0$ for $X > T$ and $X < 0$, then the two integrals are recognized as $\pm R_{ss}(\epsilon)$ and $\pm R_{ss}(T-\epsilon)$ with the sign being determined by the sign of the symbols n and n+1. Due to the fact that $R_{ss}(t)$ is an even function, it can be seen that, by symmetry, the same results apply for $\epsilon < 0$. Referring now to Fig. 4.4, the correct sign can be placed on each of the $R_{ss}(x)$ terms to obtain Fig. 4.6

m	m_{i+} $(\epsilon \geq 0)$	m_{i-} $(\epsilon < 0)$
m_1	$-R(T\epsilon) - R(T[1-\epsilon])$	$-R(T\epsilon) - R(T[1-\epsilon])$
m_2	$-R(T\epsilon) + R(T[1-\epsilon])$	$-R(T\epsilon) - R(T[1-\epsilon])$
m_3	$-R(T\epsilon) - R(T[1-\epsilon])$	$-R(T\epsilon) + R(T[1-\epsilon])$
m_4	$-R(T\epsilon) + R(T[1-\epsilon])$	$-R(T\epsilon) + R(T[1-\epsilon])$
m_5	$+R(T\epsilon) - R(T[1-\epsilon])$	$+R(T\epsilon) - R(T[1-\epsilon])$
m_6	$+R(T\epsilon) + R(T[1-\epsilon])$	$+R(T\epsilon) - R(T[1-\epsilon])$
m_7	$+R(T\epsilon) - R(T[1-\epsilon])$	$+R(T\epsilon) + R(T[1-\epsilon])$
m_8	$+R(T\epsilon) + R(T[1-\epsilon])$	$+R(T\epsilon) + R(T[1-\epsilon])$

Fig. 4.6 Mean Values for Eight Symbol Sequences

It is apparent that $m_i(\epsilon)$ depends on whether ϵ is greater or less than zero. Therefore, 4.10 can be written as two integrals, one ranging over $-1/2 < \epsilon < 0$ and the other over $0 < \epsilon < 1/2$. The corresponding values of $m_i(\epsilon)$ for each range are m_{i-} and m_{i+}. From Fig. 4.6 the

following equalities are noted.

$$m_{1+} = m_{1-} = m_{2-} = m_{3+} = -m_{6+} = -m_{7-} = -m_{8+} = -m_{8-}$$
$$m_{2+} = m_{3-} = m_{4+} = m_{4-} = -m_{5+} = -m_{5-} = -m_{6-} = -m_{7+} \qquad 4.13$$

Using these equalities, 4.10 can be written as

$$P_{d.e.} = 1/8 \int_{-1/2}^{0} p(\epsilon) \left[4\Phi(\frac{-m_{1-}}{\sigma}) + 4\Phi(\frac{-m_{3-}}{\sigma})\right] d\epsilon$$
$$+ 1/8 \int_{0}^{1/2} p(\epsilon) \left[4\Phi(\frac{-m_{1+}}{\sigma}) + 4\Phi(\frac{-m_{2+}}{\sigma})\right] d\epsilon \qquad 4.14$$

Observe now that $m_{1-} = m_{1+}$ and $m_{3-} = m_{2+}$ so that if $p(\epsilon)$ is symmetrical about 0, then these two integrals are equal and the probability of detection error becomes, for this special case

$$P_{d.e.} = \int_{0}^{1/2} p(\epsilon)\left[\Phi(\frac{-m_{1+}}{\sigma}) + \Phi(\frac{-m_{2+}}{\sigma})\right] d\epsilon$$
$$= \int^{1/2} p(\epsilon)\left[\Phi(-\frac{1}{\sigma}[R(T\epsilon)+R[T-\epsilon T]) + \Phi(-\frac{1}{\sigma}[R(T\epsilon)-R(T-\epsilon T)])\right] d\epsilon \qquad 4.15$$

To put this into terms of one of the standard signal to noise ratios, $2E/N_o$, refer to 4.3 and note that for the white gaussian noise case,

$$\sigma^2 = \overline{\Delta^2} = \overline{\left(\int_0^T n(X-[\epsilon+n]T)\ S(X)dX\right)^2}$$
$$= \int_0^T \int_0^T S(y)\ S(X)\ \frac{N_o}{2}\ \delta(X-y)dXdy = \frac{N_o}{2}E \qquad 4.16$$

which, since $R(0) = E$, becomes

$$\sigma^2 = \frac{N_o}{2} R(0)$$

If now, $R(0)$ is factored from $R(T\epsilon) \pm R(T-\epsilon T)$ to obtain

$$R(0)[r(T\epsilon) \pm r(T-T\epsilon)], \qquad 4.17$$

then

$$\frac{R(T\epsilon) \pm R(T-T\epsilon)}{\sigma} = \frac{\sqrt{R^2(0)}}{\sqrt{\frac{N_o}{2}R(0)}} \left\{r(T\epsilon) \pm r(T-T\epsilon)\right\} \qquad 4.18$$

may be written as

$$\sqrt{2E/N_o} \left\{r(T\epsilon) \pm r(T-T\epsilon)\right\} \qquad 4.19$$

Also, to put the result in terms of erf(x) the identity

$$\Phi(X) = 1/2(1 + \text{erf}(x/\sqrt{2})) \qquad 4.20$$

is used to obtain

$$P_{d.e.} = \int_0^{1/2} p(\epsilon)\left[1-1/2 \text{ erf}\left(\frac{\sqrt{2E/N_o}}{\sqrt{2}} \left\{r(T\epsilon) + r(T-T\epsilon)\right\}\right)\right.$$

$$\left. - 1/2 \text{ erf } \left(\frac{\sqrt{2E/N_o}}{\sqrt{2}} \left\{r(T\epsilon) - r(T-T\epsilon)\right\}\right)\right] d\epsilon \qquad 4.21$$

As a verification of this equation, the timing becomes more precise $p(\epsilon) \Rightarrow 1/2\ \delta(\epsilon)$ and

$$P_{d.e.} = 1/2\left[1 - \text{erf}\left(\frac{\sqrt{2E/N_o}}{\sqrt{2}}\right)\right] \qquad 4.22$$

This is the well-known expression for the probability of error for a correlation detector.

4.3 Signal to Noise Ratio Degradation

The results of the previous section give the new (higher) probability of detection error when the detector has noisy synchronization. While this number is fundamental, the result may be put in a slightly more instructive form if the probability of error degradation is converted into its equivalent signal to noise ratio degradation. If it is assumed that

a digital system is to perform with a fixed probability of error, then any increase of this error probability due to synchronization inaccuracy must be made up by a corresponding increase in the received signal to noise ratio. In this section an approximate solution is obtained for the necessary increase in the signal to noise ratio.

For binary anticorrelated signaling, the probability of error is given as

$$P_{d.e.} = 1/2\left(1 - \text{erf}(\sqrt{R/2})\right) \qquad 4.23$$

where $R = 2E/N_o$. Since the performance degradation that is of primary interest is of necessity limited to small increments around the operating signal to noise ratio R_o, it is reasonable to find the straight line approximation to 4.23. To do this, the Taylor series about the operating value of R_o is found. The first two terms of the series for $P_{d.e.}(R)$ are

$$P_{d.e.}(R) = P_{d.e.}(R_o) + \frac{d}{dR}[P_{d.e.}(R_o)][R-R_o] \qquad 4.24$$

Imperfect synchronization causes an increase in probability of error to P_1 which is the probability of detection error that would be obtained with a lower signal to noise ratio R_1 and perfect synchronization. The fractional degradation in signal to noise ratio is computed as

$$\frac{R_1 - R_o}{R_o} = \left[\frac{P_{d.e.}(R_1) - P_{d.e.}(R_o)}{P_{d.e.}(R_o)}\right]\left[\frac{P_{d.e.}(R_o)}{R_o\left(\frac{d}{dR} P_{d.e.}(R_o)\right)}\right] \qquad 4.25$$

Define

$$\Delta P = \frac{P_{d.e.}(R_1) - P_{d.e.}(R_o)}{P_{d.e.}(R_o)}$$

and

$$\Delta R = \frac{R_1 - R_o}{R_o}$$

and observe that

$$\frac{d}{dR}(P_{d.e.}(R)) = -(\exp[-R/2])/\sqrt{8\pi R}$$

4.25 is now written as

$$-\Delta R = \Delta R^1 = \left(\frac{P_{d.e.}(R_o)\sqrt{8\pi}}{\sqrt{R_o}\ \exp(-R/2)}\right)\Delta P$$

where ΔR^1 is seen to be the resulting fractional increase that is required in R in order to bring the probability of detection error back to P_o.

4.4 Performance with Typical Symbol Waveshapes

Inspection of 4.21 shows that the degradation in probability of detection error is effected by the shape of the density function for ϵ and the shape of the autocorrelation function of the symbol pulse. It is apparent that the broader the density function becomes, the more significant the degradation will be. The role of R(x) in the degradation is most easily explained in terms of the "ideal" shape for R(x). Consider an R(x) which is defined as

$$R(x) = R(0) \qquad 0 \leq x < T/2$$

$$R(x) = 0 \qquad \text{elsewhere}$$

For such an autocorrelation function, the terms

$$r(\epsilon T) \pm r(T - \epsilon T)$$

in 4.21 would effectively reduce to $r(\epsilon T)$ since $0 < \epsilon < 1/2$ in the integral. Thus 4.21 reduces to

$$P_{d.e.} = \int_0^{1/2} p(\epsilon)\left\{1 - \operatorname{erf}\left(\frac{\sqrt{2E/N_o}}{\sqrt{2}}\right)\right\} d\epsilon \qquad 4.27$$

which after integrating over ϵ becomes

$$1/2\left(1 - \operatorname{erf}\left\{\sqrt{2E/N_o}\,/\sqrt{2}\right\}\right) \qquad 4.28$$

This result is the probability of detection error for perfect synchronization. The departure of R(x) from the ideal shape has the effect of reducing the size of the arguments in the terms erf(y) and hence increasing the magnitude of

$$1 - 1/2\ \operatorname{erf}\left(\sqrt{E/N_o}\,\{r(T\epsilon)+r(T-T\epsilon)\}\right) - 1/2\ \operatorname{erf}\left(\sqrt{E/N_o}\,\{r(T\epsilon)-r(T-T\epsilon)\}\right)$$

for a given value of ϵ.

In order to find out what kind of performance can be expected with noisy synchronization, 4.21 has been evaluated for the conditions of the suboptimum synchronizer of Chapter III. The probability density function for ϵ that was assumed there was given by 3.29 with the change of variable $\theta = 2\pi\epsilon$. The choice of autocorrelation functions was made by considering specific symbol waveshapes that are either used or could be easily used.

These pulses, all defined over the interval [0,T] are:

1. Square Pulse — $S(t) = A$
2. Half Sine Pulse — $S(t) = A \sin((\pi/T)t)$
3. Raised Cosine Pulse — $S(t) = A\,(1 - \cos((2\pi/T)t))$

It is possible to place a lower limit on degradation as a function of waveshape by calculating the degradation for a special autocorrelation function. According to Boas and Kac [11] the best upper bound on $R(\epsilon T)$ under the constraints that $R(\epsilon T) = 0$ for $\epsilon > 1$ and that the pulse is physically realizable is

$$R(\epsilon T) \leq R(0)\ \cos\left(\frac{\pi}{1 + [1/\epsilon]}\right)$$

where $[1/\epsilon]$ denotes the greatest integer not exceeding $1/\epsilon$. The results

using this function are identified as the "optimum" waveshape results.

The results presented in Fig. 4.7 to Fig. 4.12 have been computed by numerically integrating 4.21 for each of the above waveshapes using a range of values of $|\overline{\epsilon}|$ for various values of $2E/N_o$.

Fig. 4.7 shows the degradation in $2E/N_o$ for various qualities of synchronizer performance as measured by $|\overline{\epsilon}|$ for the case of the "optimum" pulse waveform. For each performance measure, the results for all practical pulses will lie to the left of these curves. One of the more interesting results as shown by these curves is the rather pronounced threshold that occurs. Below the threshold the detection errors are caused primarily by the noise at the detector. Above the threshold, the performance is badly degraded by synchronizing inaccuracies. Fig. 4.8 and 4.9 show the performance for the three waveshapes compared to the "optimum" for two values of $|\overline{\epsilon}|$. The significant results here are that the square pulse seriously degrades performance but both the half sine and the raised cosine cause performance to be near optimum.

Fig. 4.10 presents the same data as the previous figures, but in a slightly different form. The effect of synchronizer performance is plotted for fixed values of $2E/N_o$ for the optimum pulse shape. Here it is easy to see the threshold effect beginning to take effect in the range $.04 < |\overline{\epsilon}| < .06$. This indicates that the worst case performance should be set in this range. Fig. 4.11 and 4.12 compare the waveshapes with the "optimum". These curves can be used to compare the results in the following way.

It is typical for parameter estimators to have measures of performance such as $|\overline{\epsilon}|$ that vary inversely with the square root of the

effective measurement time. For all but the lowest signal to noise ratios, this is true for the suboptimum system derived in Chapter III. The ratio of measurement times required to provide the same amount of degradation is thus equal to the inverse square of the respective values of $|\bar{\epsilon}|$. In Fig. 4.12 for example, for 0.1 db degradation the value of $|\bar{\epsilon}|$ for the square wave is 0.009 and for the half sine it is 0.036. The ratio of required measurement times to provide the same degradation is thus 16. The ratio is typical of the difference in performance between these two waveshapes. This result, it should be noticed, assumes that each waveshape will cause equivalent synchronizer performance--a situation that the results in Chapter VI will show is not the case.

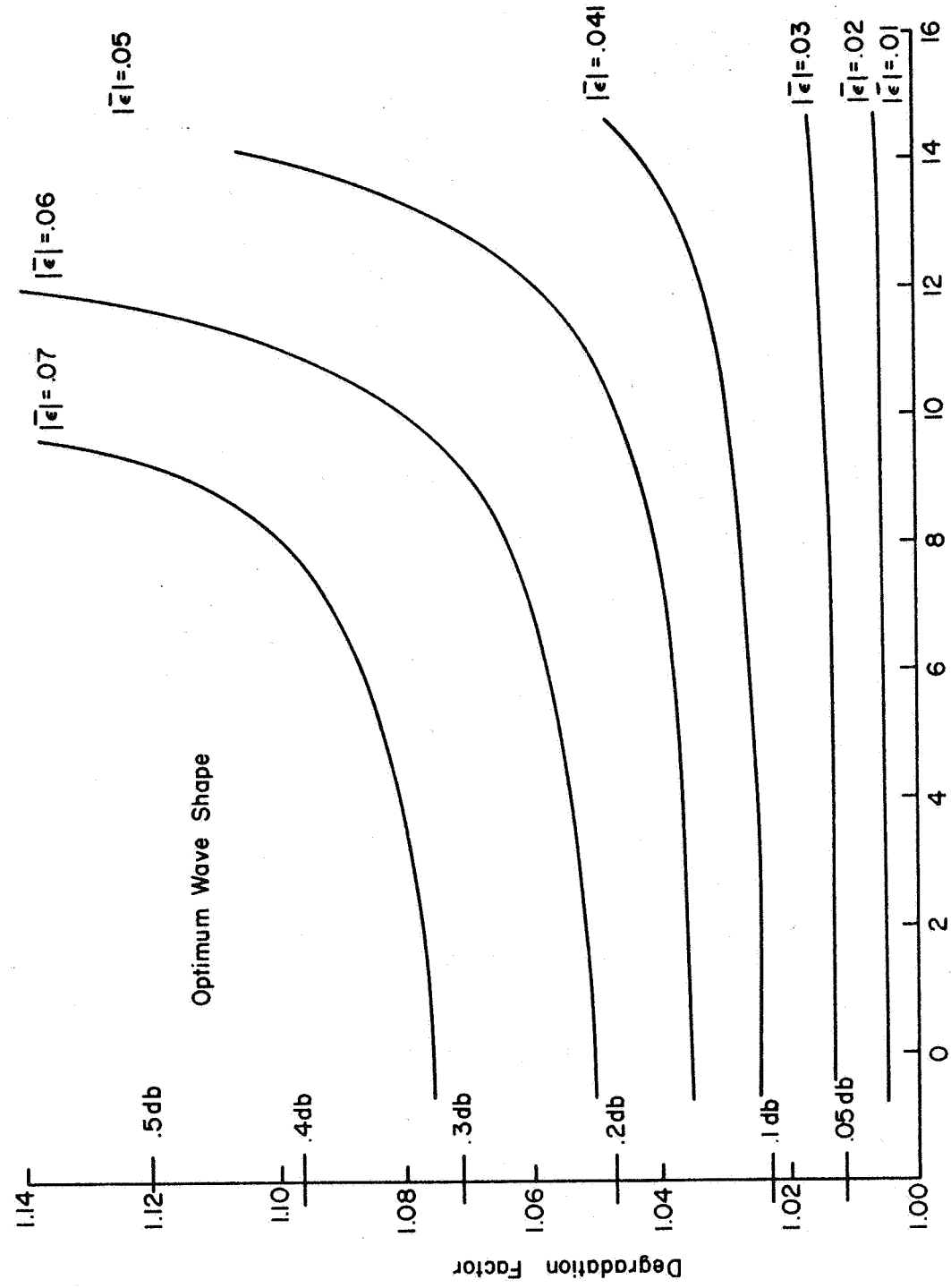

Fig. 4.7 Degradation of $2E/N_o$ for Selected Values of $|\bar{\epsilon}|$ with Optimum Wave Shape

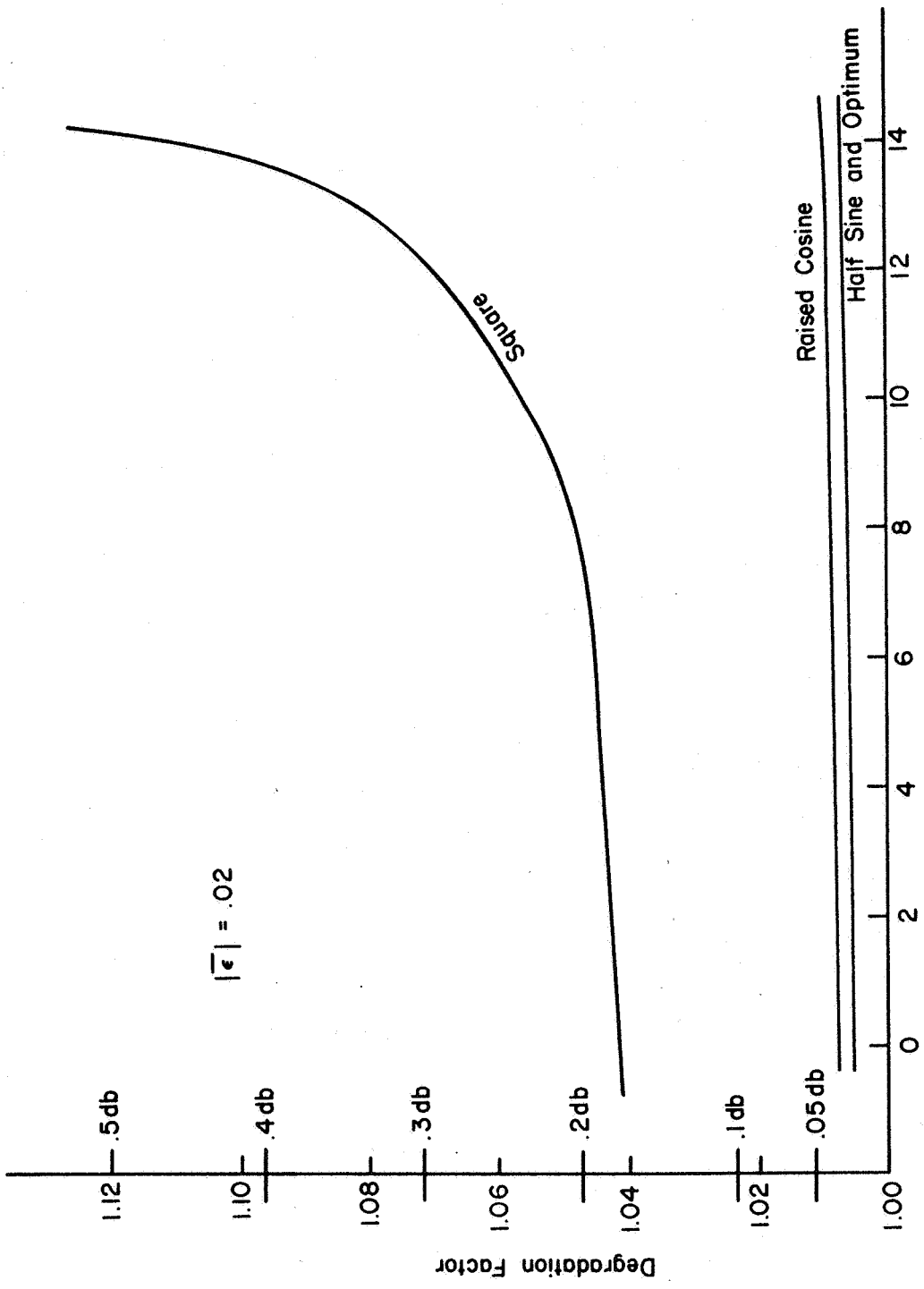

Fig. 4.8 Degradation of $2E/N_o$ for Selected Wave Shapes with $|\overline{\epsilon}| = .02$

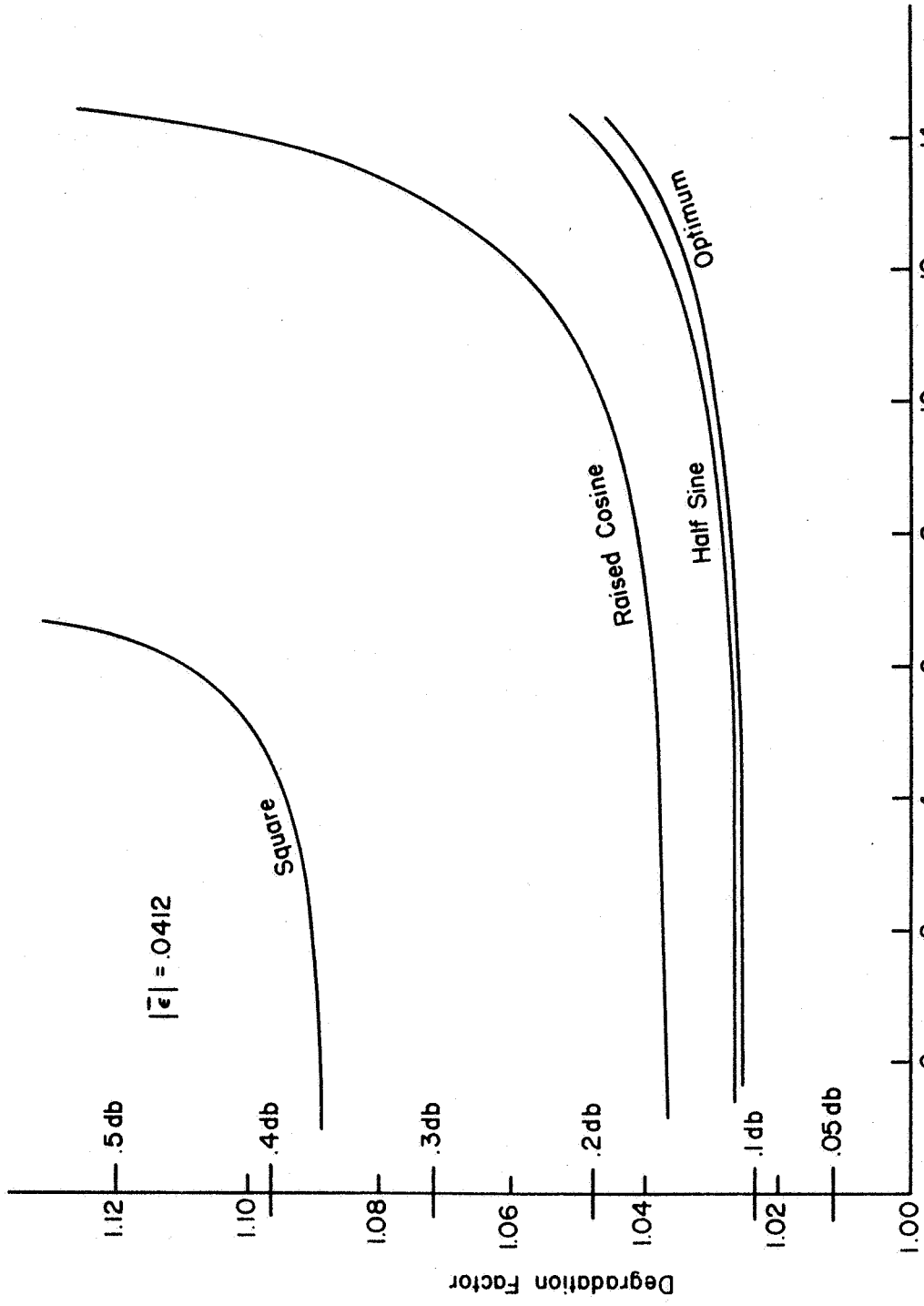

Fig. 4.9 Degradation of $2E/N_o$ for Selected Wave Shapes with $|\bar{\epsilon}| = .0412$

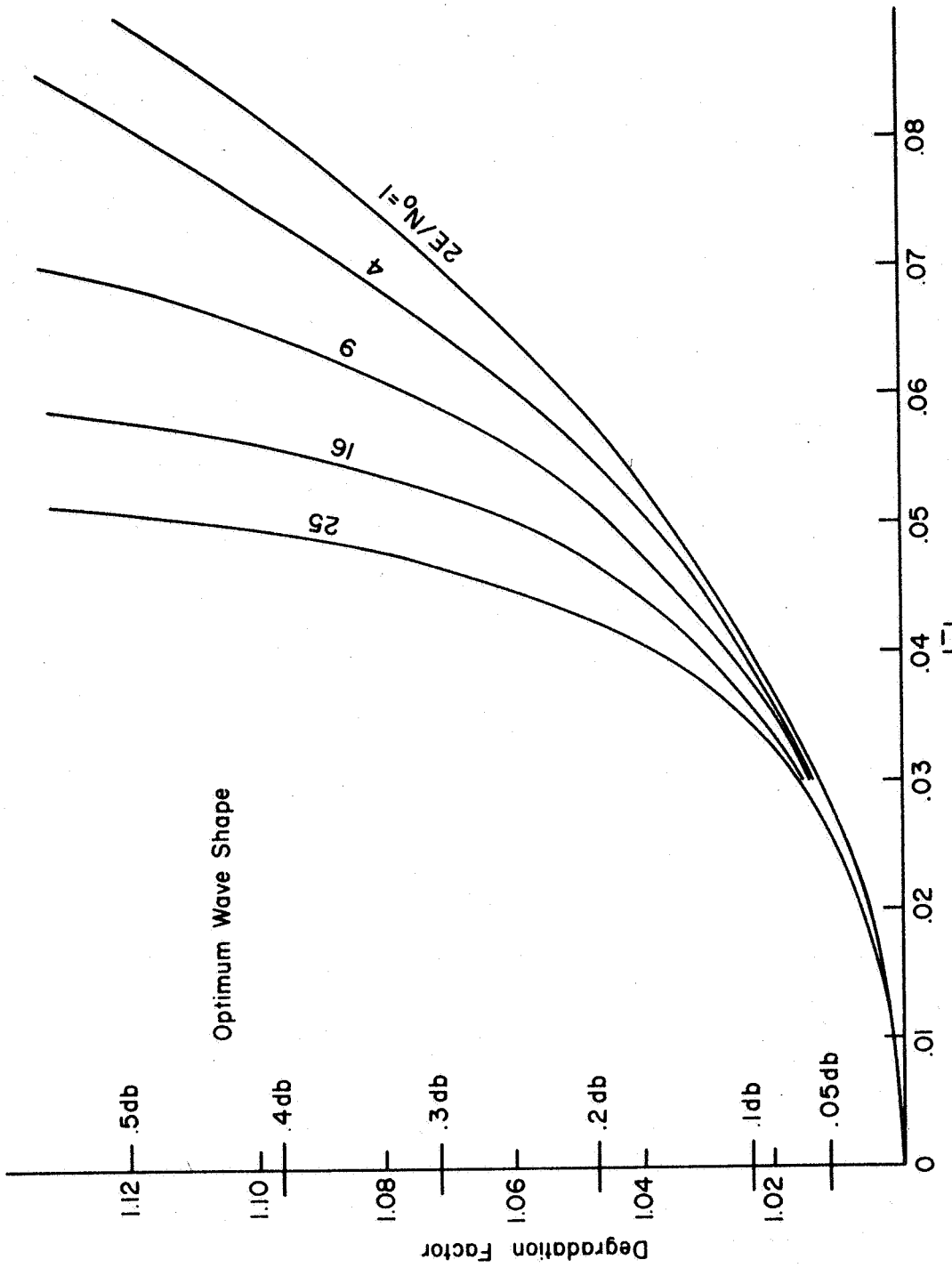

Fig. 4.10 Degradation of $2E/N_o$ for Selected Values of $2E/N_o$ with Optimum Wave Shape

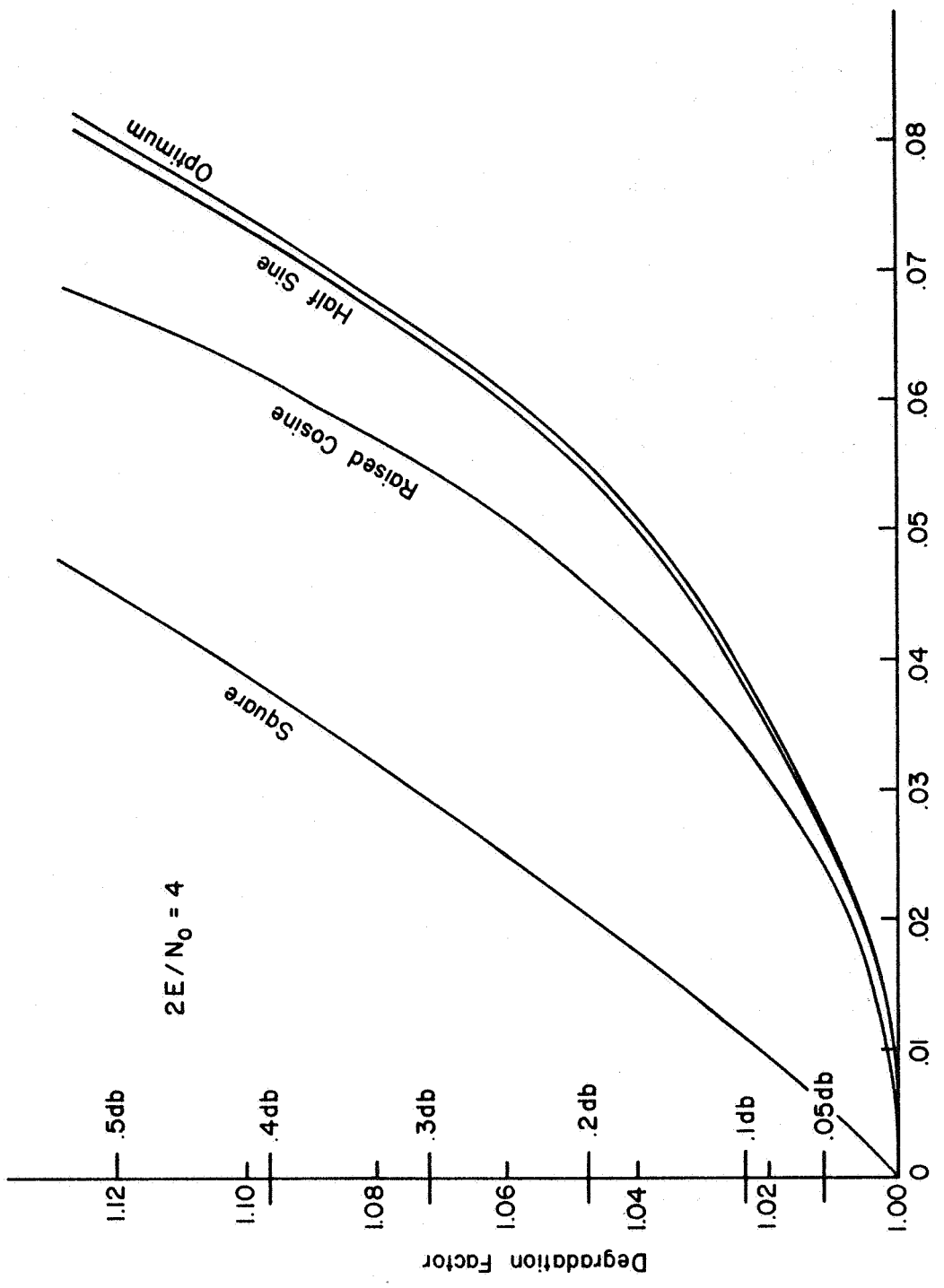

Fig. 4.11 Degradation of $2E/N_o$ for Selected Wave Shapes with $2E/N_o = 4$

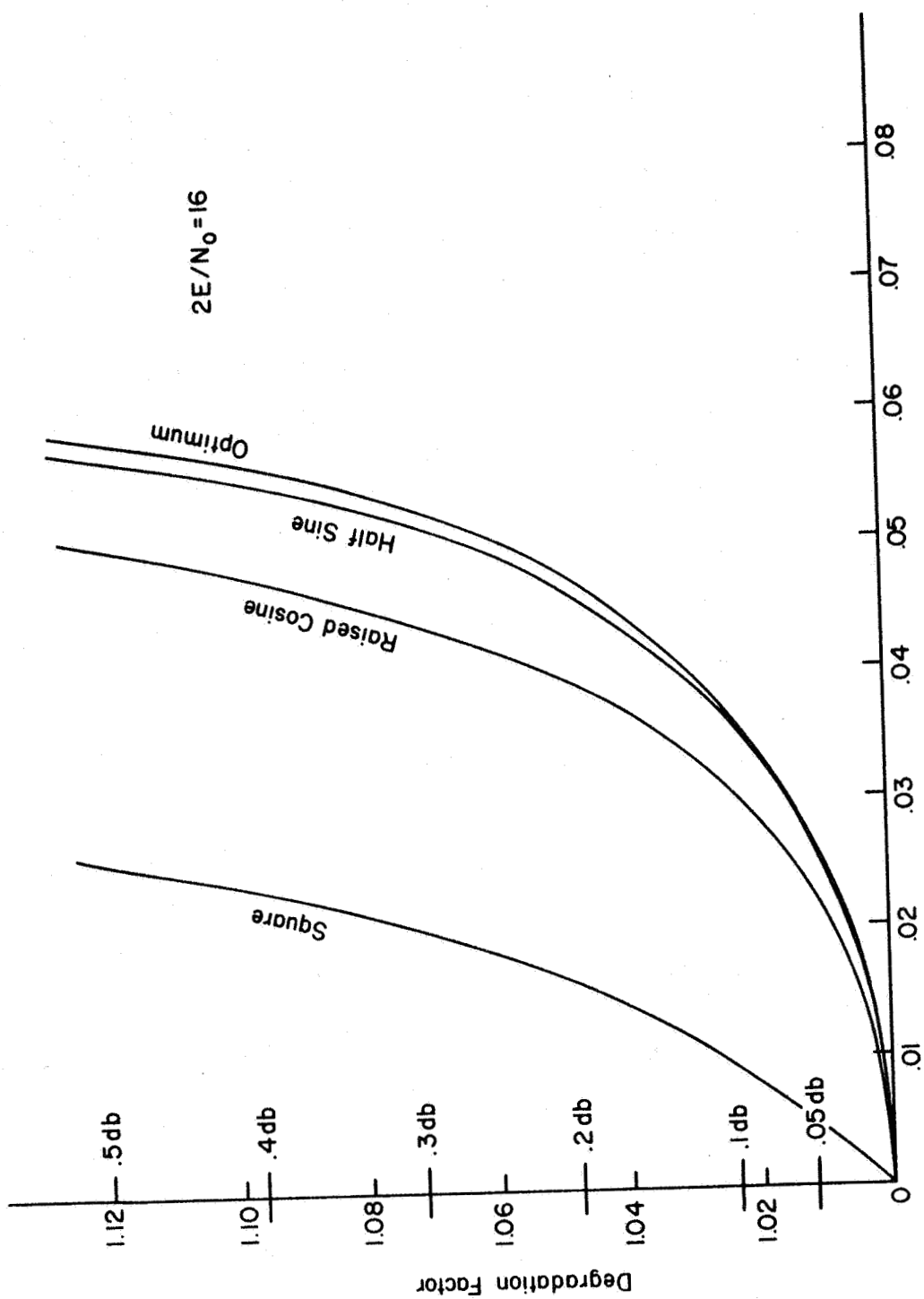

Fig. 4.12 Degradation of $2E/N_o$ for Selected Waveshapes with $2E/N_o = 16$

V. PROTOTYPE SYSTEM

The solution presented in Chapter III for the suboptimum synchronizer carried the problem to the point of computing a signal to noise ratio at the narrowband filter. It was hypothesized there that the probability density function of synchronizing error could be modeled by a single parameter function like that obtained with a sine wave and additive narrowband gaussian noise. The prototype system described in this chapter was designed to verify this assumption and to find the relationship between the computed signal to noise ratio and the desired density function parameter. In addition, the prototype is used to verify the correctness of the model as far as it describes the other aspects of the synchronizer. Finally, the model describes performance with a square law nonlinearity. The prototype system allows a comparison to be made between this and other possible synchronizers, including the infinite clipper--differentiator, or hard limiter, system commonly in use.

5.1 Obtaining an Error Signal

To be able to measure the performance of a prototype synchronizer, it is necessary to have an error signal which is in a convenient form for processing. This section describes a simple method for generating one such useful error signal.

If fractional error, ϵ, is considered to be limited to the range $-1/2 < \epsilon \leq +1/2$, then the timing error can be given a magnitude such that

$0 \leq |\epsilon T| < T/2$, and an algebraic sign. A system which generates a pulse of duration $|\epsilon T|$ with algebraic sign determined by the lead or lag of the synchronizing error is shown in Fig. 5.1. The correct synchronizing time is represented by the leading edge of a short pulse. The noisy sinusoidal output of the suboptimum synchronizer, described in Chapter III, can be passed through a hard limiter, such as a Schmitt trigger, then differentiated, and finally half-wave rectified to give a sequence of positive pulses whose leading edges represent the synchronizer's estimate of the correct synchronizing time. The time difference between the occurrence of these two pulses is the synchronization error.

In order to generate a new signal which has this time difference as its chief defining parameter, these two pulses are applied to identical bistable circuits. The output of one bistable is then subtracted from the other. This difference signal is a sequence of pulses whose duration is the same as the synchronizing error. Fig. 5.2a-f shows the various waveshapes for cases where the synchronizer time both leads and lags the correct time.

In the difference waveshape of 5.2e, where the noisy square wave is subtracted from the reference, the polarity gives no indication of lead or lag. To get a pulse train where polarity can represent the lead or lag of the error, a simple switching system is used. The pulse of Fig. 5.2e is switched off during every other cycle; for example, during the times $1/2T < t < 3/2T$, $5/2T < t < 7/2T$,

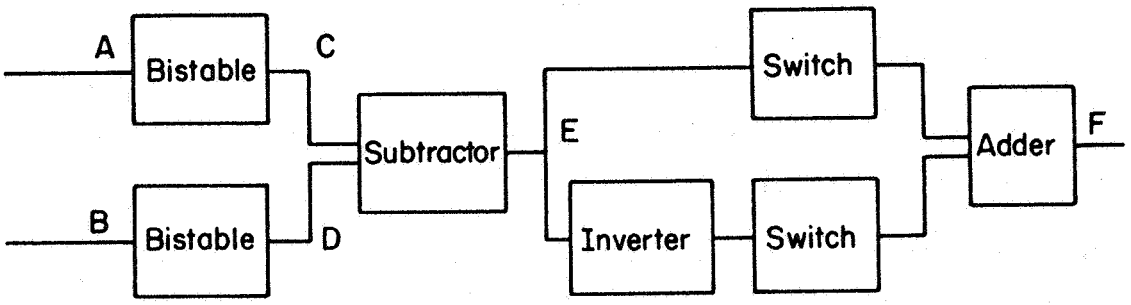

Fig. 5.1 Block Diagram of Error Signal Generator

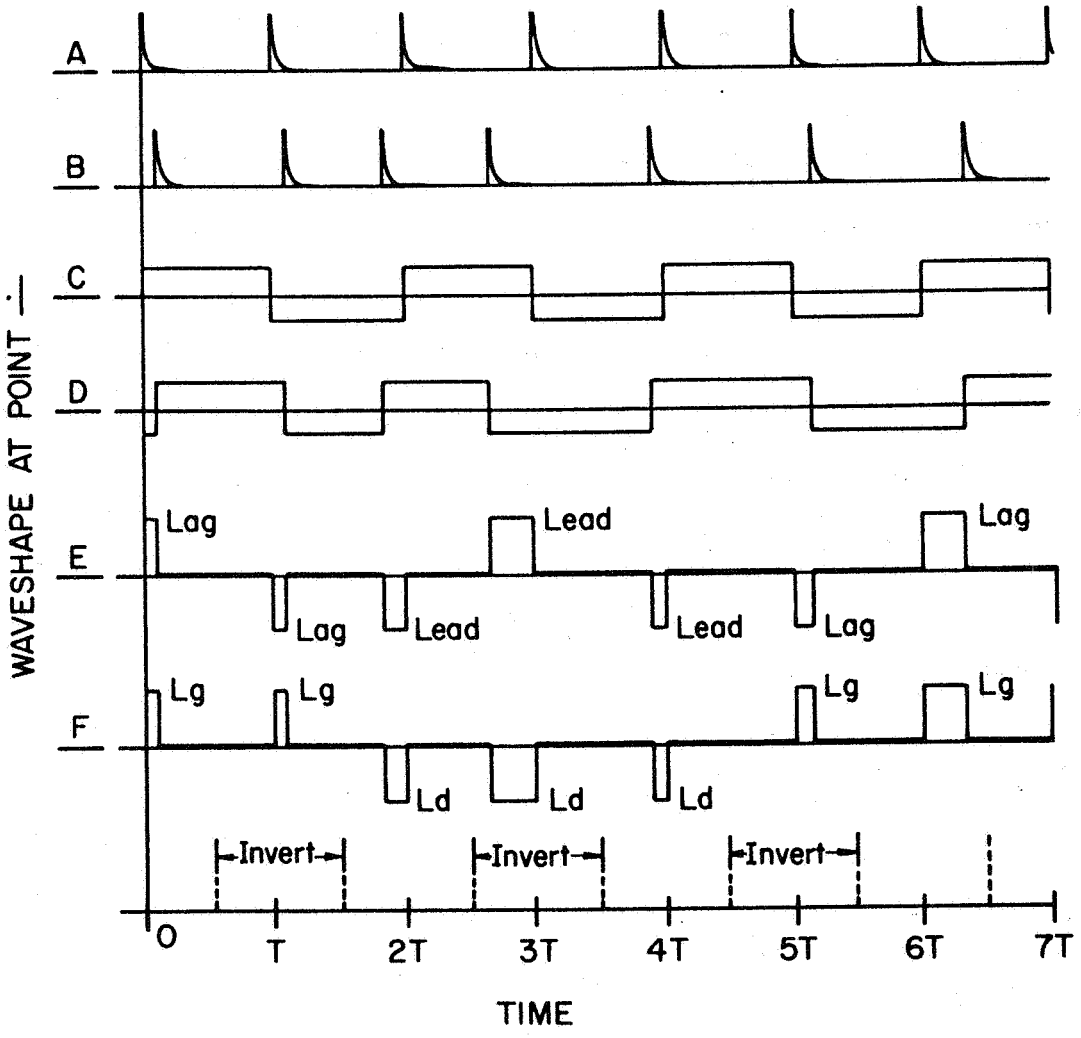

Fig. 5.2 Wave Shapes of Voltage at Various Points of Error Signal Generator

$9/2T < t < 11/2T$, etc. At the same time, the negative of the pulse train is formed and switched off during the times $-1/2T < t < 1/2T$, $3/2T < t < 5/2T$, etc. The two resulting pulse trains are added to produce the result in Fig. 5.2f. The lagging errors are now represented by positive pulses and the leading errors by negative pulses.

5.2 Method of Measuring the Desired Statistical Moments

The timing errors that result from jittery synchronizing signals are a sample function of a stationary time series. The fractional error, ϵ, at the beginning of each symbol period defines a set of random variables $\epsilon_{t_1}, \epsilon_{t_2}, \ldots, \epsilon_{t_n}$ at the times $t_1 = KT$, $t_2 = (K+1)T$, $\ldots$, $t_n = (K+n)T$ which have a joint probability density function. Because the time series is stationary, $\bar{\epsilon}_{t_1} = \bar{\epsilon}_{t_2} = \ldots \bar{\epsilon}_{t_n} = \mu$. Now the mean $M = \frac{1}{n}(\epsilon_{t_1} + \epsilon_{t_2} + \ldots \epsilon_{t_n})$ is an unbiased estimator of μ since $\bar{M} = \frac{1}{n}(\bar{\epsilon}_{t_1} + \bar{\epsilon}_{t_2} + \ldots \bar{\epsilon}_{t_n}) = \frac{1}{n}(n\mu) = \mu$. Consider the time average of the error signal that is generated by the process described in Sec. 5.1. If a record of NT seconds is available, the average value of that signal is

$$V_{AVG} = \frac{1}{NT} \sum_{i=1}^{N} \epsilon_i T = \frac{1}{N} \sum_{i=1}^{N} \epsilon_i$$ where ϵ_i is the error at the i-th symbol period. Thus, the average value of the error signal is an unbiased estimate of the mean μ of the fractional timing error.

In order to measure the expected value of the absolute error, the error signal is full-wave rectified. This new signal is a sequence of

positive pulses whose durations are the period-by-period measure of the absolute timing error. These absolute values of timing error define a time series of random variables $X_t = |\epsilon_t|$. In a way exactly analagous to the case of measuring the mean of ϵ, the estimate of the average value of $|\epsilon|$ is obtained by measuring the average value of the full-wave rectified error signal.

For both measurements, the variance of this estimate is quite large because of the high correlation from one symbol period to the next. From measurements of the timing error of the suboptimum synchronizer, it was found that measurement times of 10-20, 000 time periods were necessary to reduce the fluctuations about the mean value to $\pm$ 5%.

5.3 The Test System

The block diagram of the test set-up which was used to evaluate the performance of the self synchronizers is shown in Fig. 5.3. Briefly, the operation of the system is as follows: The master clock, which is driven by an external variable frequency oscillator, provides the necessary timing pulses for the entire system. The pseudo-random word generator produces a sequence of positive and negative square pulses which are used to drive a switch. The switch chooses either the positive or negative symbol that has been generated by the periodic waveform synthesizer. The resulting pseudo-random symbol sequence is combined with additive gaussian noise from the Random Noise Generator and the sum is applied to the self synchronizer that is being tested. The output of the synchronizer is applied to the phase meter and moment estimator system. The components of each of the blocks are described below.

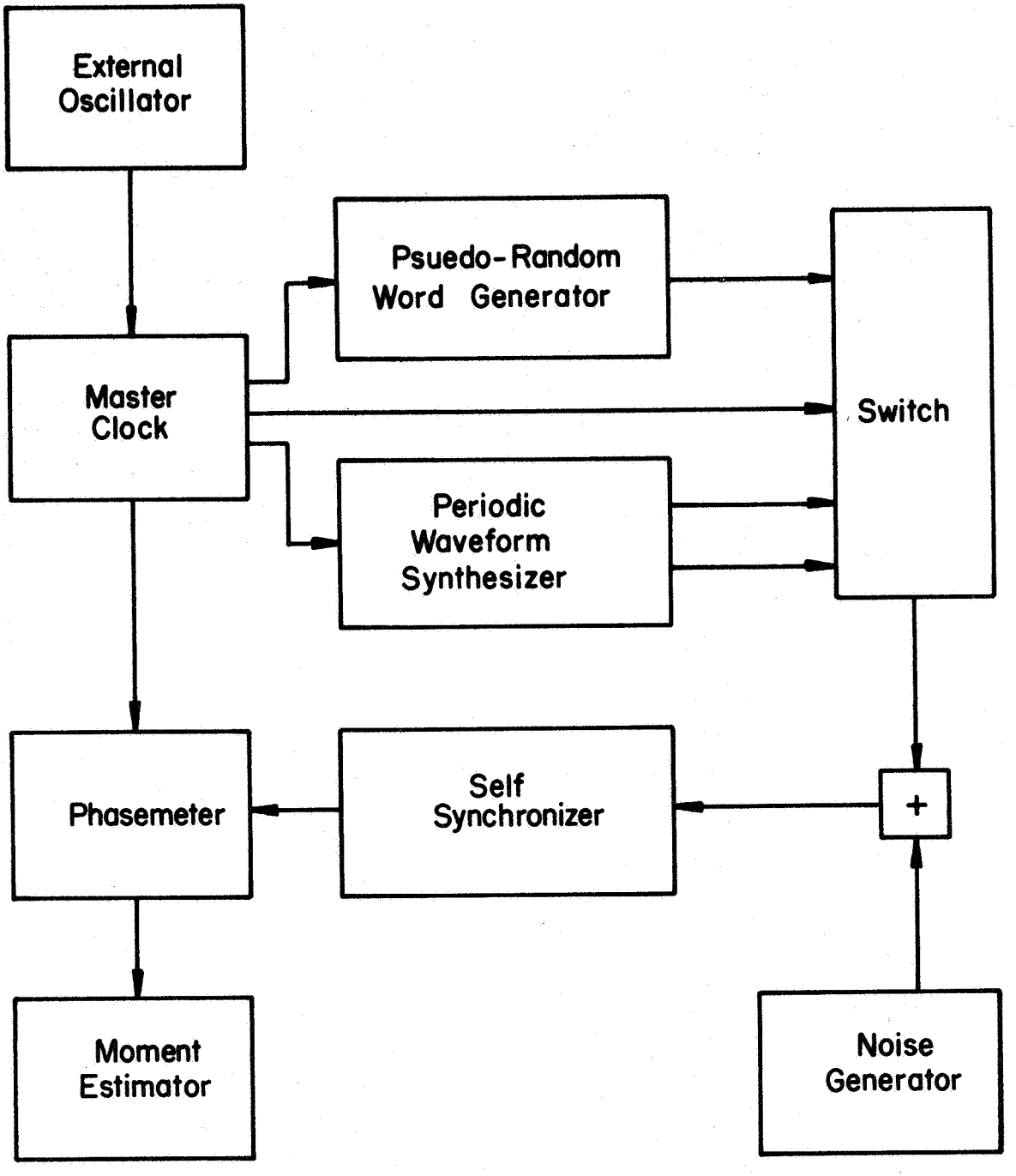

Fig. 5.3 Block Diagram of Test Set Up

5.3.1 External Oscillator

The external oscillator was a General Radio 1210-C unit oscillator.

5.3.2 Pseudo-Random Word Generator

Constructed by the Purdue University Communication Sciences Laboratory, this generator produces a 127 bit pseudo-random word by means of a binary shift register. The output is square and has a separate timing pulse at the start of the word.

5.3.3 Periodic Waveform Synthesizer

The Exact Electronics, Model 1200-B produces any periodic waveform desired by a series of straight line approximations with up to 50 segments. For the waveshapes generated for tests, 20 segments were found to be sufficient.

5.3.4 Noise Generator

The noise generator used was a General Radio Model 1390-B Random Noise Generator.

5.3.5 Master Clock

The master clock was designed specifically for these experiments. It supplies the timing signals to operate the other units and is designed to supply a variable time-delayed pulse to the phase meter. This is done so that the reference phase, or time, will be in phase with the output of the self synchronizer. The phase of the self synchronizer is variable with the design parameters of the system. In the block diagram of Fig. 5.4, the output of the signal generator is shaped by a Schmitt trigger which drives the master clock bistable device. The output is at the frequency 2f where f is the frequency of symbol

transmission. This output is delivered to a bistable whose output drives the Pseudo-Random Word Generator and the Waveform Synthesizer. In order to develop a phase shifter with good resolution and fine control, the 0° - 180° output at 2f drives a monostable delay which delays the input pulse over the range $(1/8)f < t_d < (3/8)f$. This delayed pulse is applied to the bistable which is used to operate the phase meter. By selectively choosing the 0° or 180° outputs at this point, a full (1/f) seconds of delay, or 360° phase shift, is possible. The output opposite to the one chosen for the phase meter drive is chosen to drive a bistable whose outputs operate the switches in the phase meter, Fig. 5.1.

5.3.6 Phase Meter

The basic principle of the phase meter is described in Sec. 5.3. To measure $|\overline{\epsilon}|$, the timing error is full wave rectified. In order to make an accurate measurement, the rectifier output is applied to a Schmitt trigger which generates pulses of fixed amplitude. The dc level is brought to the zero base line and the resulting signal measured by a HP Model 410-C. Since the effective measurement time of the voltmeter is only about 1 second, the longer time needed is obtained by using the one milliamp full scale output of the meter amplifier to drive a microammeter circuit that has a long time constant filter. For good measurements, the time constant is set to a value near 30 seconds. The microammeter is calibrated against the dc voltmeter and has a shorting switch for quick return to zero.

5.3.7 Prototype Synchronizer

The block diagram of the prototype synchronizer is shown in Fig. 5.5. The nonlinear devices are simulated by a piecewise linear approximation

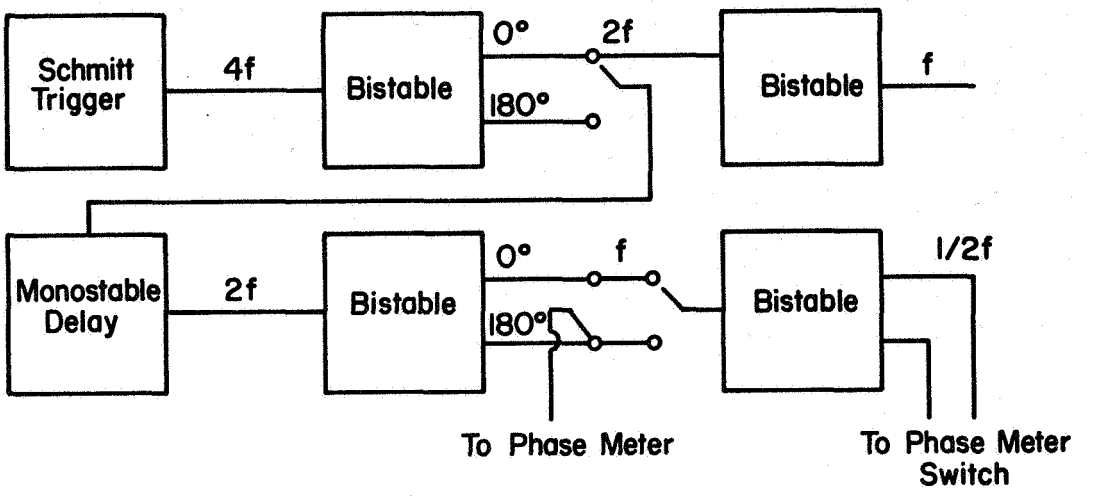

Fig. 5.4 Block Diagram of Master Clock System

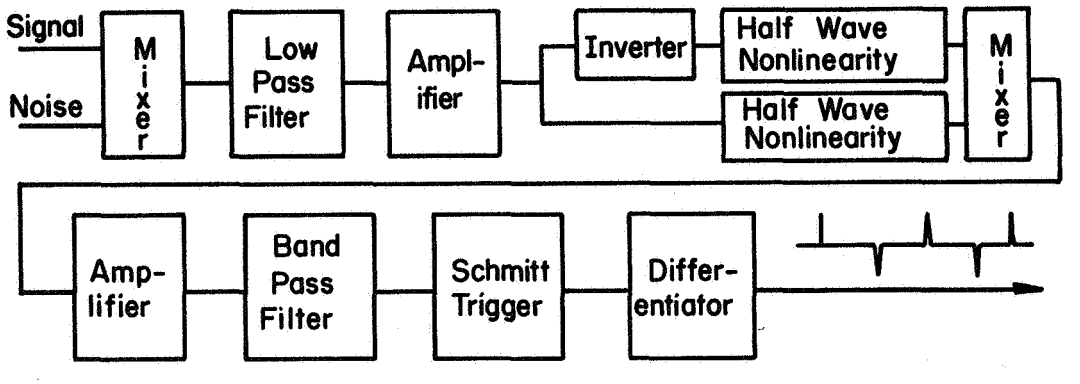

Fig. 5.5 Block Diagram of Details of the Prototype Synchronizer

produced by biased diode-resistor networks. The bandpass filter is a two stage filter with a wide bandwidth, single pole, first stage and a narrow bandwidth final stage.

5.4 Calibration and Operation of the System

This section contains brief discussions of the methods used to calibrate and operate the various parts of the measurement system. It also contains comments on how the system, as constructed, did not measure up to the ideal as conceived in the block diagrams.

The first order of necessity in operating the system is that of measuring the input signal to noise ratio $2E/N_o$. To do this, the spectral density of the noise source, N_o is needed. The manufacturer of the noise generator specifies that the spectrum level is $\pm$ 1 db flat over a 20 Hz to 20 kHz frequency range and has a typical value of $25 \cdot 10^{-6}$ v^2/Hz for a 1 volt RMS noise output. This was checked by low pass filtering the output with cutoff frequencies well within the cut-off of the generator. The resulting volts-square noise output with this filter was used in conjunction with the noise equivalent bandwidth to calculate the spectral density. The average value obtained by this method was $19.2 \cdot 10^{-6}$ v^2/Hz. To compute $2E/N_o$, the signal power and noise power were measured at the input to the mixer using an HP 3400A RMS voltmeter. Signal energy per period is $V_s^2 T$. Noise spectral density is directly proportional to the input noise power so that $N_o = (19.2 \cdot 10^{-6}\ V^2/Hz)\ V_n^2$. Hence, $2E/N_o = (2T/19.2 \cdot 10^{-6})(V_s/V_n)^2$. Thus, only RMS inputs need be measured. The greatest source of error in the final measured value of the signal to noise ratio is in the initial measurement of N_o.

The setup of the Waveform Synthesizer was accomplished by drawing the desired waveform on the face of an oscilloscope and then adjusting the synthesizer controls until the trace of the waveform that is generated was coincident with the one that was drawn. Exact coincidence was not possible and some variations occurred at points of abrupt change in the waveform. These are not really a problem though, since the deviations are the source of high harmonics and at no point were these deviations more than 5% of full scale.

The setup and alignment of the self synchronizer required establishing the nonlinear transfer function and the bandpass filter bandwidth. The half wave nonlinear devices were set up by a process of initially computing the desired settings and then making fine adjustments by statically testing the input-output characteristics. It was possible to match at least 5 points on the nonlinear input-output characteristics, but the process was slow and was complicated by the tendency of the settings to have a long term drift.

The adjustment of the bandpass filter was done in the following manner. The desired symbol rate, and hence, the fundamental component of the signal at the bandpass filter, was 2000 Hz. Instead of trying to fine tune the filter to exactly this value, it was brought to a value as close as was easily possible and the total system drive frequency was then adjusted so that the input to the bandpass was at its center frequency. This turned out to be near 2005 Hz. The minimum bandwidth that was obtained with the filter was 36 Hz. Wider bandwidths were obtained by loading the second stage of the filter to broaden its response bandwidth. The bandwidths of each stage in the

filter were measured by observing the frequency of the 3 db points with a digital frequency meter. The resulting noise equivalent bandwidth of the cascaded parallel RLC bandpass filters was then computed.

The alignment of the phase meter and calibration of the measuring system are important to the proper operation of the system. To obtain the correct error signal, the noise source to the self synchronizer was disconnected and the phase shift system in the master clock was adjusted until there was no error signal. This was easily observed as a null on the indicating instrument. After the null was achieved, the zero level adjustment was made in the moment estimator circuit.

To calibrate the meter to measure the desired moment, the phase shift circuits in the master clock were switched to provide a 180^{o} phase shift. The resulting meter indication was used to calculate the volts/degree conversion factor for the meter.

As in any practical problem, several compromises were necessary in the design of the test system. One very fundamental one was in the choice of 2000 symbols per second as the symbol rate for the pseudo-random sequence. The realization of the bandpass filter for the self synchronizer is easier as the rate is increased. This is true because it is less difficult to realize the necessary high Q inductor as frequency is increased. However, as the rate is increased, more stringent demands are made on the switching times of the various measurement circuits. For example, to produce a fair quality error signal pulse for a 1% fractional error at 500 microseconds symbol duration (2000 Hz) requires overall system rise time of 2-3 microseconds. To achieve circuits with an overall time less than this requires a significant increase in circuit

complexity. Hence, 2000 Hz is near the upper limit for simple circuit design.

Another factor in circuit design that makes 2000 Hz near the lower limit is the low frequency response that is necessary to reasonably pass the pseudo-random symbol sequence. Ideally, the amplifiers should be D.C. coupled, but practically the distortion due to low frequency cutoff can be held to a minimum with good ac coupling. To prevent a sag of more than 10% over a run of 5 consecutive positive or negative pulses, an equivalent lower cutoff frequency of 20 Hz is required. For the number of stages of amplification and isolation that are necessary, this is a relatively difficult lower limit to exceed. Thus, to lower the 2000 Hz rate would require all dc amplification.

Dynamic range is a problem in any system in which precise noise measurements are to be made. At low signal to noise ratios, the amplitude of the noise peaks is easily 10-20 times the amplitude of the signal. It is difficult to maintain linearity over such a wide range. This was especially difficult in the drive stages to the full wave nonlinear filters. Here the signal level must be maintained at a level great enough to minimize the effect of reverse conduction in the rectifier and the null zone in the forward direction. A peak signal level of 1 volt, for instance, means that peak signal plus noise voltages of 10-20 volts are common. A device to produce a square law output over such an input range is very difficult to obtain and in these experiments some peak clipping was unavoidable.

VI. RESULTS

This chapter presents the results obtained using the optimum and suboptimum synchronizers that were derived in the previous chapters. Sec. 6.1 gives the results of a computer simulation of the optimum synchronizer. Sec. 6.2 through 6.7 present the experimental completion and verification of the suboptimum model and the conclusions that can be drawn concerning its performance. Sec. 6.8 compares the optimum and suboptimum results.

6.1 Performance of the Optimum Synchronizer

A Monte Carlo computer simulation was used to evaluate the performance of the optimum synchronizer. The complete computer program is included as Appendix A. The basic concept of the procedure is to use a discrete time analog of the continuous time problem. The input signal is sampled at 50 equal time increments for each symbol duration. The sign of successive symbols is randomly chosen with each sign equiprobable. To each "time sample" of the input, a random, gaussianly distributed number is added to simulate the additive white gaussian noise assumption. It is relatively easy to relate the variance of each of these random numbers and the amplitude of the signal to the required signal to noise ratio $2\ E/N_o$.

In Chapter II it was shown that the optimum receiver tested each possible synchronizing position (measured with respect to the receiver

reference) by finding the sum of the log hyperbolic cosines of the correlation of the properly shifted reference with the received signal. That shift which produced the maximum was judged to be the proper synchronizing position. In the derivation it was assumed that the input record started uniformly over the duration of one symbol. This means that the input record will contain only a fractional part of the first symbol. To simulate this condition, the sequence of received symbols was started at each of 10 equal fractions of the first symbol. In other words, the first input symbol ranged from a full symbol to the last 1/10 of a symbol.

A histogram of the probability of position error, $p(\epsilon)$, is built up by testing synchronizing positions around the known (to the program) position. To save computation time only 20 out of the 50 possible positions were tested with the majority of these being near the correct synchronizing position.

For each signal to noise ratio and wave shape, 500 complete runs of one through eight symbols of memory were made. From the histograms that were obtained, the performance measure $|\overline{\epsilon}|$ was computed and by means of the appropriate application of the theory of Chapter IV, the probability of detection error with noisy synchronization was obtained.

Fig. 6.1, 6.2, and 6.3 show $|\overline{\epsilon}|$ plotted against $2\ E/N_o$ for each of the eight memory durations. For the case of the half sine and raised cosine pulses the results clearly show that for $2\ E/N_o > 2$, $|\overline{\epsilon}|$ decreases with the inverse of $\sqrt{2\ E/N_o}$. For values less than 2, $|\overline{\epsilon}|$ asymptotically approaches .5 and hence cannot continue to obey the inverse square root law. The results for the square pulse case are

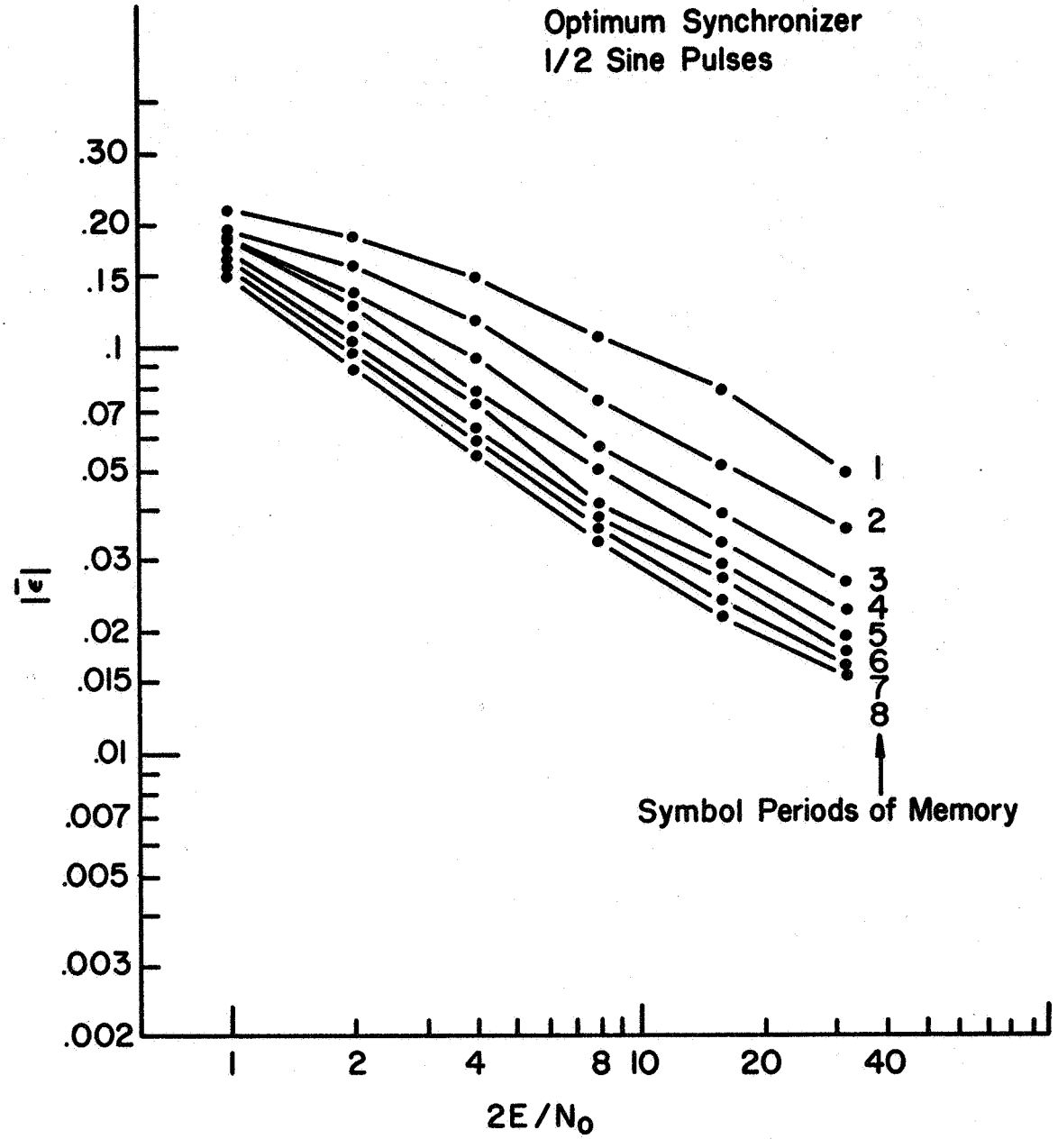

Fig. 6.1 $\overline{|\epsilon|}$ vs. $2E/N_0$ for Half Sine Symbols

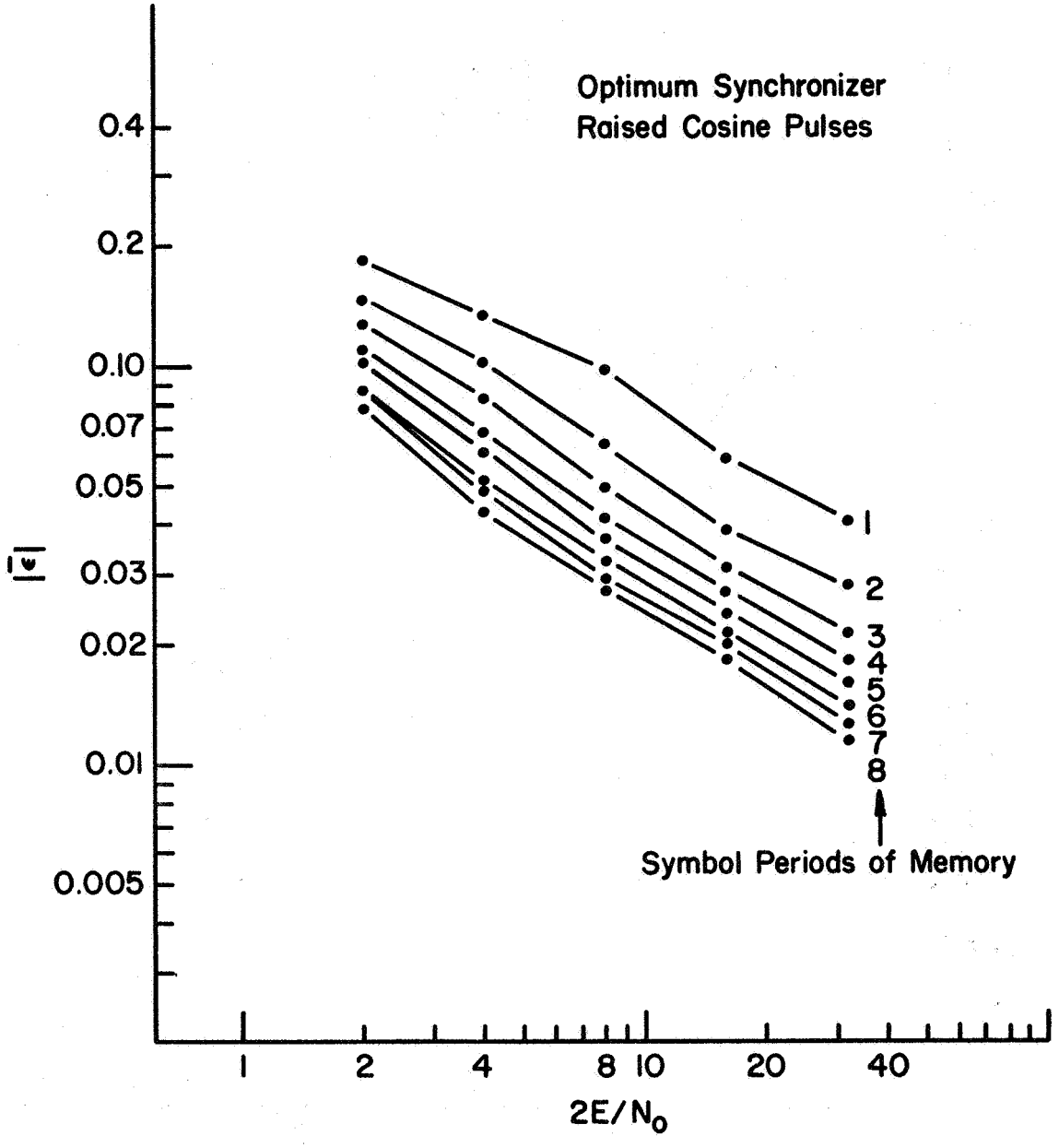

Fig. 6.2 $|\bar{\epsilon}|$ vs. $2E/N_o$ for Raised Cosine Symbols

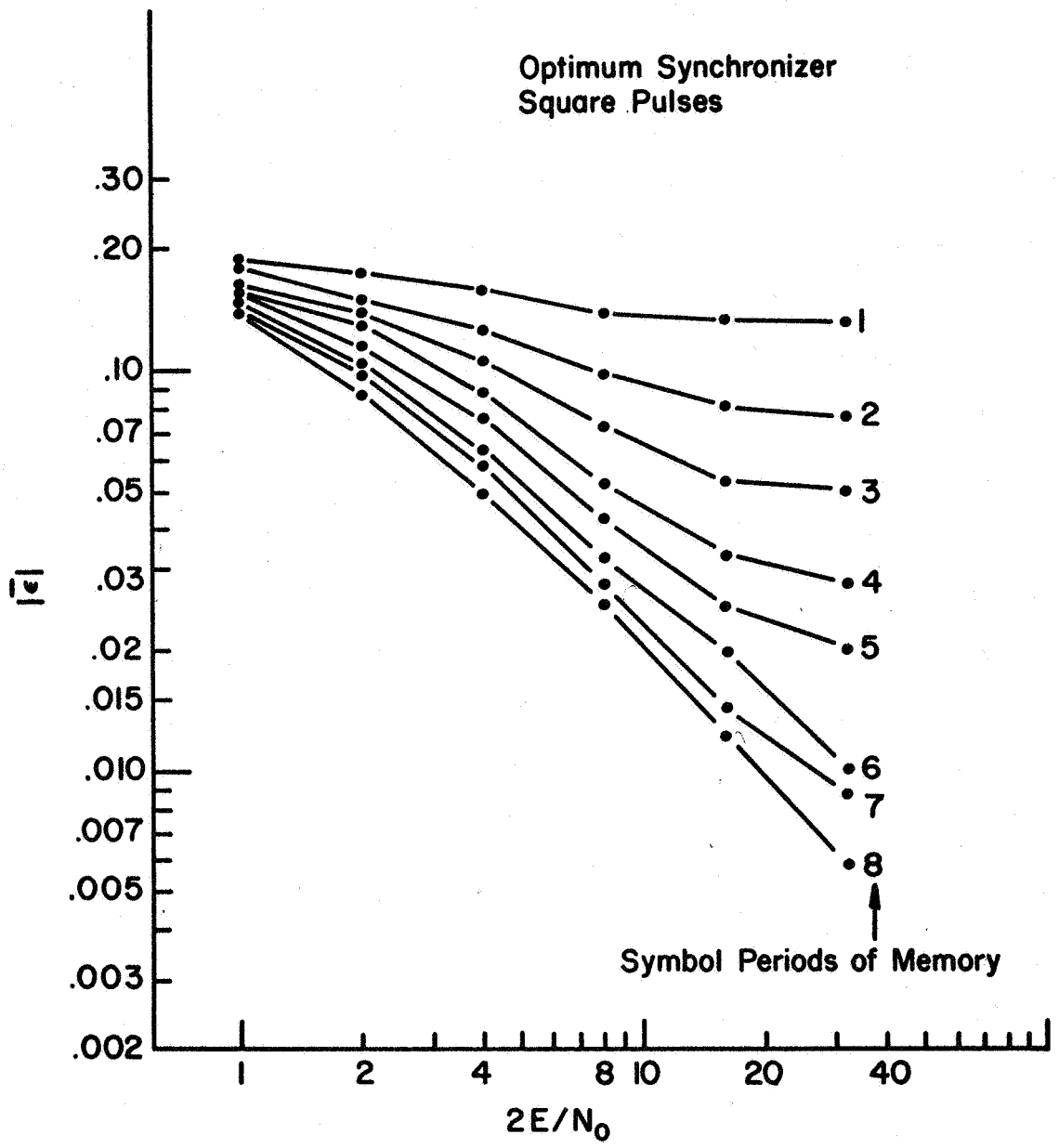

Fig. 6.3 $\overline{|\epsilon|}$ vs. $2E/N_0$ for Square Symbols

not so clear cut, but they appear to follow the same trend. The unexpected effects at the high values of $2\ E/N_o$ are due to the approximations in the computer model.

It can also be seen from these figures that $|\bar{\epsilon}|$ varies inversely with the square root of memory time as measured in symbol periods. Again, for the square pulse case, the results are not as conclusive over the complete range of signal to noise ratios, but they do fit well in the range $4 < 2\ E/N_o < 16$. Let T_m = memory time and $R_i = 2\ E/N_o$. The results can be summarized by the relationship $|\bar{\epsilon}| \sim 1/\sqrt{T_m R_i}$. Such a relationship seems to be typical for adaptive systems [12].

Fig. 6.4 shows the comparison of the three wave shapes used with the optimum synchronizer. They show that the optimum solution is relatively insensitive to pulse waveform. The synchronizer makes about the same degree of error for each case.

Fig. 6.5, 6.6, and 6.7 show the results for the optimum synchronizer when it is used to drive a correlation detector. The Monte Carlo simulation results are obtained in terms of the probability of detection error. As pointed out in Chapter IV, the degradation in effective signal to noise ratio is a more meaningful measure of the synchronizer performance than is $|\bar{\epsilon}|$. For small increases in probability of error, the results of Sec. 4.3 are used to calculate the degradation. For large increases in error, degradation is computed in the following way. For each value of detection error, there is a corresponding value of signal to noise ratio under the condition of perfect synchronization. The difference in the ratio corresponding to the detection error with no synchronization error and that error with non-perfect synchronization

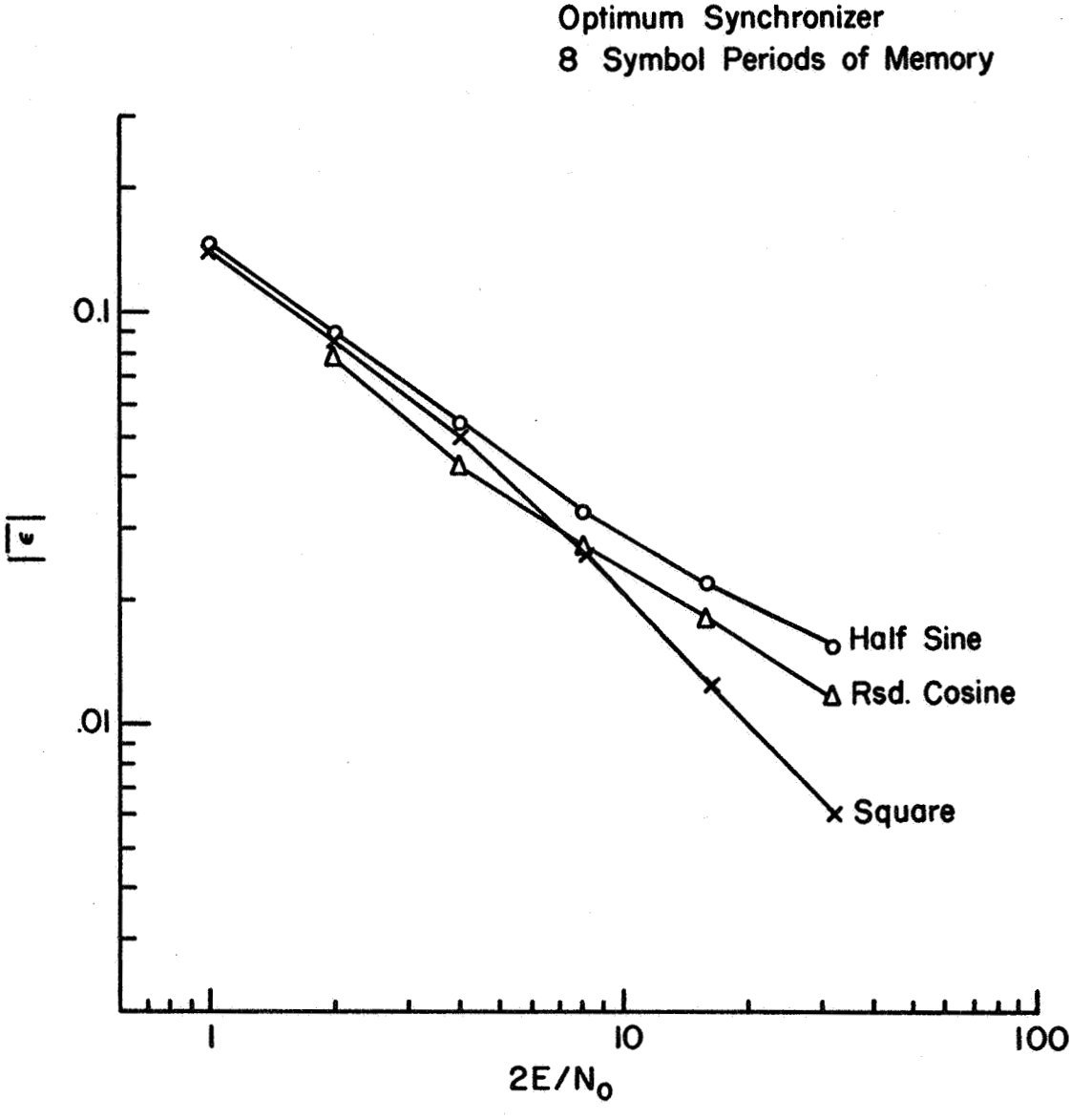

Fig. 6.4 $|\bar{\epsilon}|$ vs. $2E/N_o$ for Three Symbols Compared at 8 Periods of Memory

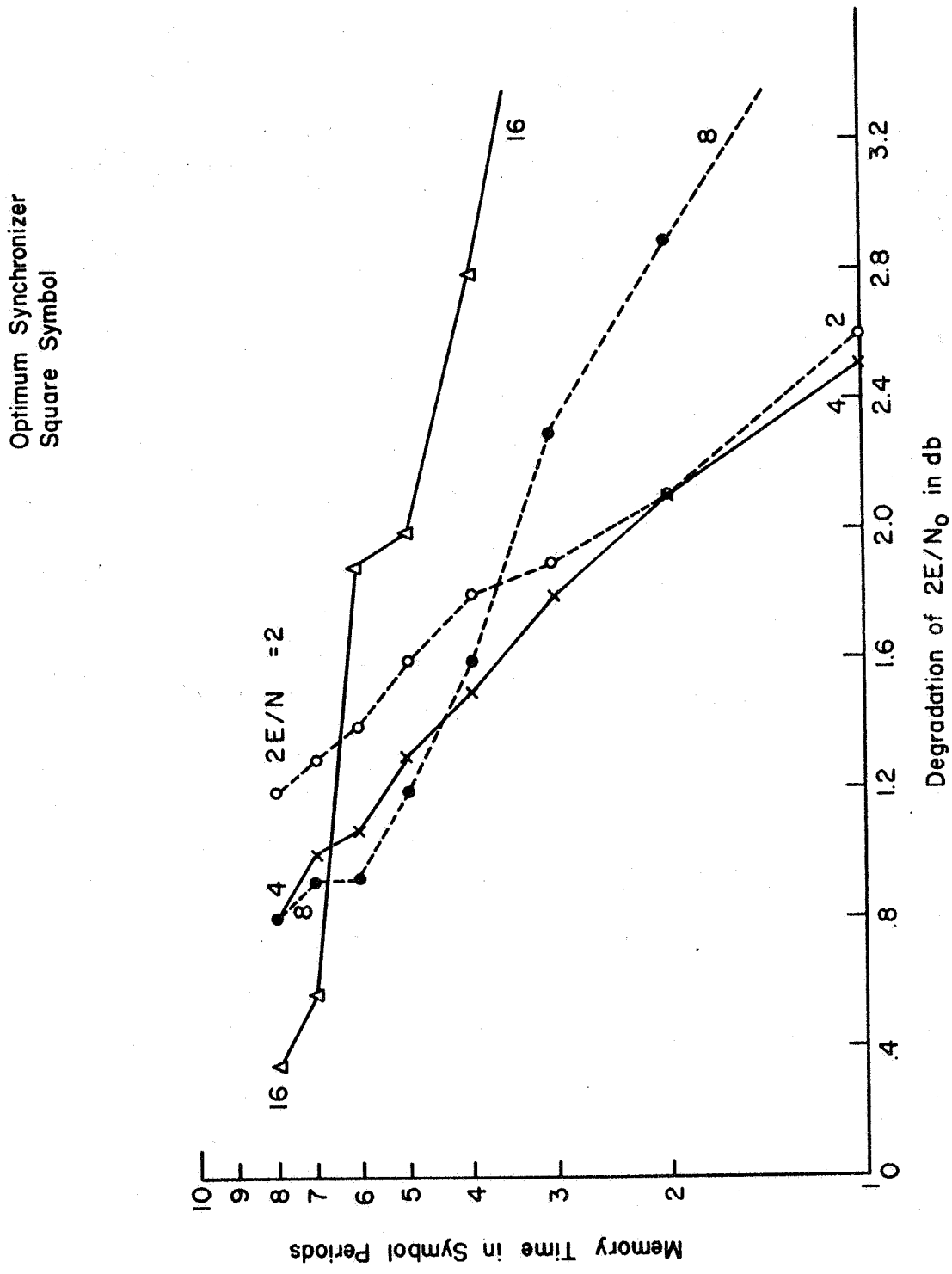

Fig. 6.5 Memory Time vs. Degradation of $2E/N_o$ for Square Symbols

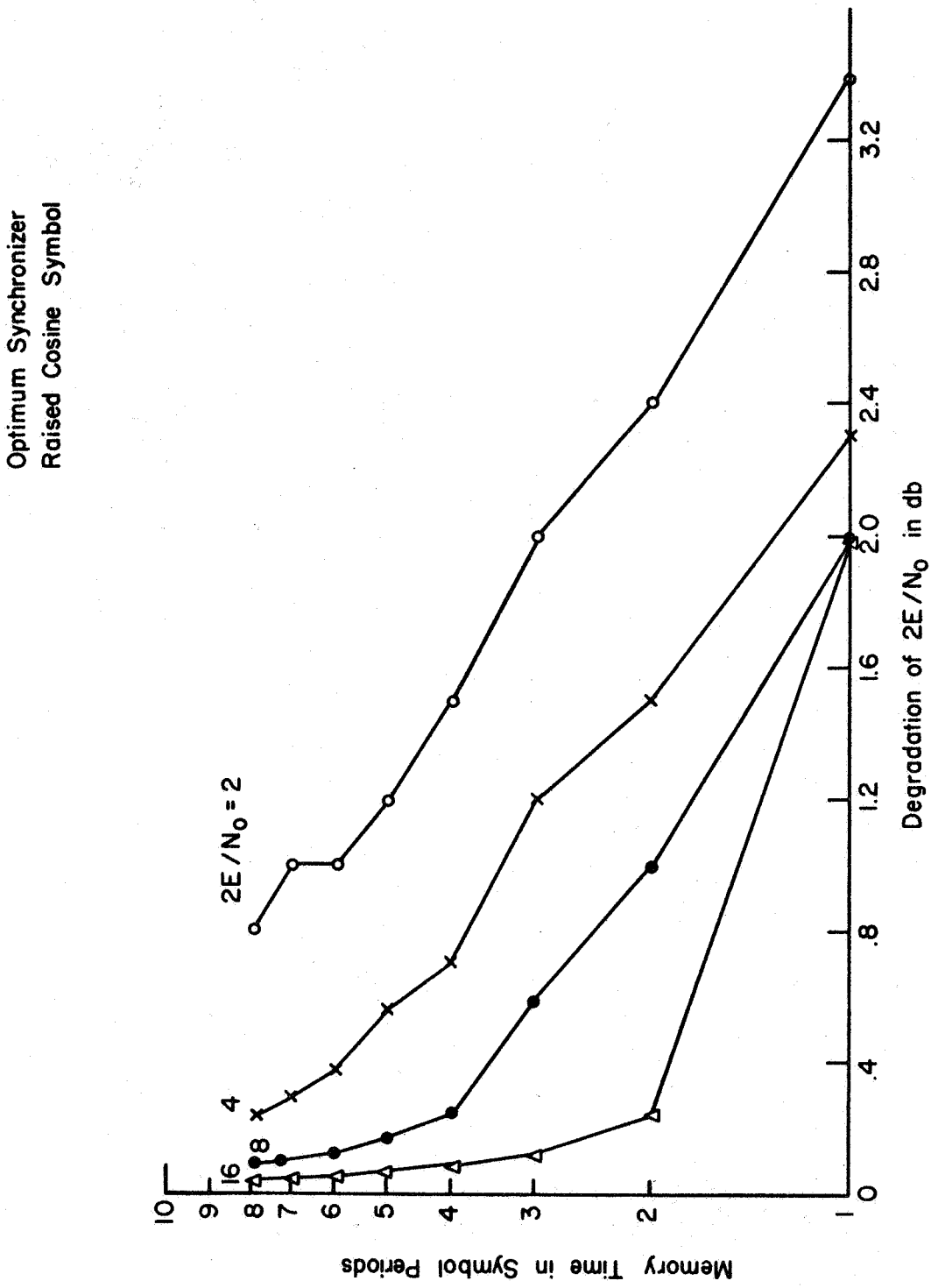

Fig. 6.6 Memory Time vs. Degradation of $2E/N_o$ for Raised Cosine Symbols

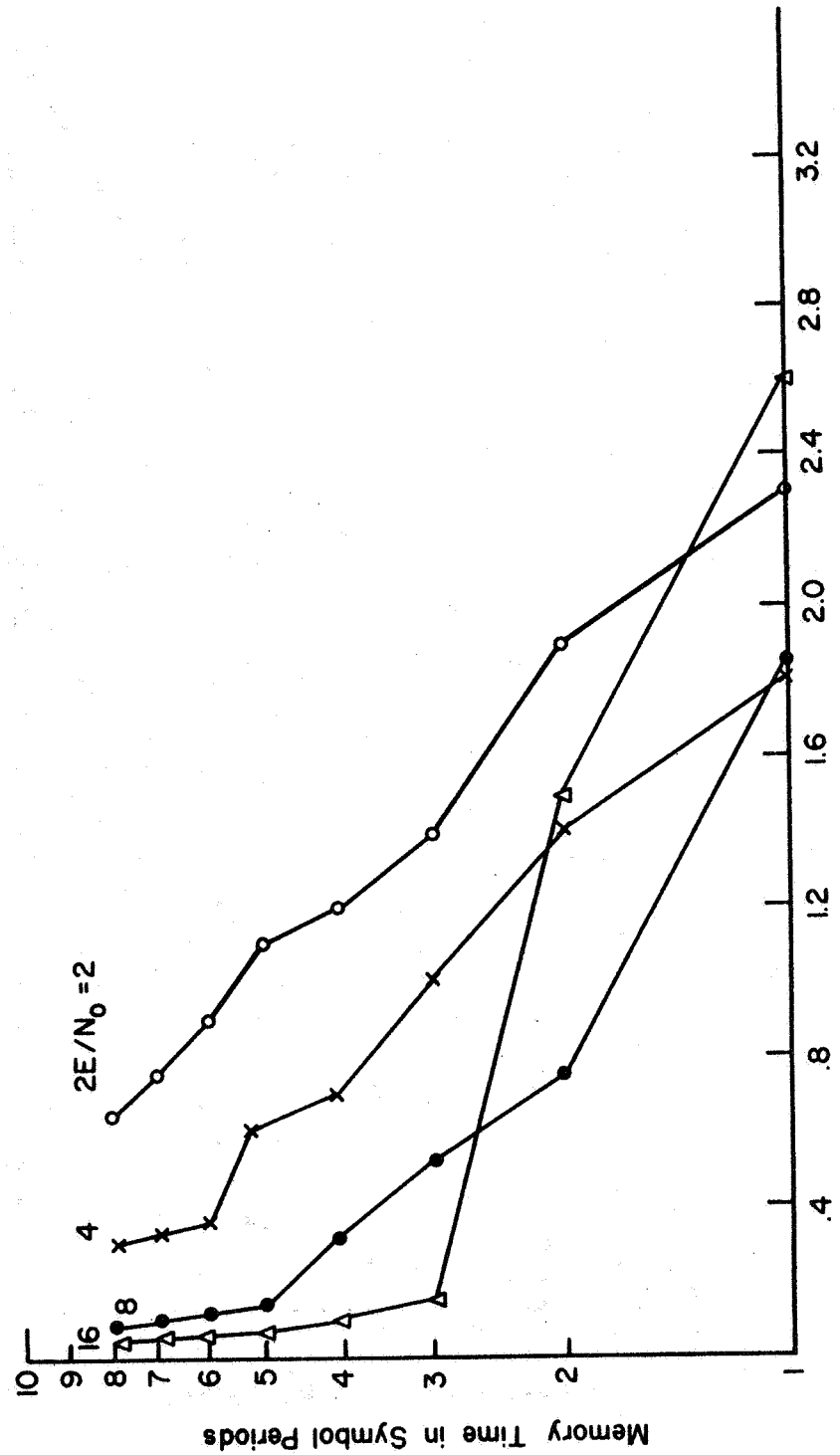

Fig. 6.7 Memory Time vs. Degradation of $2E/N_o$ for Half Sine Symbols

was taken as the degradation of signal to noise ratio. This definition is a somewhat arbitrary one which reduces the computational difficulties.

The curves show that, for the range of memory times which were used, the degradation is very sensitive to the amount of memory up until a transition point is reached. Past this point, large increases in memory are necessary to achieve even small improvements in performance. Comparison of the curves for the three different pulse wave shapes shows that the square pulse performance for a fixed degradation is poorer by a factor of 3 in memory time.

6.2 Completion of Suboptimum Model

The suboptimum synchronizer was analyzed in Chapter III. Its block diagram is repeated here as Fig. 6.8. The analysis presented

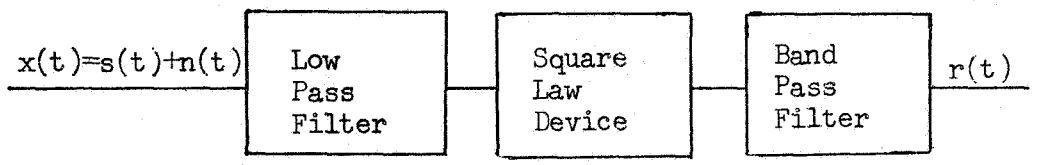

Fig. 6.8 Block Diagram of Suboptimum Synchronizer

there carried the problem to the point of computing the signal to noise ratio R_M at the output of the bandpass filter. It was conjectured there that this ratio was linearly related to the parameter R_d in the assumed density function for phase. One of the primary objectives of the experimental work was to determine if such a relationship could be verified and, as a result, a complete model of the system obtained.

In order to compute the signal to noise ratio R_M, 3.39 in

Chapter III must be evaluated. This equation was

$$R_M = \frac{S'_{ss}(1/T)}{\left[S'_{sxs} + \frac{4E_s}{(S/N)} S'_{sxN} + \frac{2E_s^2}{(S/N)^2} S'_{nxn}\right] \Delta f}$$

Here, the S'_{hxj} are the spectral densities which are computed from the unit amplitude signals as given in 3.27, 3.34, 3.36, and 3.37. The analytical form of 3.27 and 3.34 is derived in Appendix C. 3.36 and 3.37 do not lend themselves to analytical integration for the types of signals that are used. They were evaluated at the frequency 1/T by means of numerical integration. A tabulation of the results of these integrations at selected filter cutoff frequencies is included in Appendix C. Finally, in the same Appendix, R_M is tabulated for unit values of Δf. In order to determine the value of R_M for a given noise equivalent bandwidth, the tabulated value is divided by this noise equivalent bandwidth.

The formulation of the model for the suboptimum system is completed by determining the relationship between R_M and R_d. To do this, define a constant $K = R_d/R_M$. For a given set of data of $|\bar{\epsilon}|$ vs. $2\,E/N_o$ for the desired prototype synchronizer, determine the value of R_d that corresponds to a measured value of $|\bar{\epsilon}|$. The curves in Appendix B are convenient to use. Using the proper model of the synchronizer, compute the value of R_M that corresponds to the value of $2\,E/N_o$ for the measured $|\bar{\epsilon}|$. Use these to compute K.

Because the values of R_d are computed from experimental data and because it cannot be assumed that the density function for $|\bar{\epsilon}|$ is the one that precisely applies, the values of K are not necessarily the same for all values of $2\,E/N_o$. In order to achieve a simple model, the

average value of K for the range of values of $2\ E/N_o$ that are of interest is computed. For the three wave shapes that were studied, these averages are:

Half Sine — K = .36

Raised Cosine — K = .38

Square — K = .67

Fig. 6.9 and 6.10 show the experimental results, plotted as points, and the curve predicted by the model using the average value of K as given above. The results indicate that the model for the half sine and raised cosine symbols fit the experimental data very well. The results for the square pulse are not as good. For the square pulse the data for $2\ E/N_o$ greater than 210 was not used in computing a value for K. In this region, the differences between the theoretical and experimental curves become increasingly greater. This is because the low power level of the discrete signal component at the bandpass filter makes the phase error measurements very difficult to make accurately.

6.3 Verification of the Model

It was shown in the last section that it was possible to compute a single signal to noise ratio parameter, R_d, which will predict the performance of the suboptimum synchronizer. Two aspects of the model remain to be experimentally verified.

First, it is assumed in the model that the noise power is directly proportional to the noise equivalent bandwidth of the bandpass filter. This means that the value of R_M is inversely proportional to the bandwidth of the bandpass filter. The three normalized bandwidths that were used were $\Delta f = .028$, $\Delta f = .039$, and $\Delta f = .056$. Under the

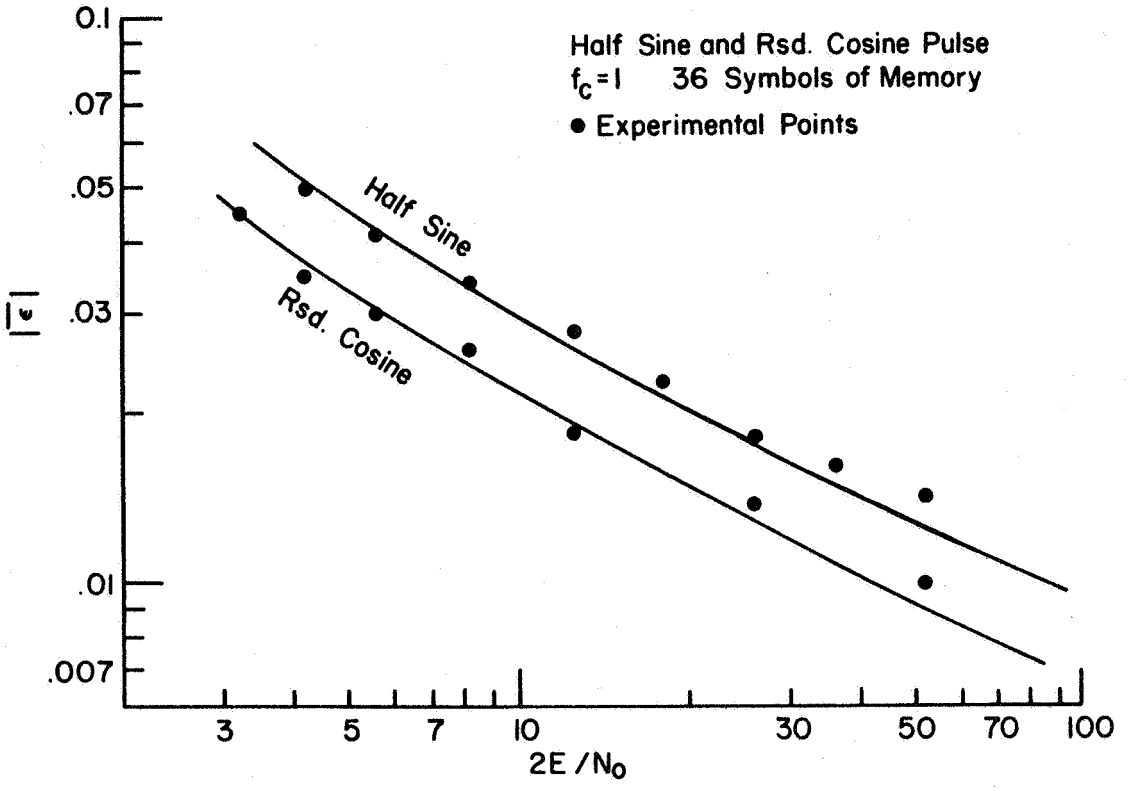

Fig. 6.9 Comparison of Theoretical and Experimental Models for Half Sine and Raised Cosine Symbols

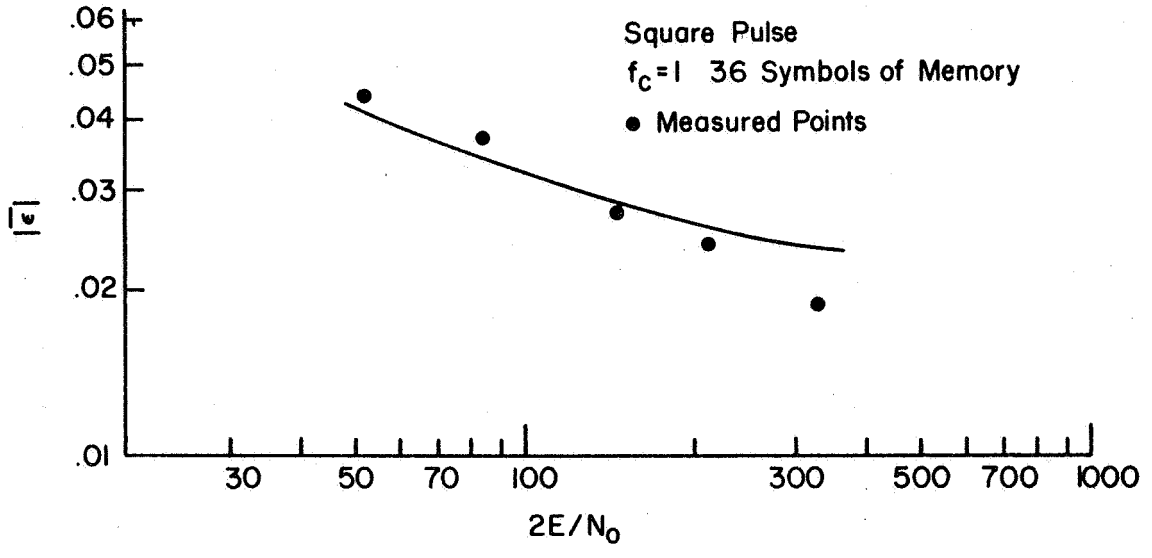

Fig. 6.10 Comparison of Theoretical and Experimental Models for Square Pulse Symbols

assumption that $|\bar{\epsilon}| = .09/\sqrt{R_M}$ (see Appendix B) so that $|\bar{\epsilon}|$ is directly proportional to $\sqrt{\Delta f}$, the experimentally determined values of $|\bar{\epsilon}|$ for $\Delta f = .028$ and $\Delta f = .056$ were adjusted to the values that they would have at $\Delta f = .039$. Fig. 6.11, 6.12, and 6.13 show the results of this. The solid lines indicate the upper and lower limits of the accuracy of the mean of the three values. These limits were determined from the experimenter's observations of the repeatability attained in the measurement system. If the bandwidth assumption is true, all three points for a given value of $2\ E/N_o$ will be coincident. These results, as shown in the figures, indicate that the prototype system signal to noise ratio at the bandpass filter output is inversely proportional to the bandwidth of the filter as assumed in the theoretical model.

Second, the model as completed in 6.3 was for only one low pass filter cutoff frequency. Whether or not the model predicts the response for other cutoff frequencies remains to be shown. That the model does do this is shown in the following way. Fig. 6.14, 6.15, and 6.16 show the graph of $|\bar{\epsilon}|$ vs. $2\ E/N_o$ for various values of filter cutoff frequency for the half sine, raised cosine, and square pulses. The performance is plotted over a greater range of $2\ E/N_o$ than was attainable by experiment in order to show the asymptotic limits of performance. In Fig. 6.17, 6.18, 6.19, and 6.20, the experimental curves of the performance as a function of $2\ E/N_o$ are presented. A close comparison of these two sets of curves indicates that, within the limits of the experimental accuracy, there is nothing to indicate a disagreement between the measured results and the results predicted by the model. Some question might be raised concerning the results with the square

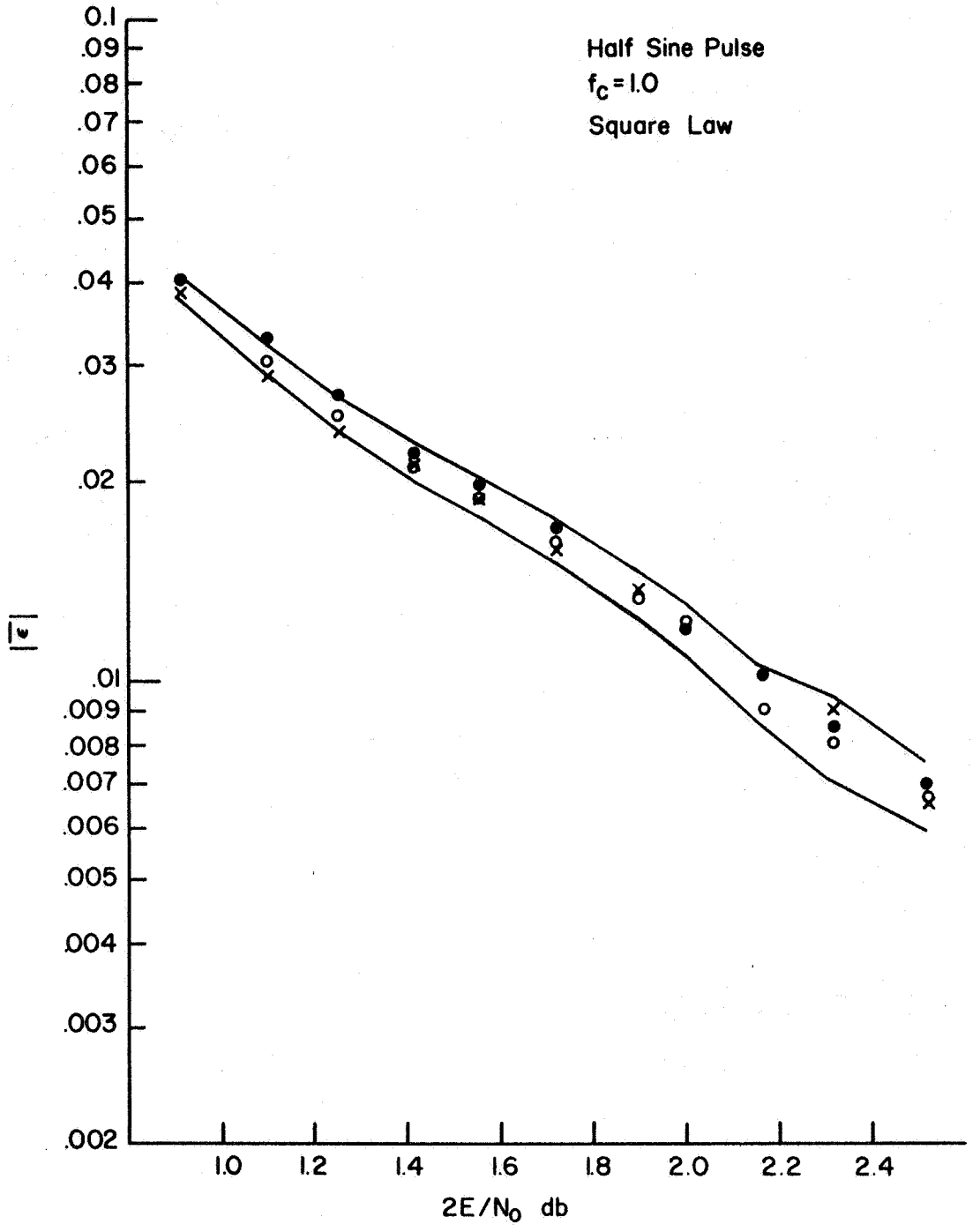

Fig. 6.11 $|\bar{\epsilon}|$ vs. $2E/N_0$ for 3 Narrowband Filters with Half Sine Symbols and Square Law Nonlinearity

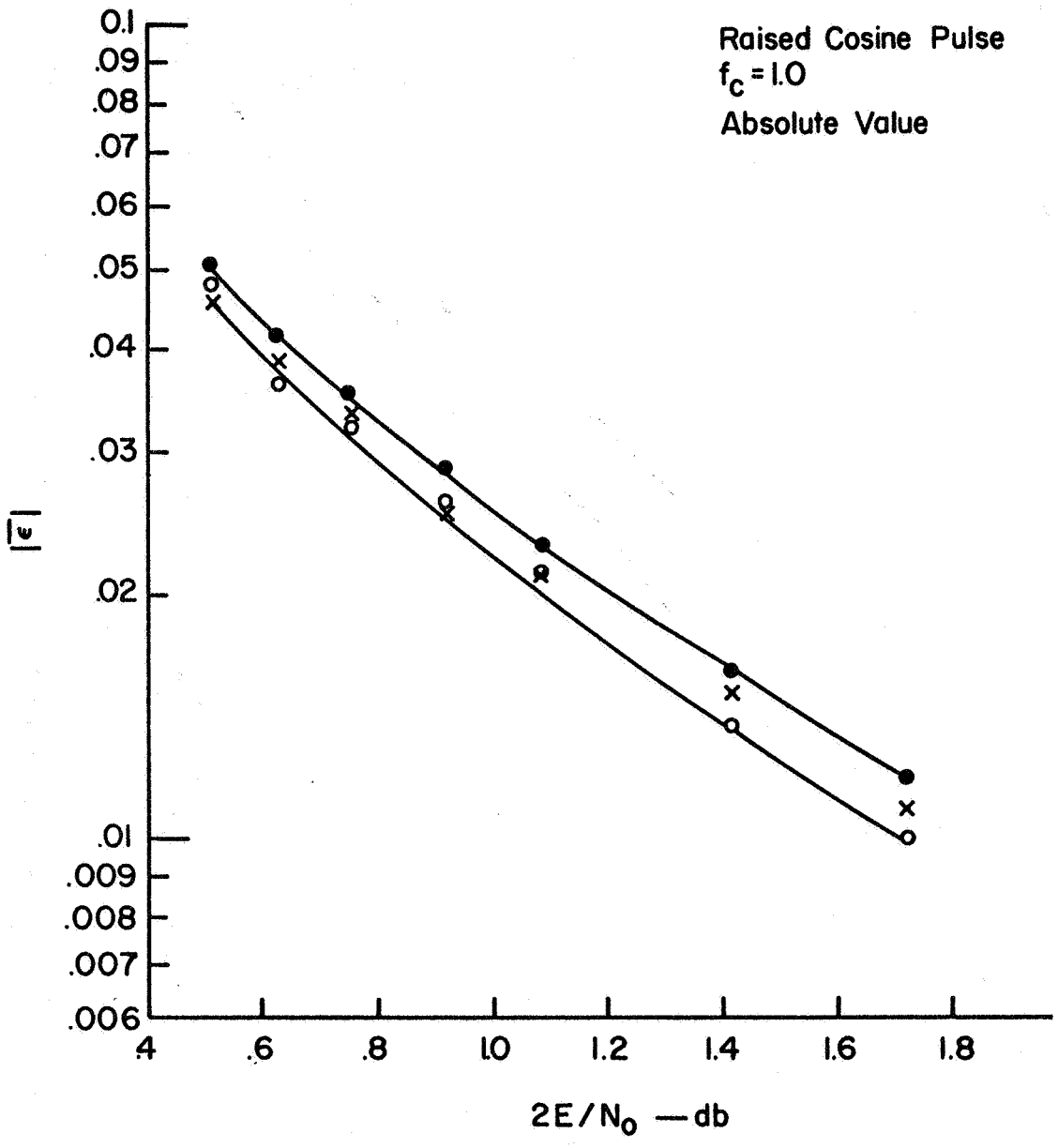

Fig. 6.12 $|\bar{\epsilon}|$ vs. $2E/N_o$ for 3 Narrowband Filters with Raised Cosine Symbols and Absolute Value Nonlinearity

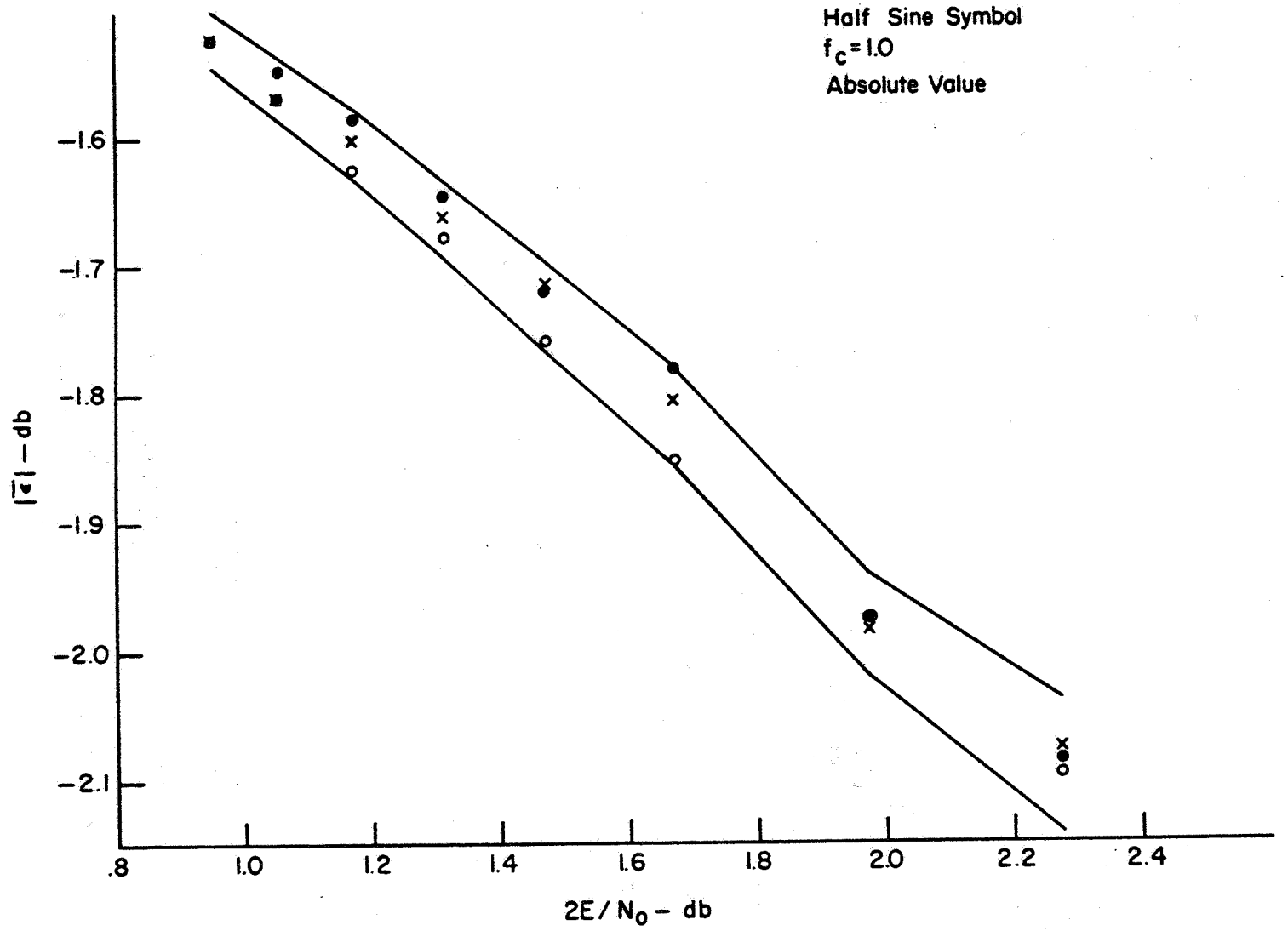

Fig. 6.13 $|\bar{\epsilon}|$ vs. $2E/N_o$ for 3 Narrowband Filters with Half Sine Symbols and Absolute Value Nonlinearity

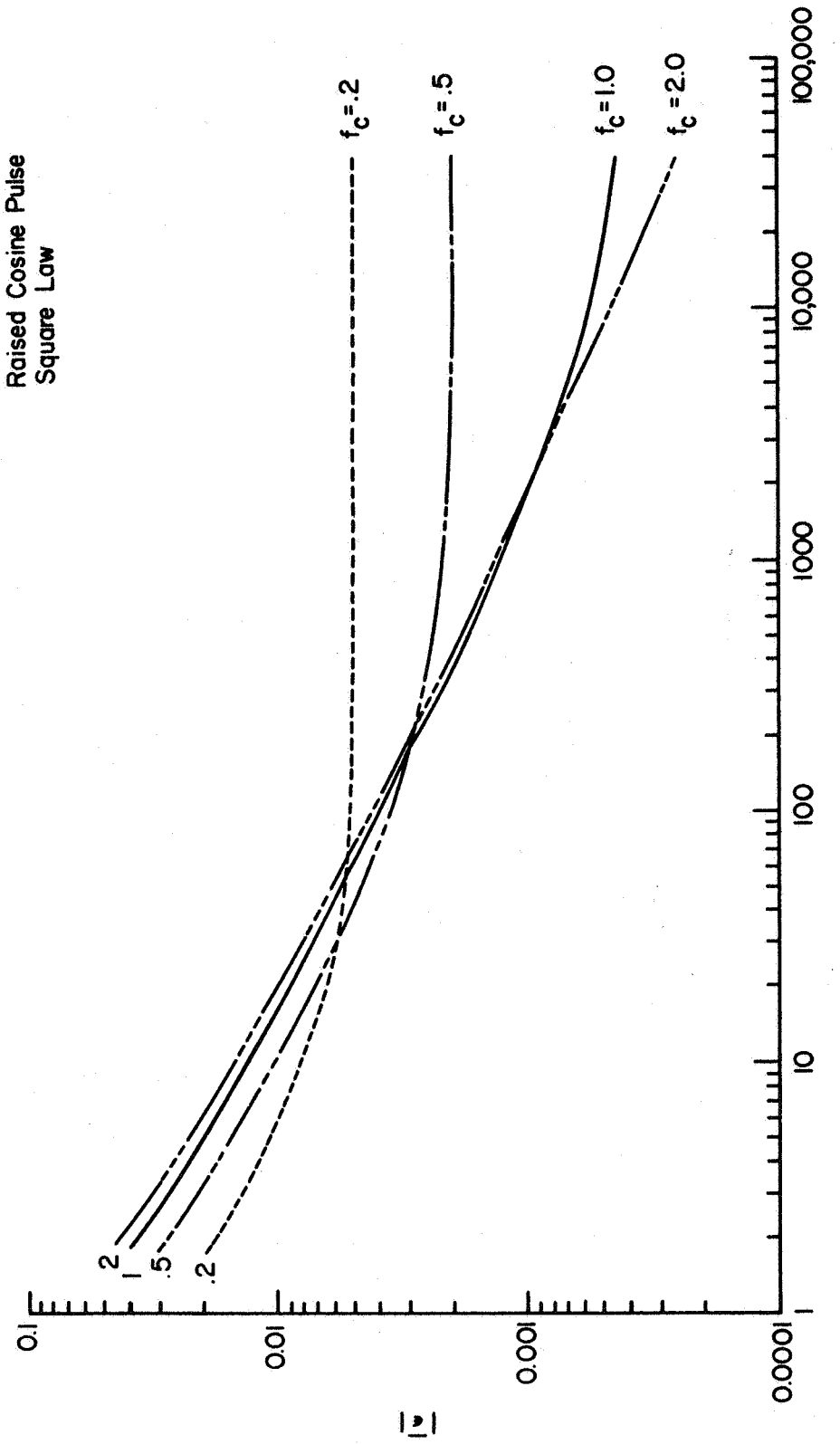

Fig. 6.14 $\overline{|\epsilon|}$ vs. $2E/N_o$ for Raised Cosine Symbols from Theoretical Model

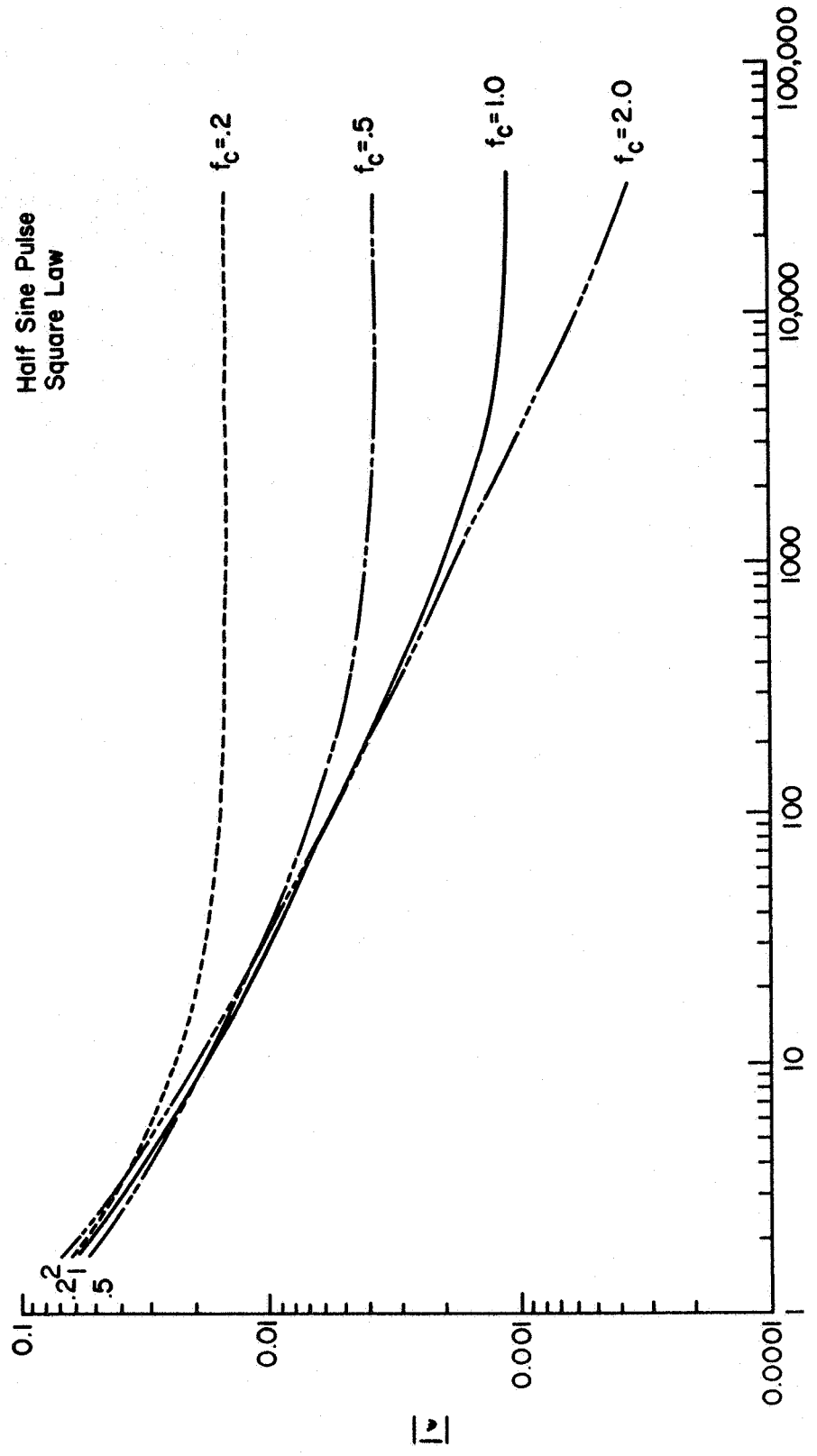

Fig. 6.15 $|\bar{\epsilon}|$ vs. $2E/N_o$ for Half Sine Symbols from Theoretical Model

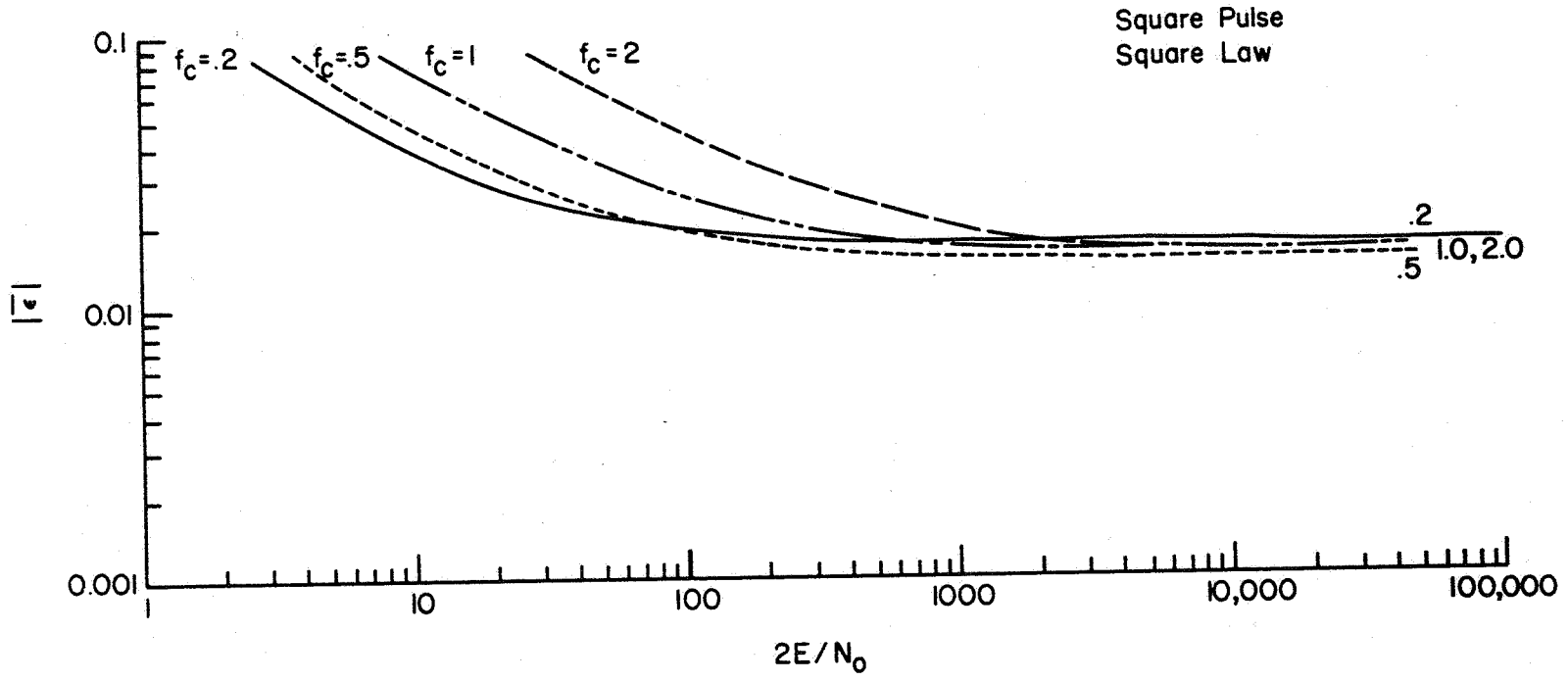

Fig. 6.16 $|\bar{\epsilon}|$ vs. $2E/N_o$ for Square Symbols from Theoretical Model

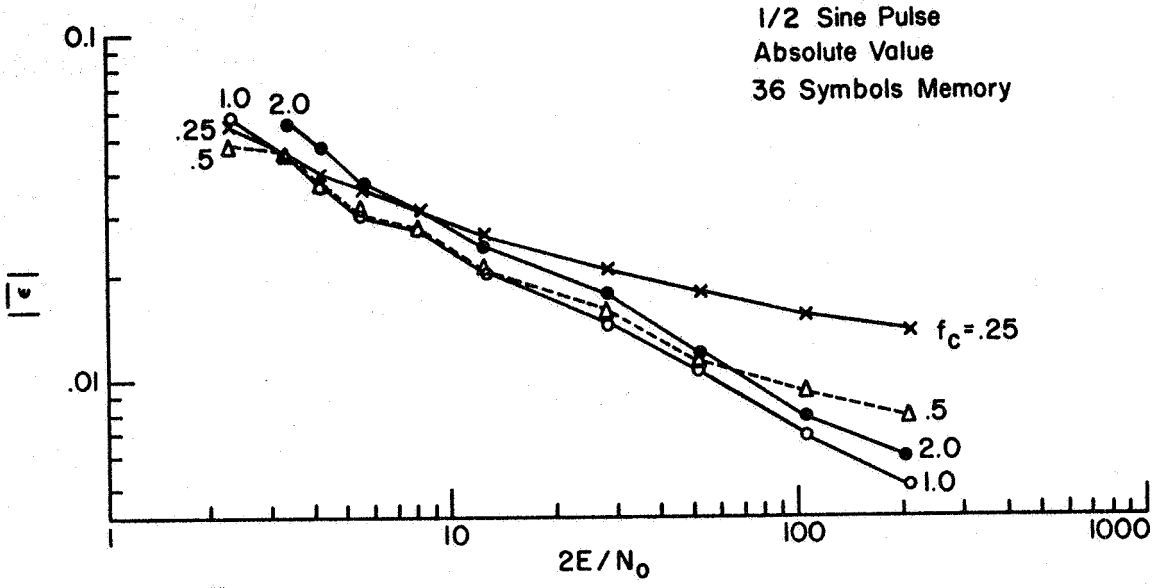

Fig. 6.17 $|\bar{\epsilon}|$ vs. $2E/N_o$ from Experiment for Half Sine Symbol and Absolute Value Nonlinearity

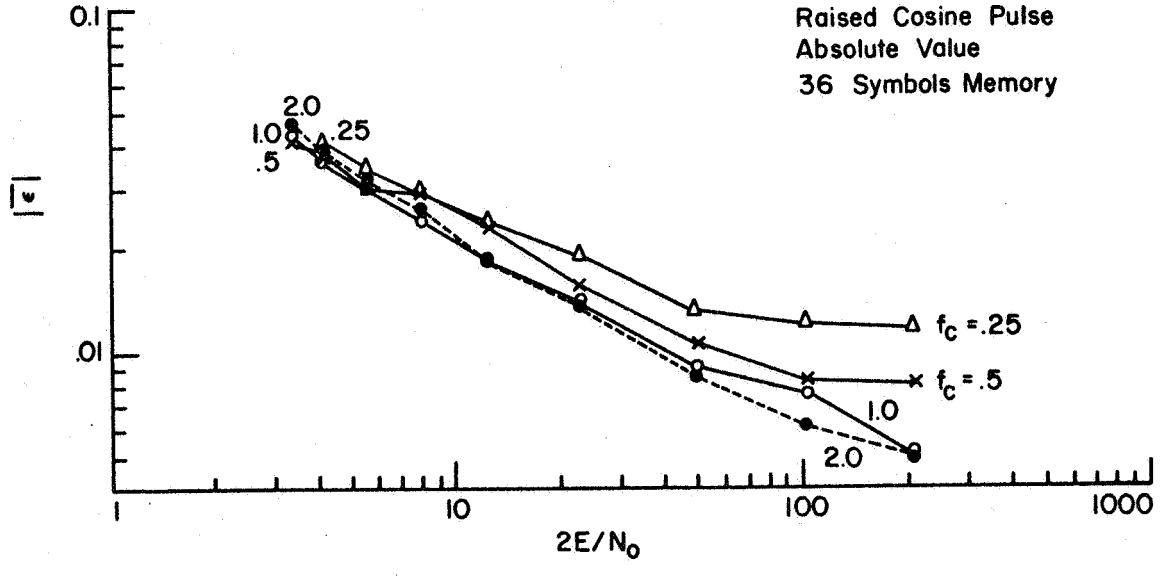

Fig. 6.18 $|\bar{\epsilon}|$ vs. $2E/N_o$ from Experiment for Raised Cosine Symbol and Absolute Value Nonlinearity

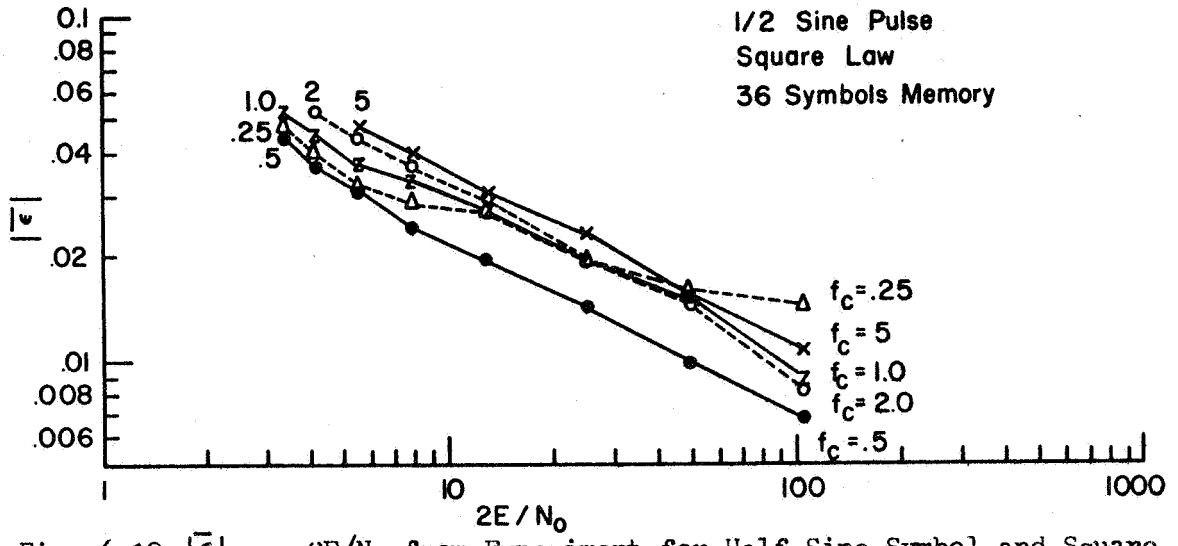

Fig. 6.19 $|\bar{\epsilon}|$ vs. $2E/N_o$ from Experiment for Half Sine Symbol and Square Law Nonlinearity

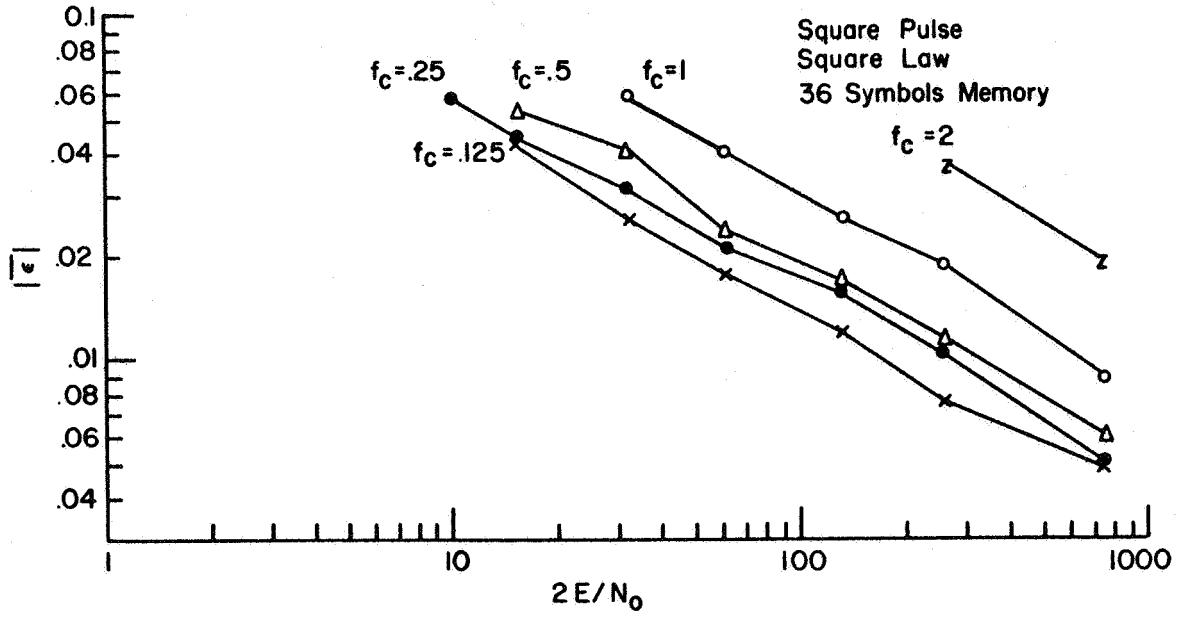

Fig. 6.20 $|\bar{\epsilon}|$ vs. $2E/N_o$ from Experiment for Square Symbol and Square Law Nonlinearity

pulse, since the model shows all bandwidths producing the same performance at high values of $2\ E/N_o$, while the experimental data does not show this. Again, it is pointed out that there was extreme difficulty in measuring the performance with the square pulse at high value of $2\ E/N_o$ so that the data in this range is somewhat suspect.

Two of the sets of curves are for an absolute value instead of square law nonlinearity. It is shown in the next section that there is no significant difference in performance with these two nonlinearities.

6.4 Effect of Nonlinearity

The nonlinear operation that is assumed in the analytical solution is a square law operation. This is necessary if a direct solution for the noise power spectrum at the output of the nonlinearity is to be made. The question remains, however, whether the square law is the best nonlinearity. Obviously any even function characteristic, $e_o = (e_i)^a$ is useable. Values of $a = 1/2$ and 1 as well as the square law, $a = 2$, were used and the results are presented in Fig. 6.21 - 6.25. While it appears that there were slight differences with different wave shapes, the best conclusion that can be made is that the type of nonlinearity does not make a significant difference. The model of Eq. 3.29 can be used with equal success with an absolute value of square root nonlinearity. This result is useful since the absolute value nonlinearity is much more easily implemented in practice. Remember also that the optimum solution called for a log cosh operation which is square law at low signal to noise ratios and absolute value at high ratios.

Many self synchronizers now in use are built with a nonlinearity which is constructed of a hard limiter, or infinite clipper, followed

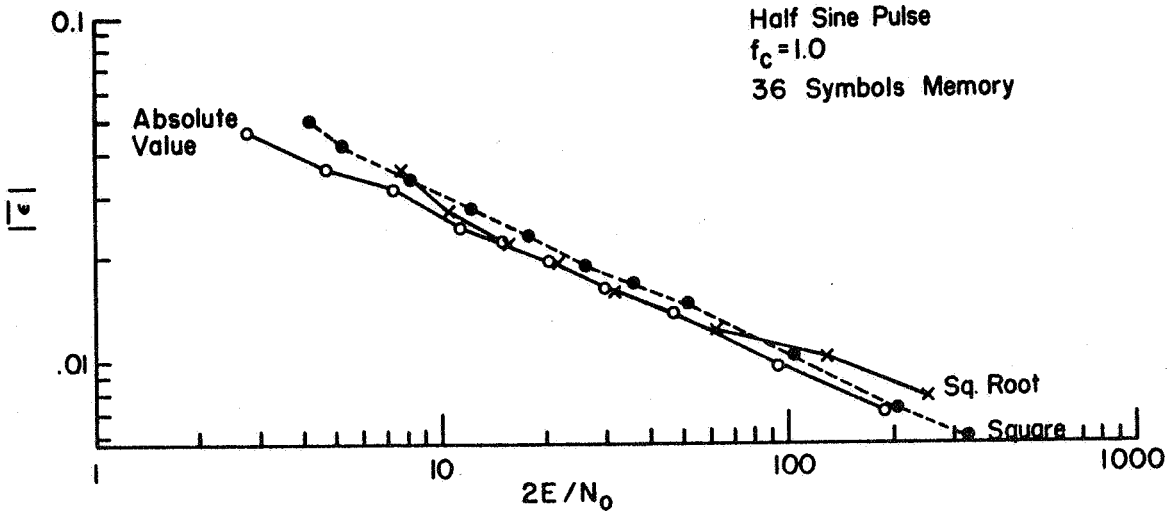

Fig. 6.21 Three Nonlinearities Compared with Half Sine Symbol $f_c = 1.0$

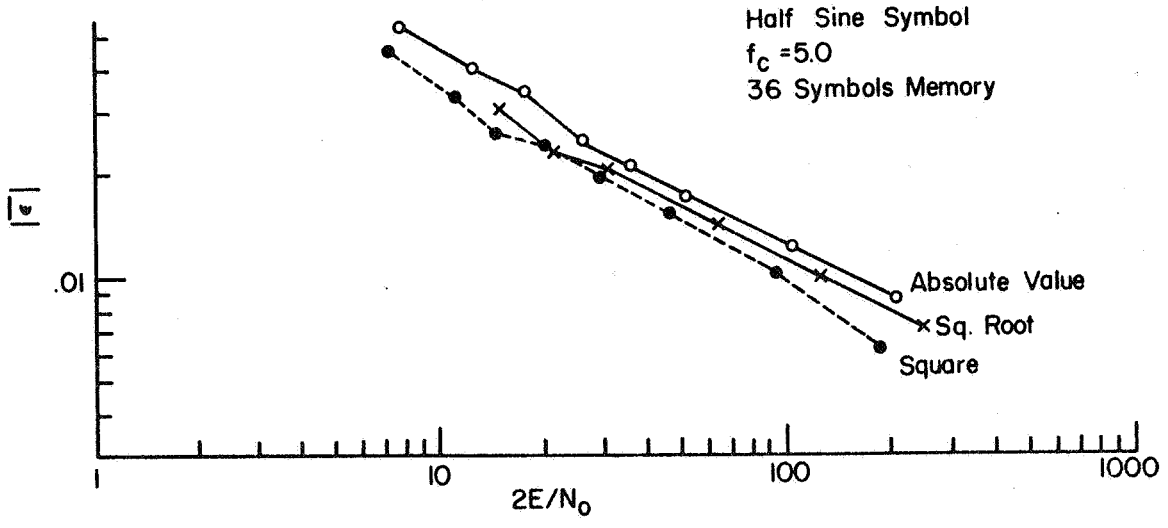

Fig. 6.22 Three Nonlinearities Compared with Half Sine Symbol and $f_c = 5.0$

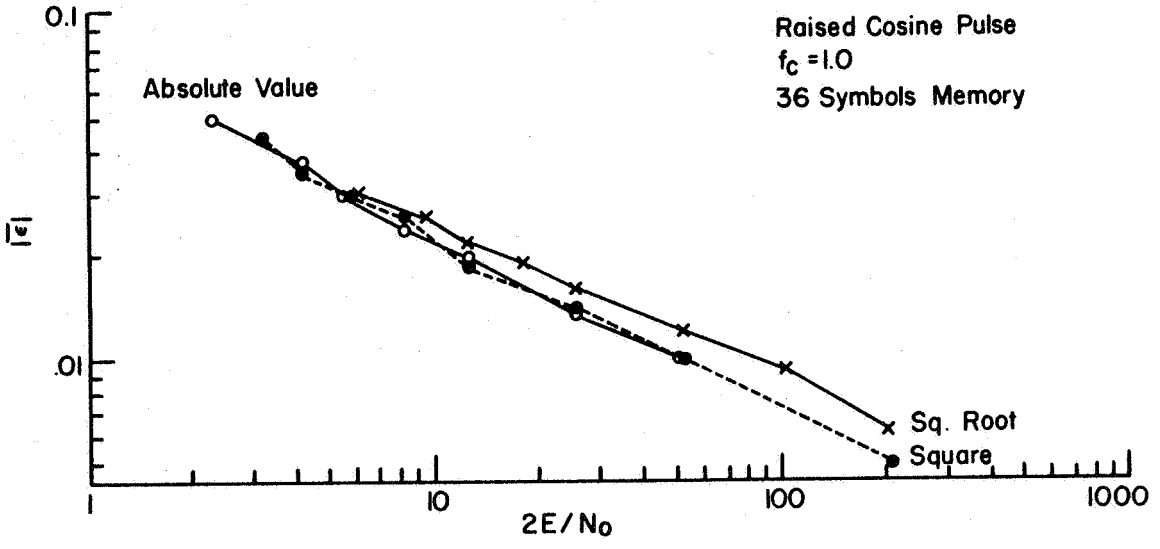

Fig. 6.23 Three Nonlinearities Compared with Raised Cosine Symbol and $f_c = 1$

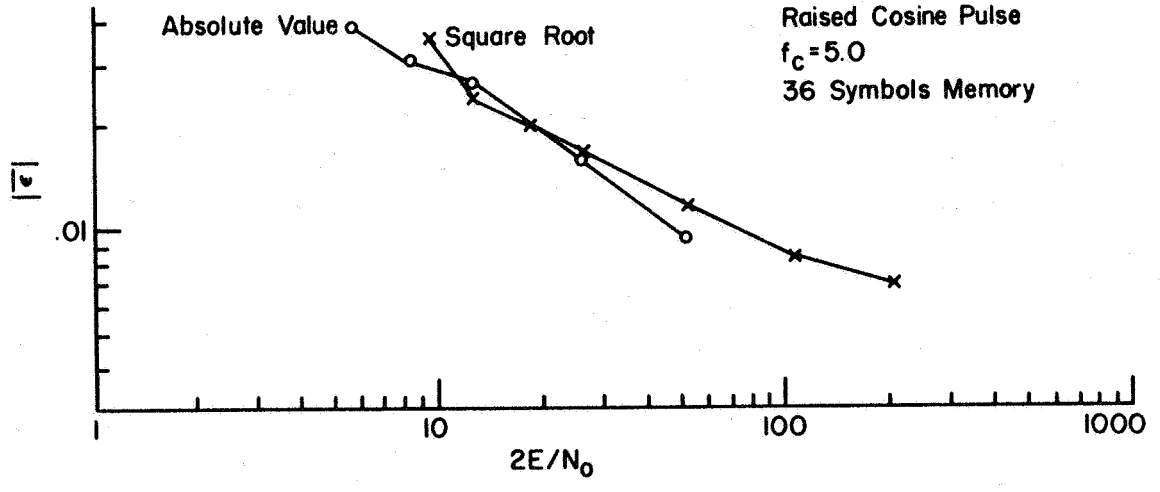

Fig. 6.24 Three Nonlinearities Compared with Raised Cosine Symbol and $f_c = 5.0$

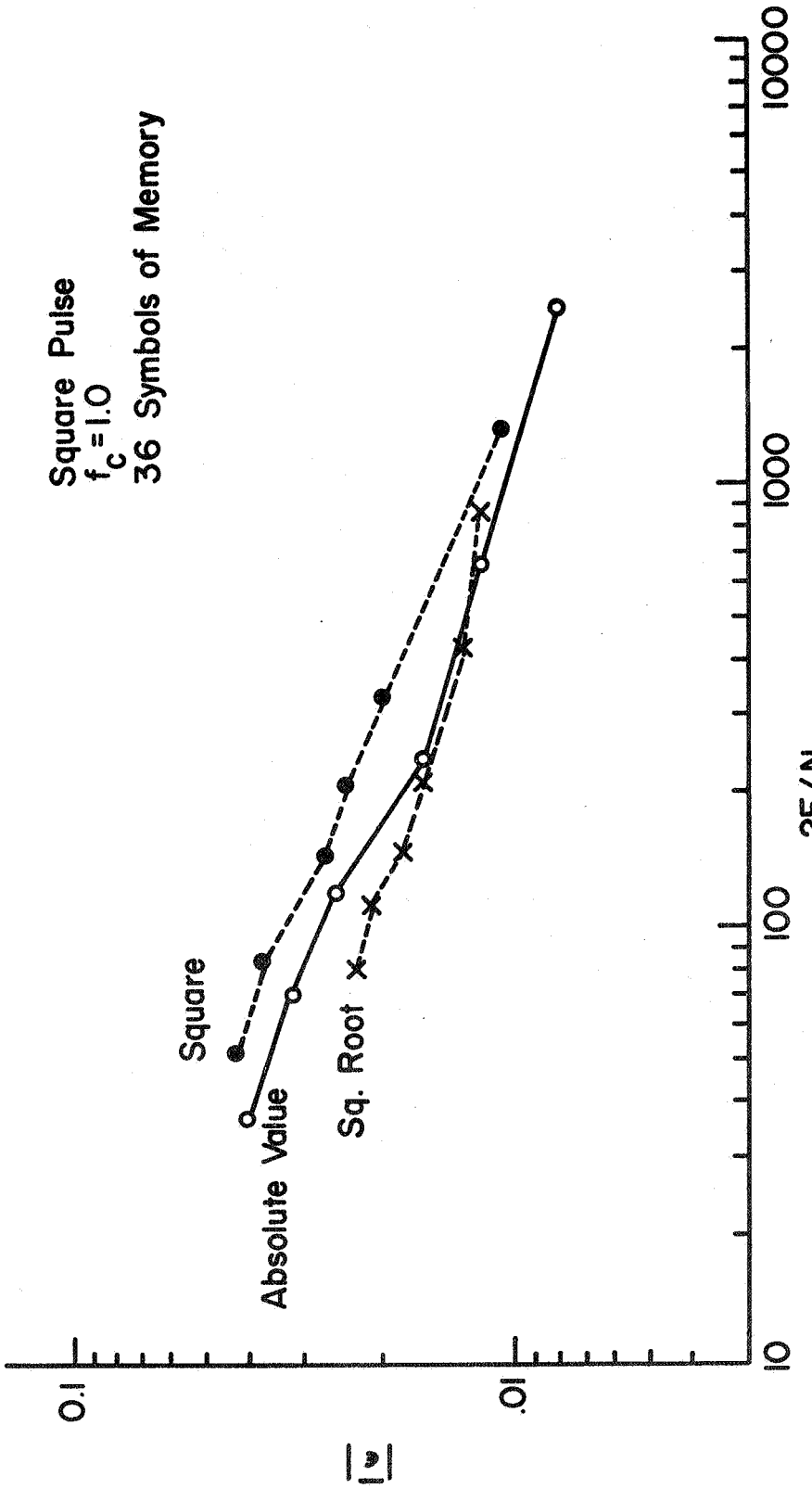

Fig. 6.25 Three Nonlinearities Compared with Square Symbol and $f_c = 1.0$

by a differentiator and a full wave rectifier. Under zero noise conditions the output of the differentiator will be a series of spikes which occur when symbol transitions take place. With additive noise, extraneous spikes are added. Such a nonlinearity was used in the experimental setup in place of the even function type nonlinearity. The results for two of the three wave shapes are plotted in Fig. 6.26 and compared with the results for an absolute value nonlinearity. As can be seen from the curves, for square pulses the infinite clipper or hard limiter performs somewhat better than the absolute value circuit. However, for all but the very low signal to noise ratios the absolute value circuit performs better than the hard limiter for the other wave shapes. It appears that by extrapolating the curves to very low values of signal to noise ratio, the performance for the two nonlinearities is about the same. The most significant conclusion that can be drawn is that even with this completely different nonlinearity the performance is more heavily dependent on wave shape than on nonlinearity.

6.5 Input Filter Bandwidth

The roll of the input filter in the performance of the suboptimum synchronizer is graphically presented in Fig. 6.14, 6.15, and 6.16. In these graphs, $|\bar{\epsilon}|$ vs. $2\ E/N_o$ is plotted as function of cutoff frequency.

Consider first Fig. 6.14 and 6.15 which show the results for the half sine and raised cosine pulses. Two significant observations can be made. First, at the low values of $2\ E/N_o$ the filter cutoff frequency is not a large factor in the operation. For the half sine symbol, the optimum value of cutoff frequency is between .5 and 1.0. Other choices

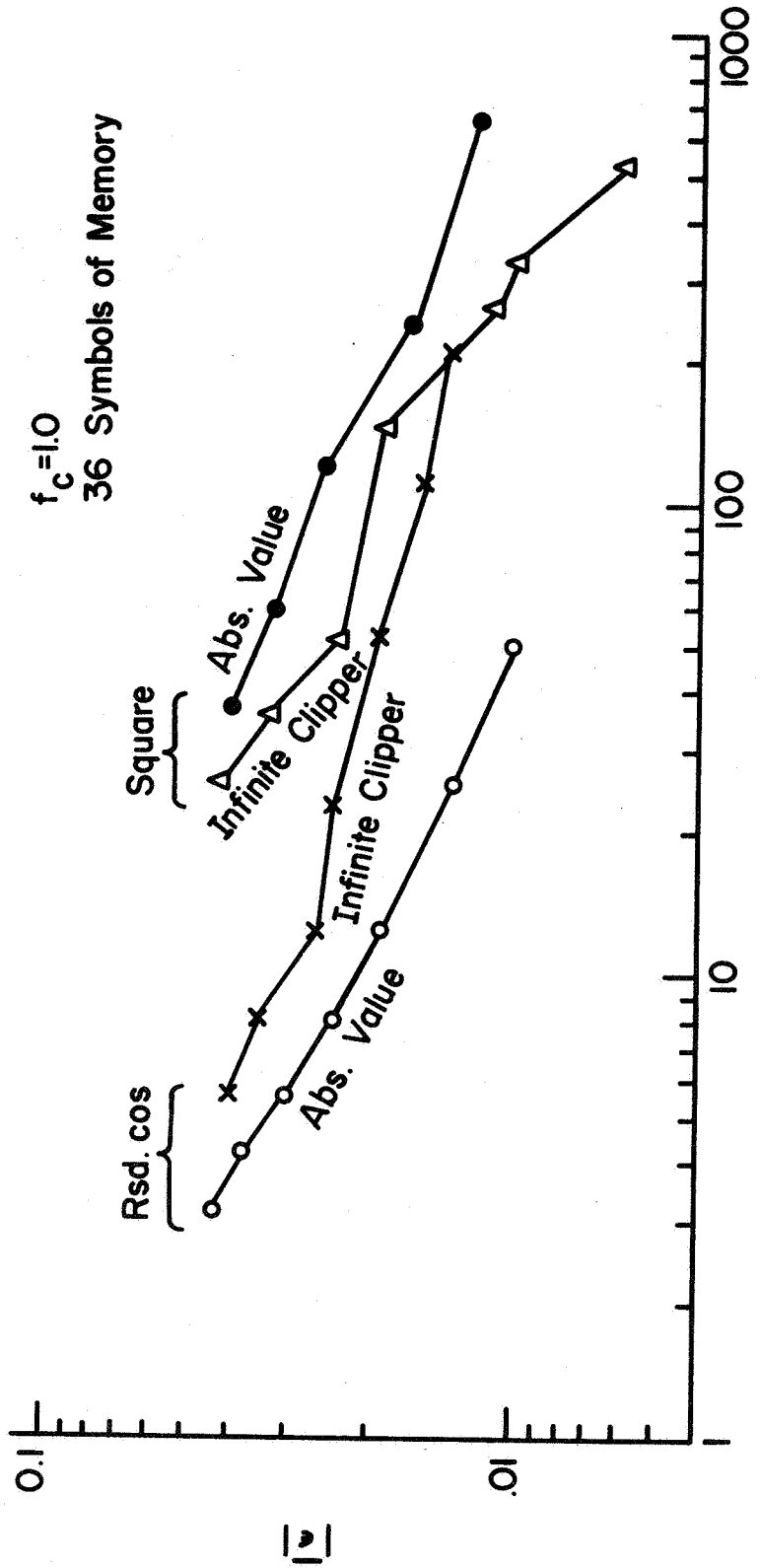

Fig. 6.26 Comparison of Absolute Value and Infinite Clipper Nonlinearities

around these values cause only a few percent degradation in $|\bar{\epsilon}|$. For the raised cosine, it appears that a cutoff frequency of .2 is best for very low values of $2\ E/N_o$. However, as $2\ E/N_o$ is raised, the performance with $f_c = .2$ and .5 is badly degraded compared to operation at higher cutoff frequencies. For a system that may operate over a range of values of $2\ E/N_o$, a compromise value of $f_c = 1.0$ appears to be more desirable.

The second observation is that these curves show a minimum value for $|\bar{\epsilon}|$ as $2\ E/N_o$ approaches infinity. This is due to the noise generated by the filtering of the random signal process. As the value of f_c is reduced, this noise increases. Hence low cutoff frequencies are not desirable for systems that operate with high values of $2\ E/N_o$.

The results for the square pulse case, Fig. 6.16, are somewhat different. Here performance at low values of $2\ E/N_o$ is progressively improved by reducing the cutoff frequency. For all values of f_c, the model predicts the same performance at high values of $2\ E/N_o$. There is, however, a practical problem in reducing f_c to a very low value. As f_c is reduced, the amplitude of the filtered signal component that is to be applied to the nonlinear filter is reduced to a very small value and it becomes very hard to maintain a workable D.C. system at these very low levels. It may be very difficult to design a synchronizer to take advantage of the improvement offered by very hard filtering.

6.6 The Function of Wave Shape

The suboptimum model was solved for three pulse wave shapes; the half sine, raised cosine, and square. In addition to these three, the prototype synchronizer was also tested with a sawtooth pulse. The results for comparing pulse wave shapes using an absolute value for the nonlinearity and a low pass cutoff of 1.0 are shown in Fig. 6.27 and 6.28. The obvious conclusion is that raised cosine pulses offer the best performance. The preference for the raised cosine pulse is even better if, in the light of the discussion of Sec. 6.5, the cutoff frequency of the input filter is reduced to .5. For the square pulse, even the improvement in $|\overline{\epsilon}|$ for $f_c = .2$ to .5 is not sufficient to put square pulses on a competitive level with either half sine or raised cosine pulses.

Fig. 6.29 presents the data comparing pulse shapes with the infinite clipper nonlinearity. Here again, the raised cosine and half sine perform about equally well and the square pulse somewhat worse at low values of $2\ E/N_o$. At higher values of $2\ E/N_o$ all three wave shapes result in about the same performance.

In summary, it can be concluded that, using $|\overline{\epsilon}|$ as a measure of performance, the best pulse shape to use is the raised cosine. The half sine produces a slight degradation, and depending on the input filter cutoff frequency and nonlinearity, the square pulse results in a more serious degradation--up to a factor of 3 in $|\overline{\epsilon}|$.

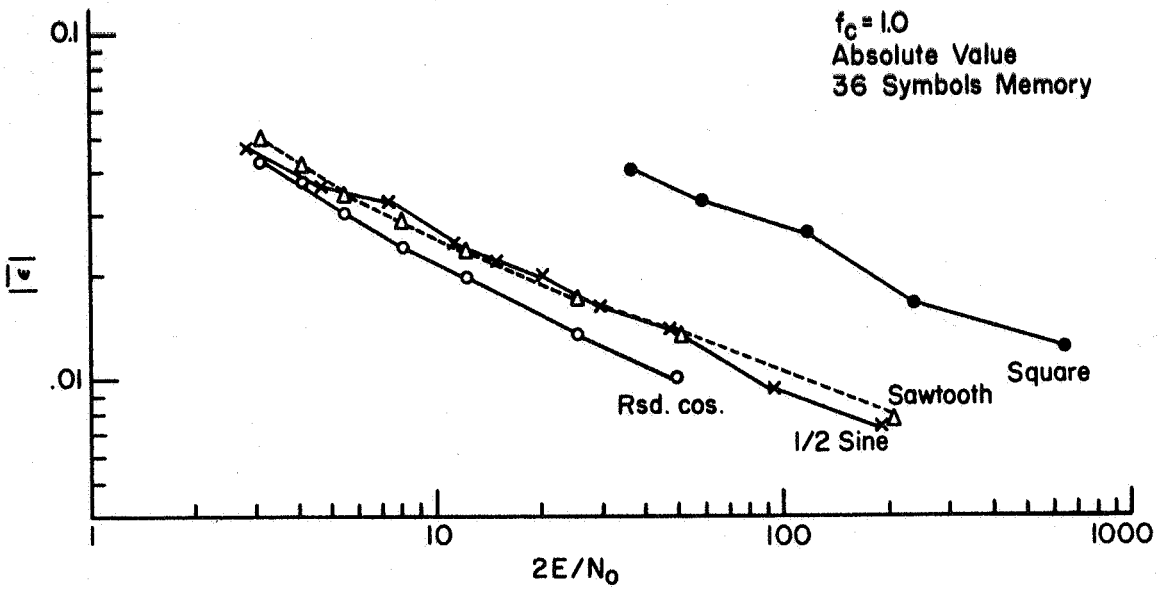

Fig. 6.27 Comparison of Symbols with Absolute Value Nonlinearity and 36 Memory Periods

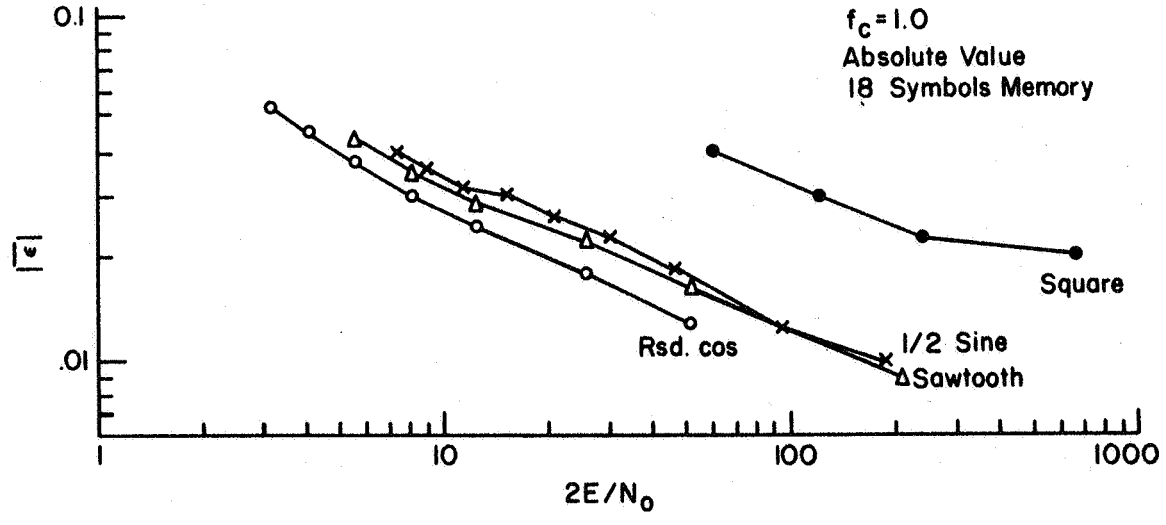

Fig. 6.28 Comparison of Symbols with Absolute Value Nonlinearity and 18 Memory Periods

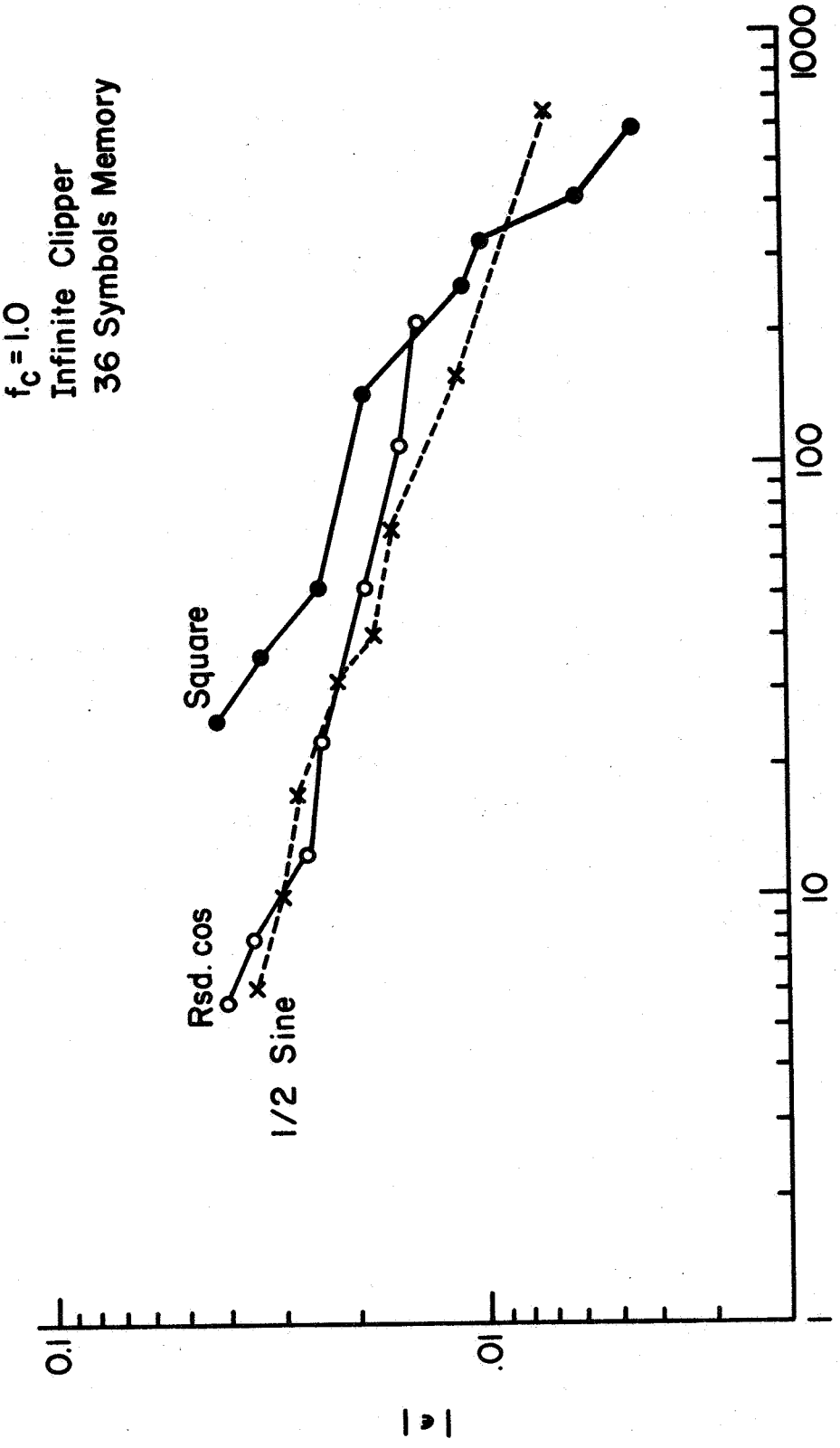

Fig. 6.29 Comparison of Symbols with Infinite Clipper Nonlinearity

6.7 Suboptimum Synchronizer Used with a Correlation Detector

The performance of a correlation detector when it is synchronized with the suboptimum system is shown in Fig. 6.30 and 6.31. In order to compute these curves, the results of Chapter IV were used. There, curves were derived for the degradation of $2\ E/N_o$ vs. $|\bar{\epsilon}|$ for given values of $2\ E/N_o$. For a given minimum value of degradation, these curves supply the corresponding maximum value of $|\bar{\epsilon}|$ for each of the wave shapes at several different values of $2\ E/N_o$. Either the model or the results of the experiments may be used to compute the required value of bandwidth of the bandpass filter necessary to produce this value of $|\bar{\epsilon}|$.

The equivalent memory time is defined in the following way. A single pole bandpass filter has an impulse response which decays exponentially with a time constant $1/\alpha = 2/\Delta\omega = 1/2\Delta f_{neb}$ where Δf_{neb} has been normalized to a center frequency of 1. Hence, each successive cycle, i, of the response is weighted by the factor $C_i = \exp(-i2\Delta f_{neb})$. For cases of varied weighting into the past, a commonly used equivalent memory or measurement time, in symbol periods, is

$$\gamma = \left(\sum_{i=1}^{\infty} C_i\right)^2 \Big/ \sum_{i=1}^{\infty} C_i^2 \qquad 6.1$$

Using this for a bandpass filter results in

$$\gamma = (1+\exp[-2\Delta f_{neb}])/(1-\exp[-2\Delta f_{neb}]) \qquad 6.2$$

If $2\Delta f_{neb} \leq .5$, this can be approximated by $1/\Delta f_{neb}$ with less than 1% error. Hence, memory time is inversely proportional to bandwidth for

all but the shortest memory times. The curves of Fig. 6.30 and 6.31 were computed on the basis that this relationship holds for all the bandwidths.

Fig. 6.30 shows the results for the suboptimum system using the even function nonlinearity. Here, it is seen that the degradation using this measure of performance for square pulses is much more severe than using $|\overline{\epsilon}|$ as the performance measure. This is due to the fact, as shown in Chapter IV, that correlation detectors are more sensitive to errors when signaling is with square pulses. Also, it is seen that the apparent superiority of the raised cosine pulse over the half sine is reduced and even reversed at low value of $2\ E/N_o$. Again, the reason is that the half sine pulse is less sensitive to synchronizer error at the correlator. Fig. 6.31 shows the results for the infinite clipper nonlinearity. They are very similar to those of Fig. 6.30.

Perhaps the most interesting conclusion that can be drawn from these curves is that the price paid in equivalent memory time becomes exceedingly high as degradation is reduced toward zero. A "knee" exists in all of the curves in the region of .05 to .1 db degradation. Increases in memory time in the range of 0 to .05 db buy very little in improved performance. On the other hand, for degradation greater than .05, small increases in memory time bring great improvement in performance.

6.8 Comparison of Optimum and Suboptimum Synchronizers

How good are the suboptimum synchronizers? Fig. 6.32 and 6.33 compare the optimum and even function nonlinearity suboptimum synchronizer on the basis of memory time vs. degradation of $2\ E/N_o$. The low pass cutoff for all the suboptimum systems is $f_c = 1$. For half sine and raised

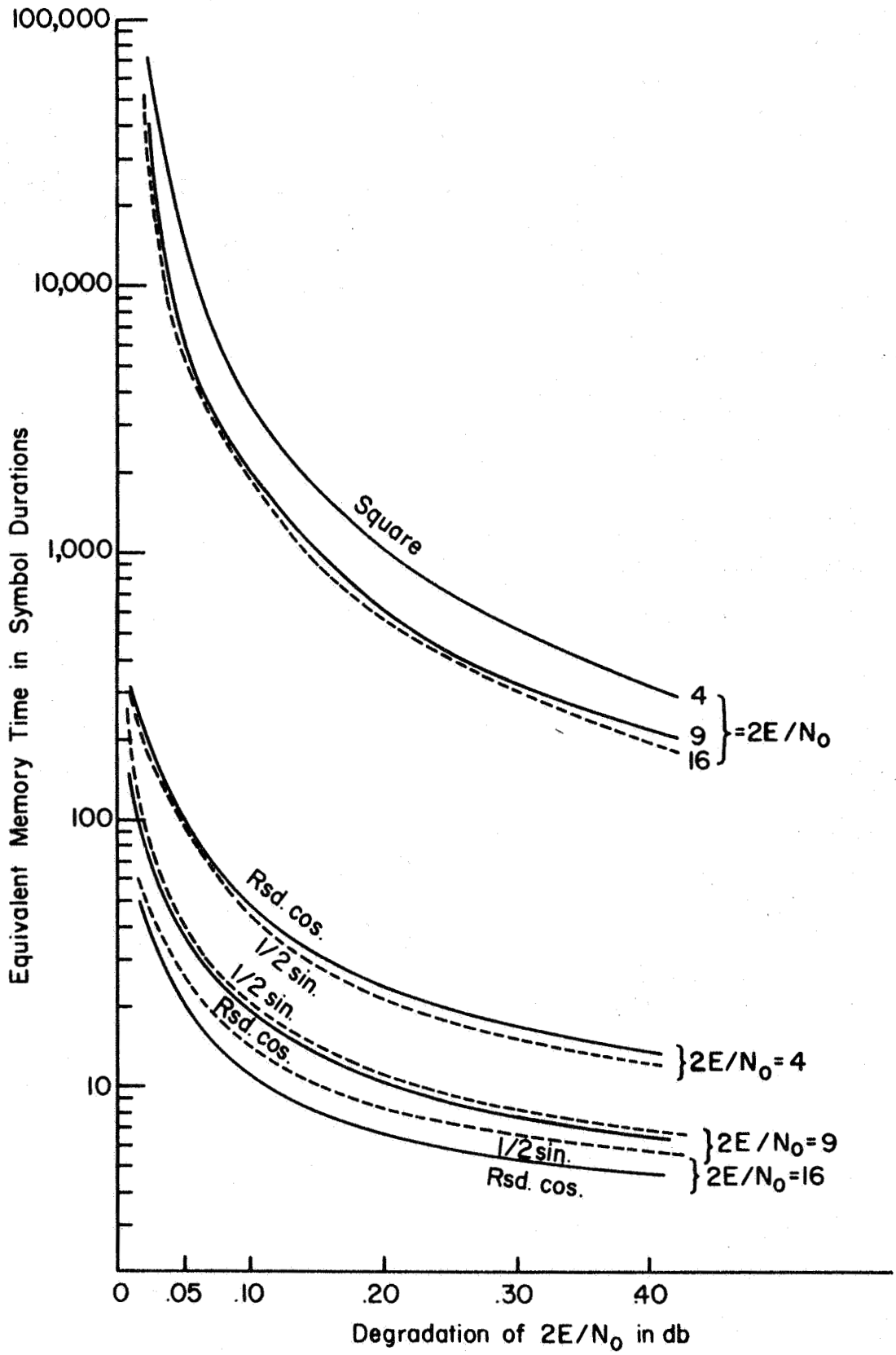

Fig. 6.30 Memory vs. Degradation for Suboptimum Synchronizer

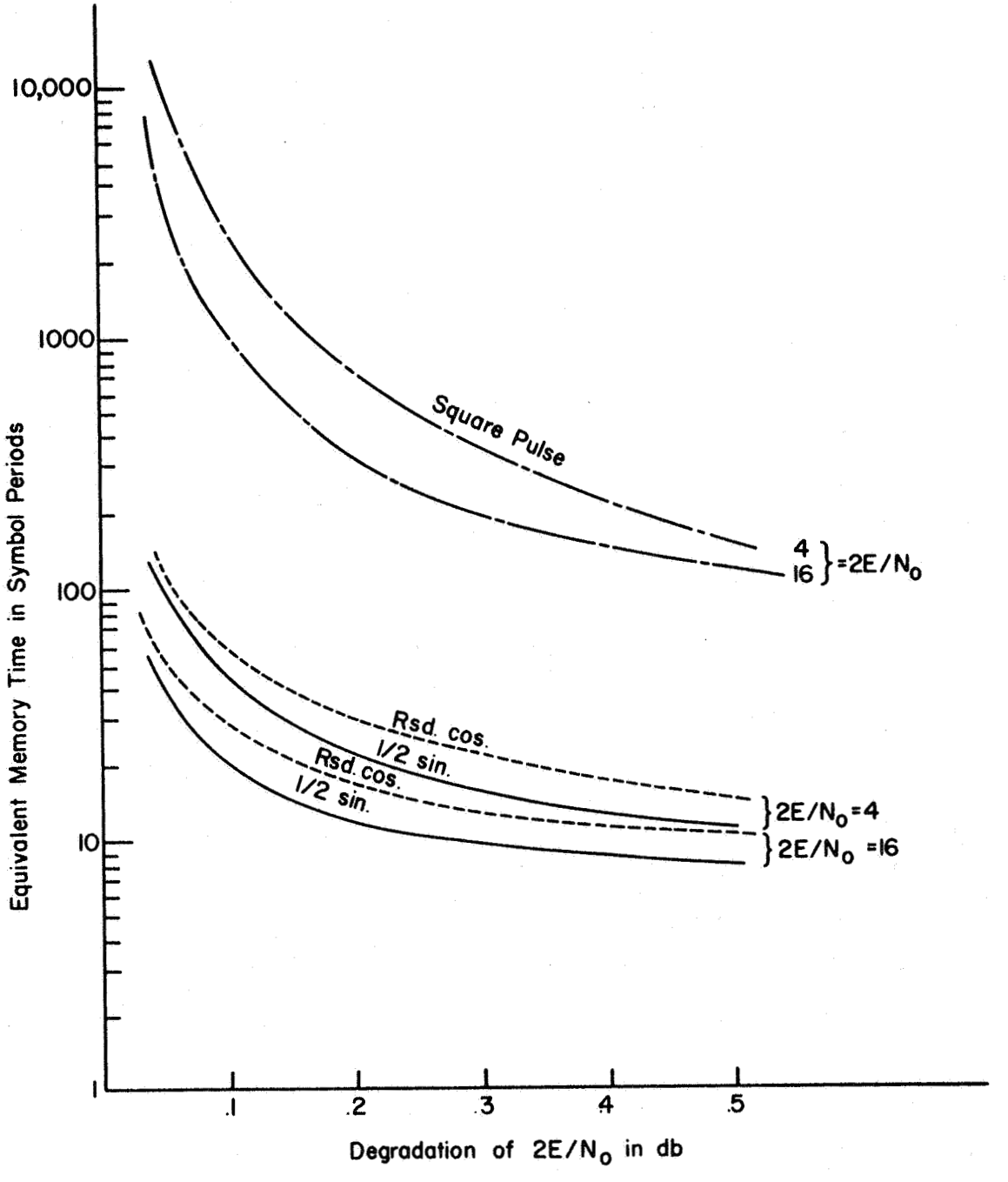

Fig. 6.31 Memory vs. Degradation for Suboptimum Synchronizer with Infinite Clipper Nonlinearity

cosine pulses, the suboptimum system is worse than the optimum by a factor of 2.5 in memory time. For the square pulse, the degradation is a factor of 15. The optimum and suboptimum are farther apart for the square pulse because the optimum synchronizer makes timing errors, as measured by $|\bar{\epsilon}|$, about the same as for other pulses, while the suboptimum performance, as measured by $|\epsilon|$, is considerably worse for square pulses.

Considering the simplicity of the suboptimum synchronizers, performance as compared to the optimum is quite favorable and no effort is warranted in trying to find a better self synchronizer.

The series of curves Fig. 6.34 - 6.39 compare the performance of the three synchronizers for values of $2\ E/N_o$ of 4 and 16. For half sine and raised cosine pulses, the even function nonlinearity is always equal to, or superior to, the infinite clipper nonlinearity. For the square pulse, there is a slight advantage to the infinite clipper.

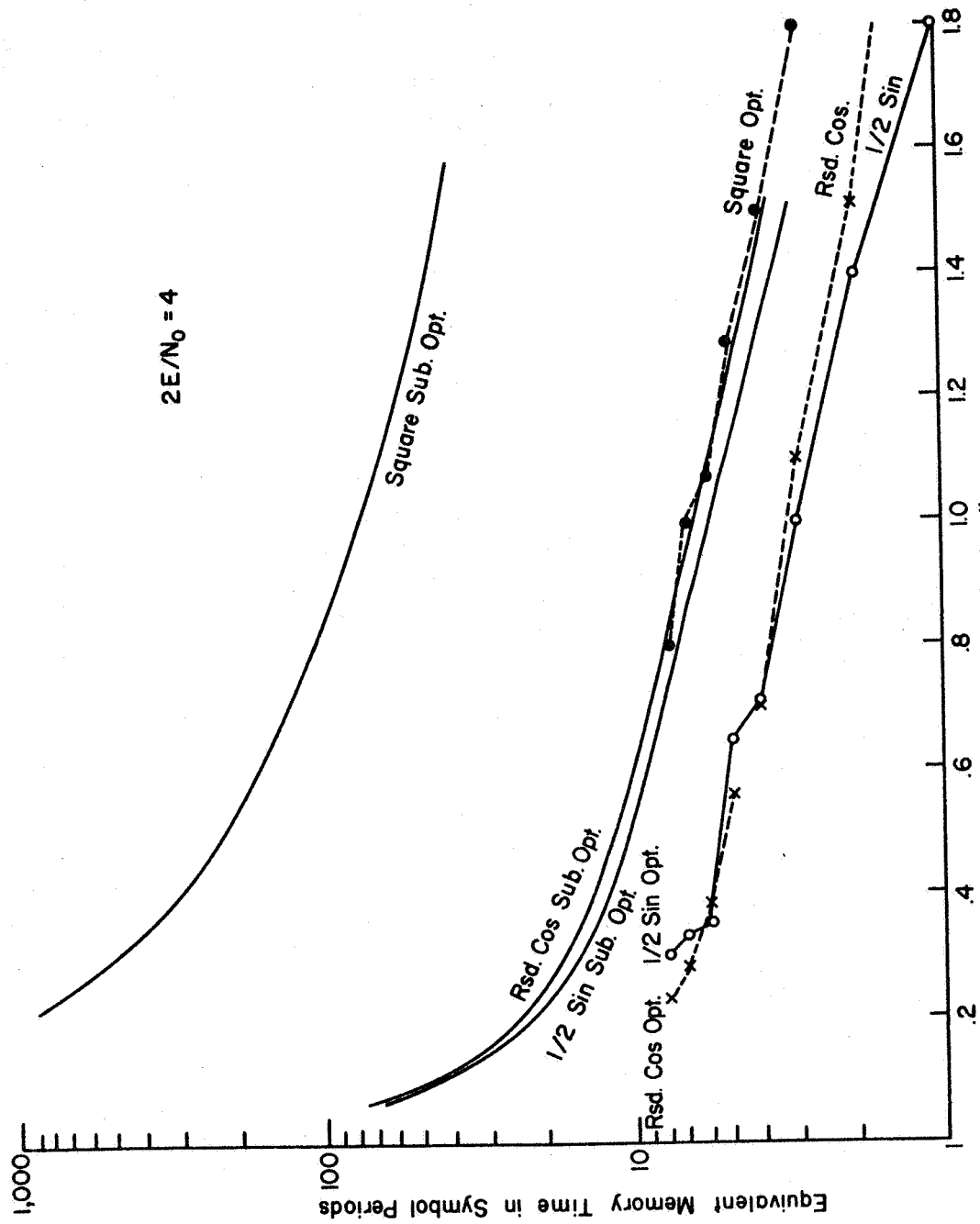

Fig. 6.32 Optimum and Suboptimum Compared for $2E/N_o = 4$

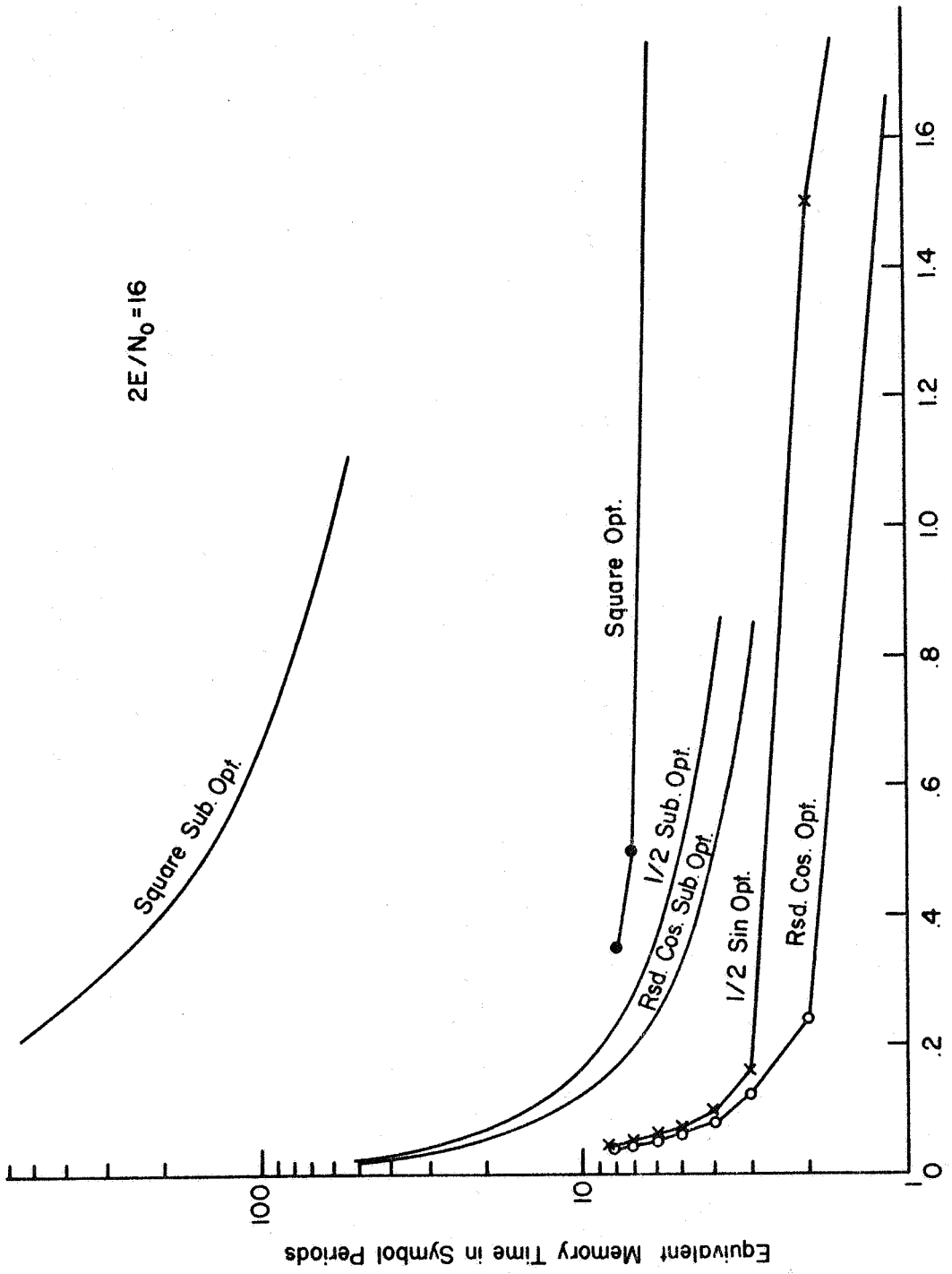

Fig. 6.33 Optimum and Suboptimum Compared for $2E/N_o = 16$

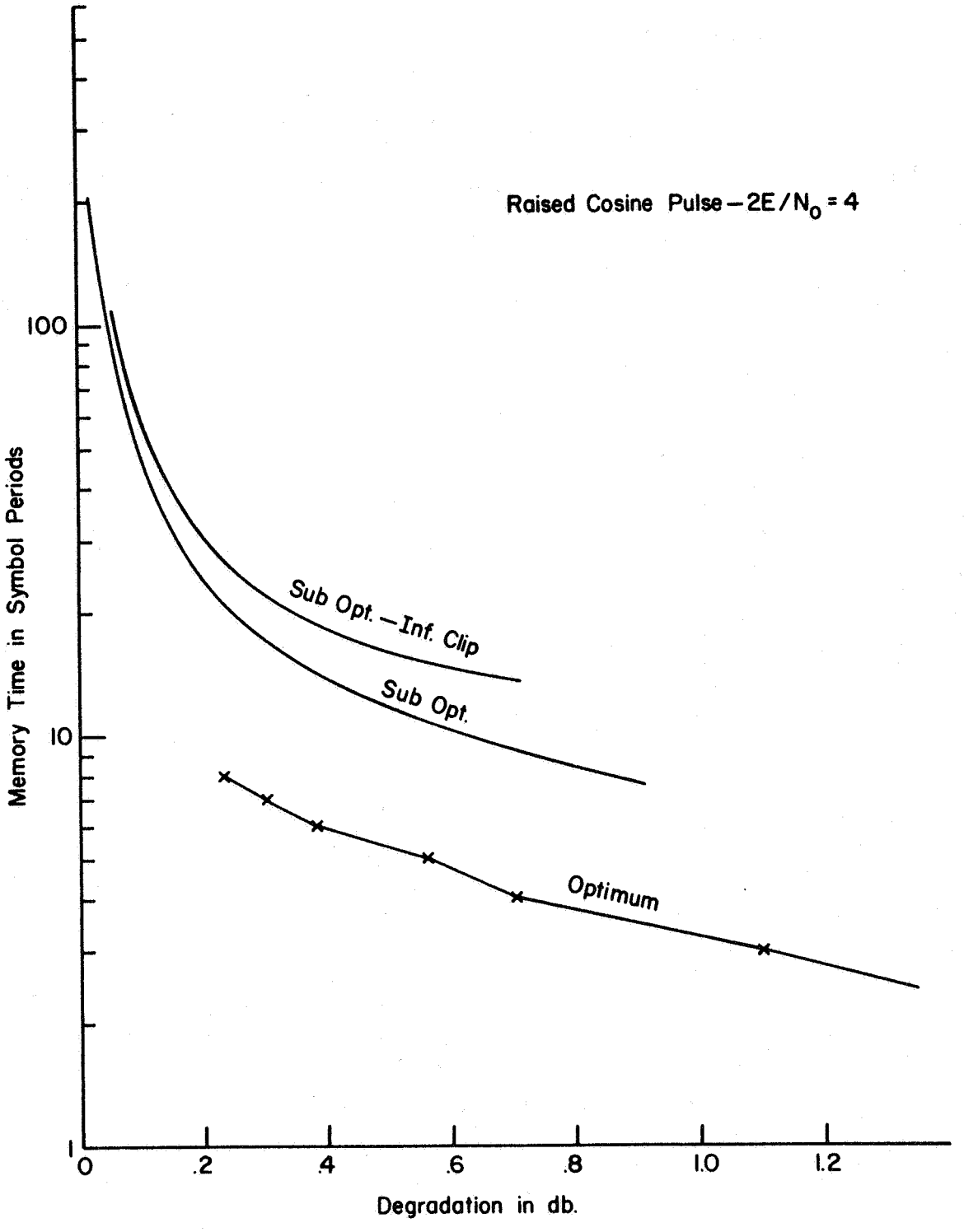

Fig. 6.34 Three Synchronizers Compared for Raised Cosine Symbol and $2E/N_o = 4$

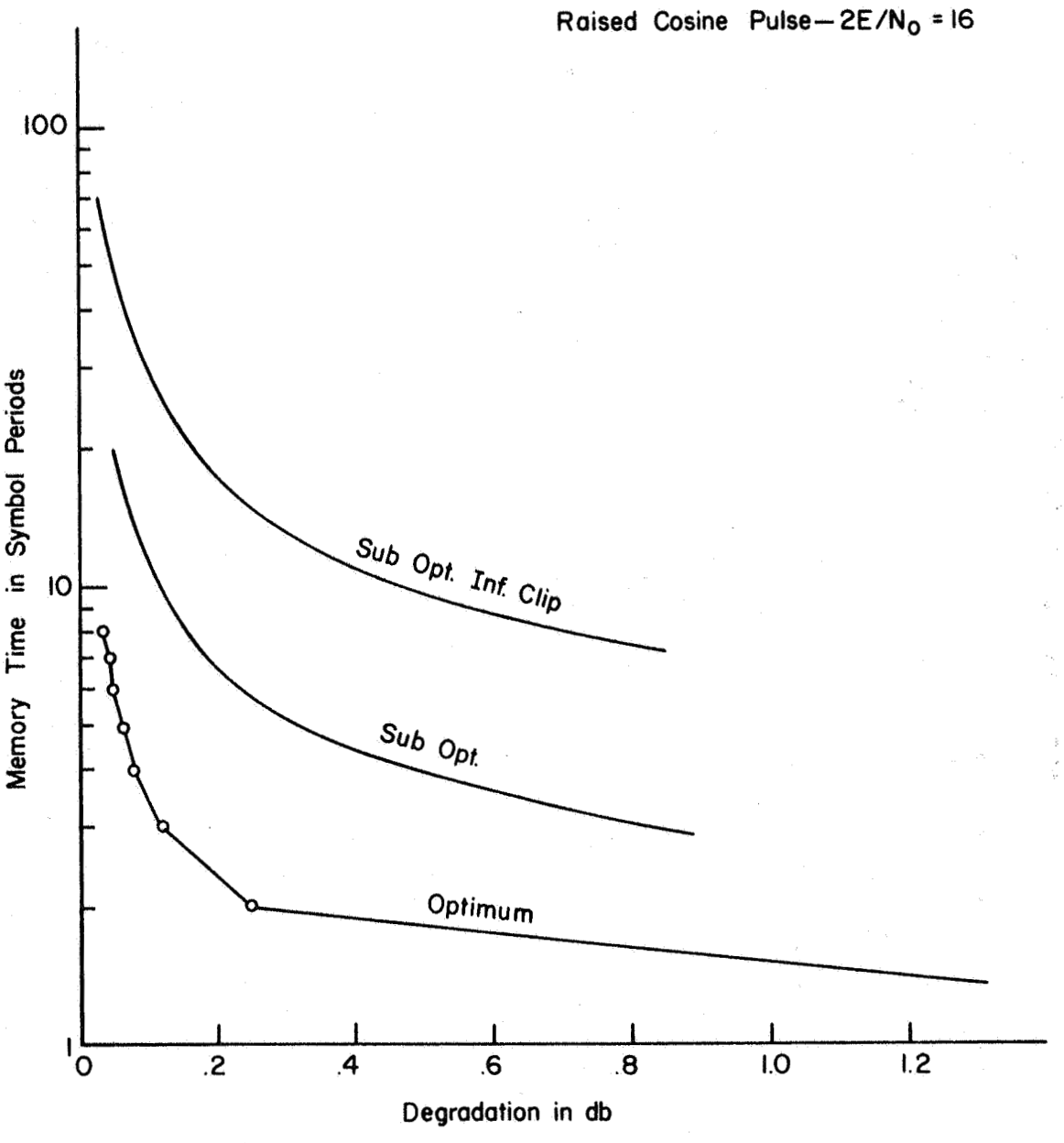

Fig. 6.35 Three Synchronizers Compared for Raised Cosine Symbol and $2E/N_o = 16$

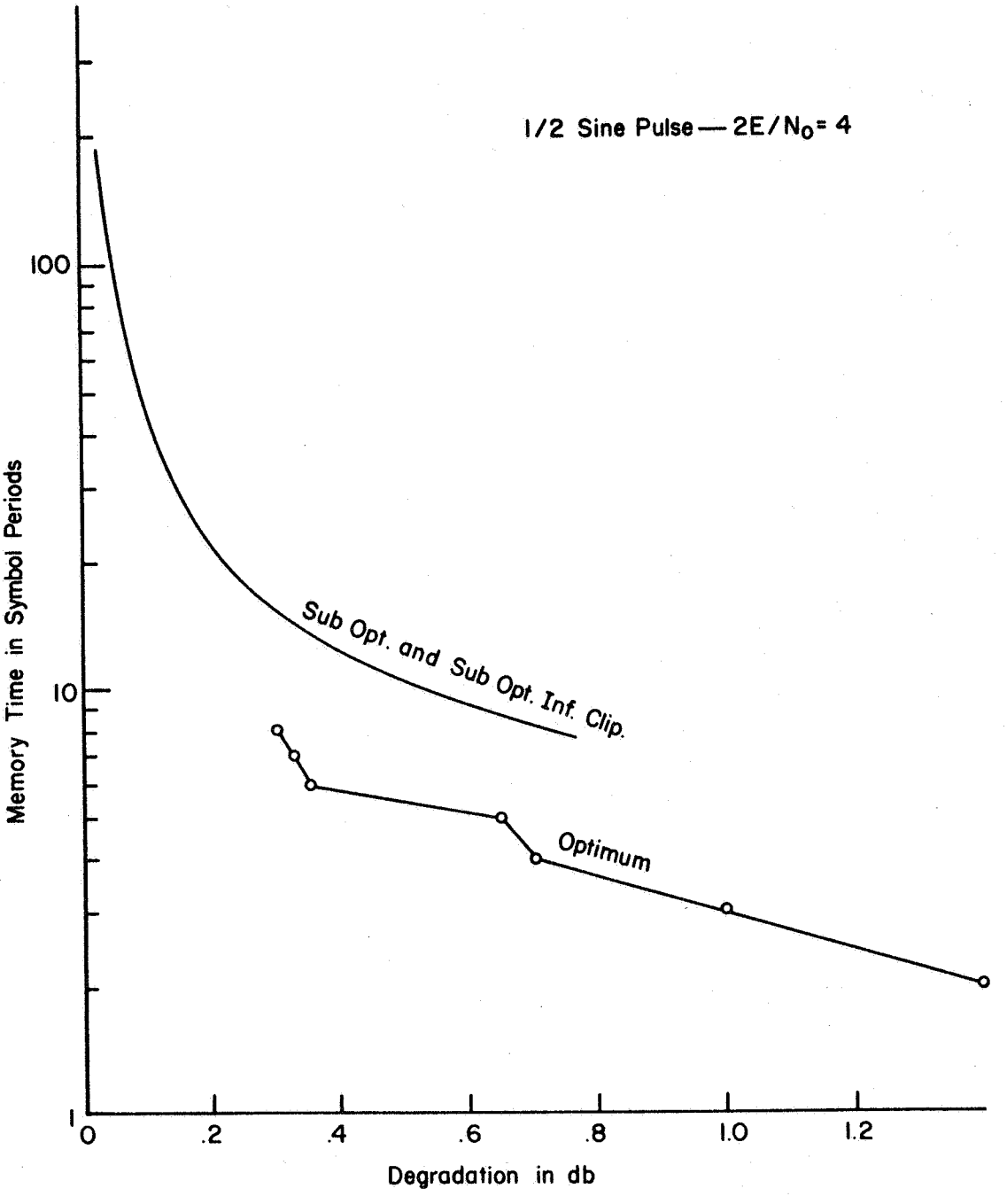

Fig. 6.36 Three Synchronizers for Half Sine Symbol and $2E/N_o = 4$

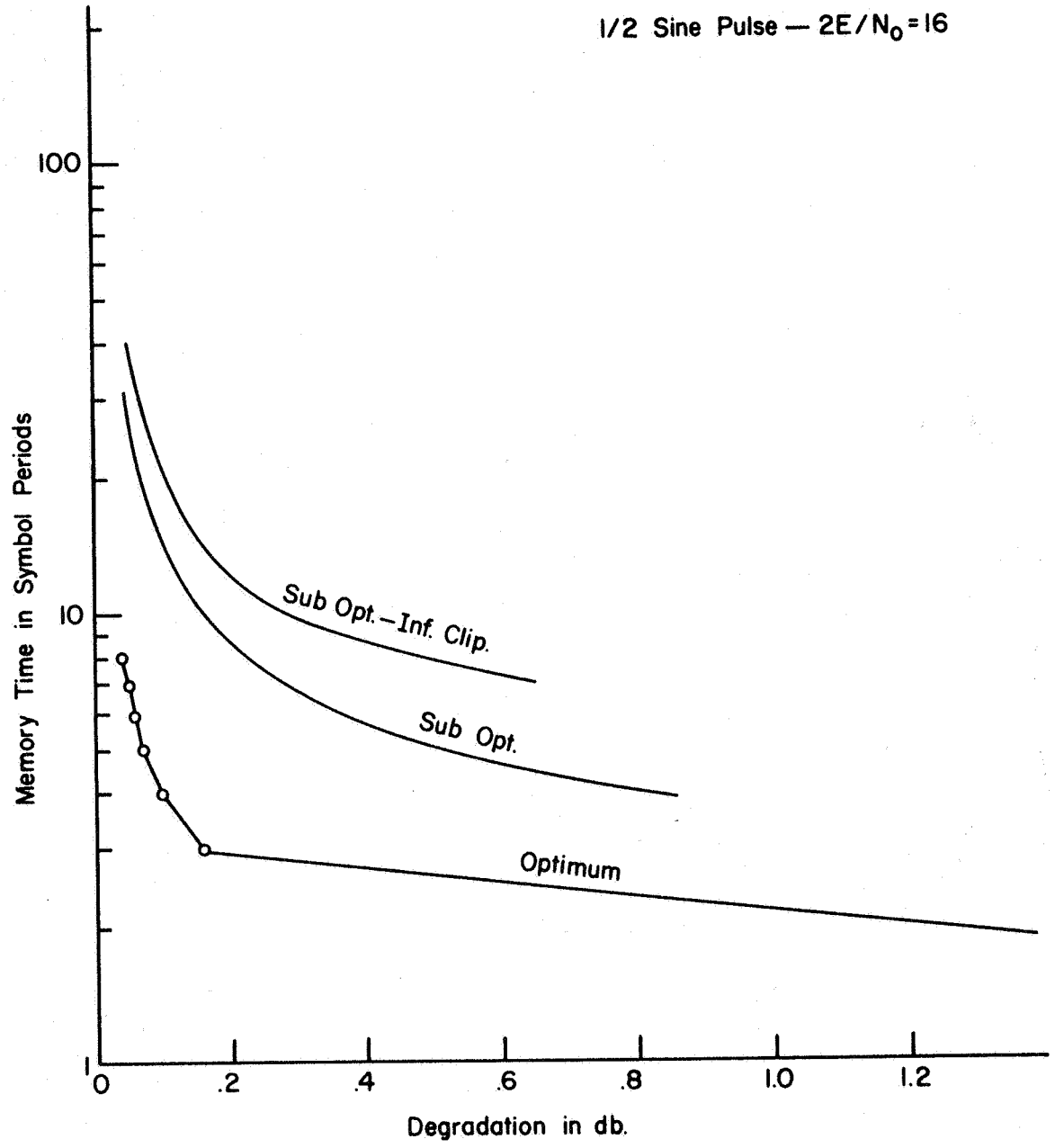

Fig. 6.37 Three Synchronizers Compared for Half Sine Symbol and $2E/N_o = 16$

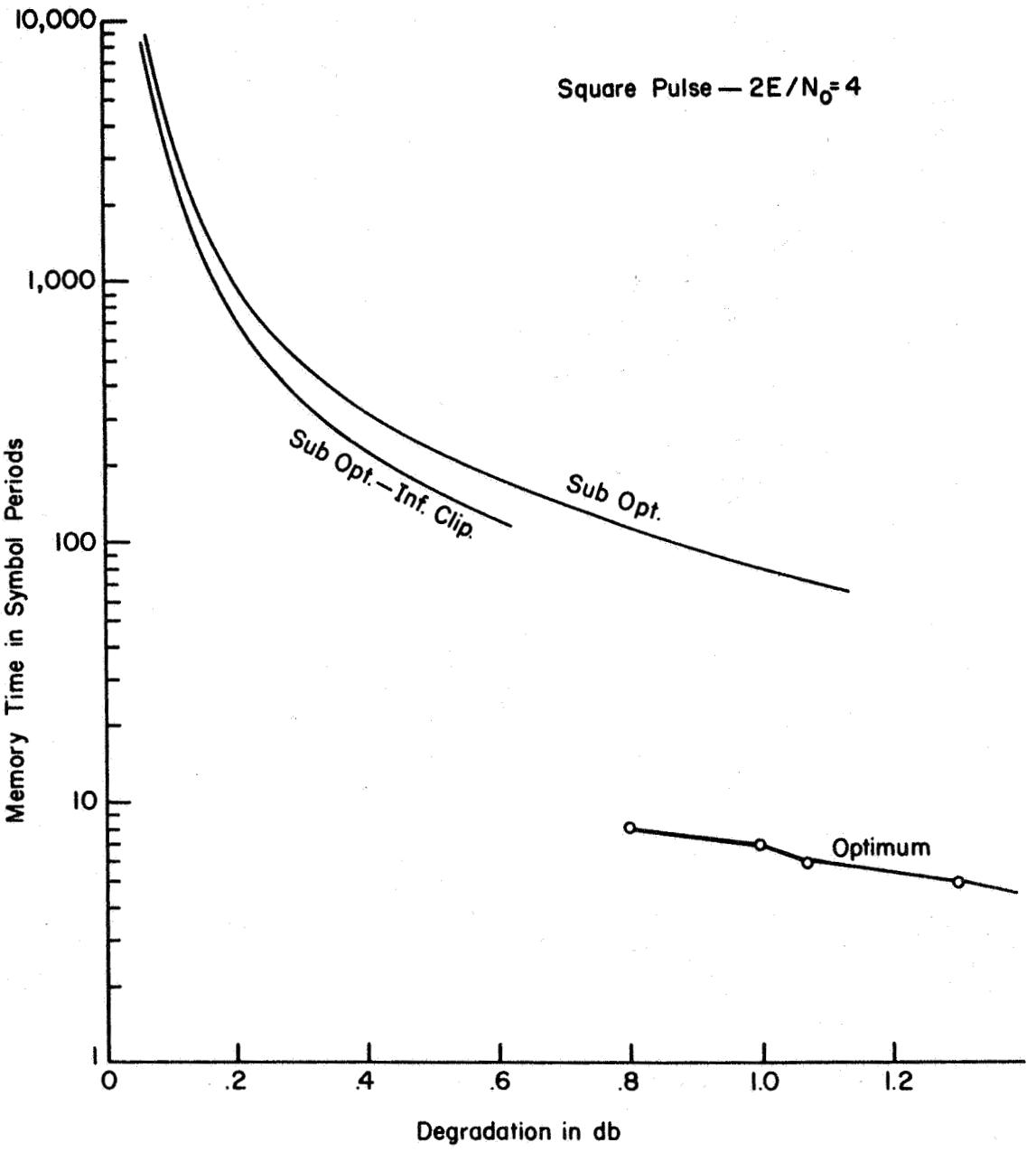

Fig. 6.38 Three Synchronizers Compared for Square Symbol and $2E/N_o = 4$

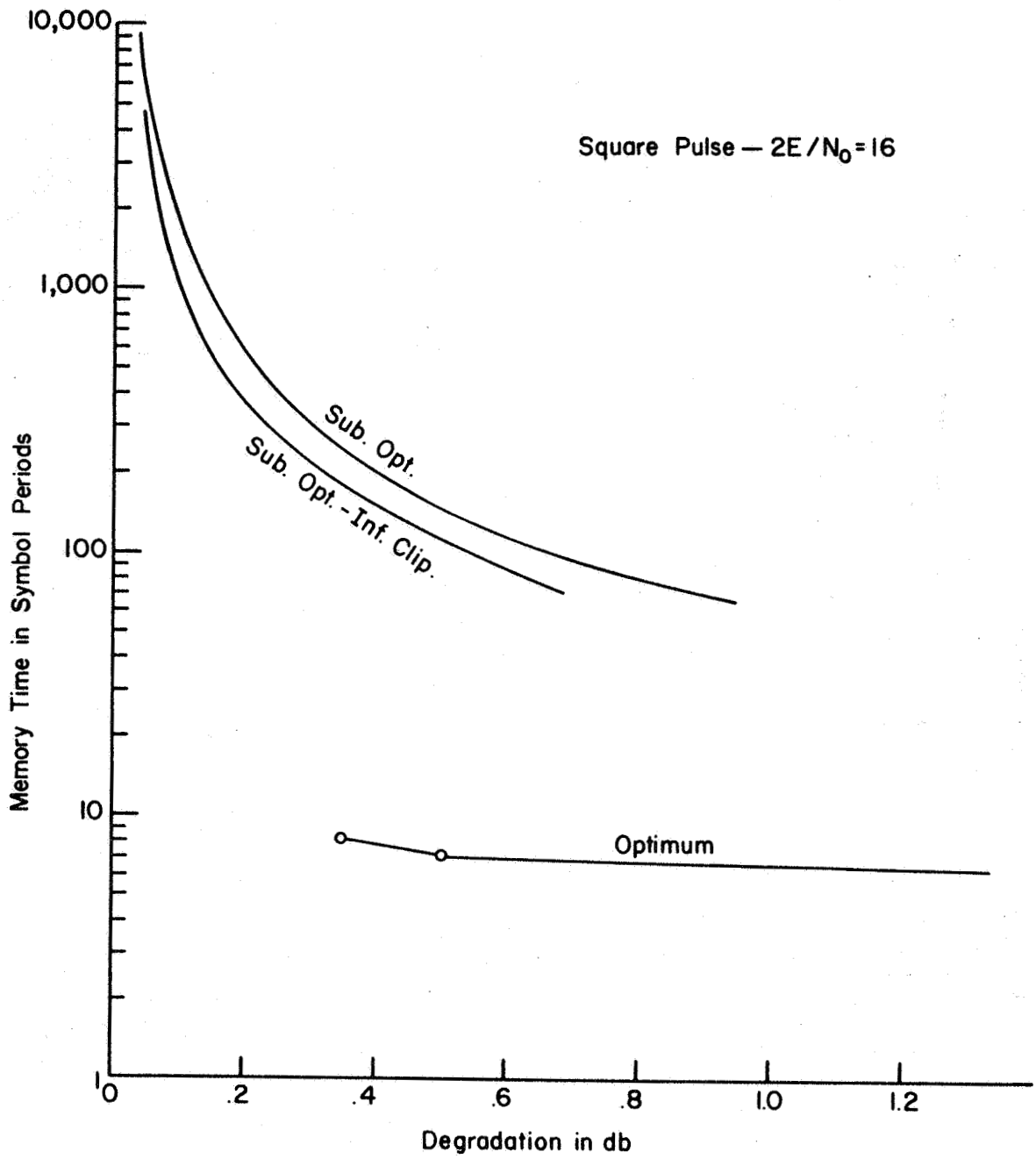

Fig. 6.39 Three Synchronizers Compared for Square Symbol and $2E/N_o = 16$

VII. CONCLUSIONS

Most of the conclusions that can be made from this research have been reported in Chapter VI. They are repeated here in the interest of clarity and emphasis.

7.1 Review of Results

This study is concerned with the performance of an optimum and a suboptimum synchronizer. The significant variables for either case are the input signal to noise ratio, the amount of memory time used in the estimation of synchronization position, and the waveshape used for the signaling pulse. Two measures of performance are used to measure the role of these variables. One is expected absolute error, $|\overline{\epsilon}|$, in synchronization time and the other is related to the probability of detection error for a correlation detector that is driven by the synchronizers that were studied. This second measure points up one conclusion which is not directly related to the form of the synchronizer. For the three waveshapes that were studied, it was observed that a correlation detector is significantly more sensitive to the synchronization error when the symbol is a square pulse than when it is either the raised cosine or half sine symbol. In fact, the half sine performance is nearly equal to that of the optimum physically realizable pulse.

The results for the optimum synchronizer indicate the following. Using $|\overline{\epsilon}|$ as a measure, performance is inversely proportional to the

square root of the product of signal to noise ratio and duration of memory time for all three waveshapes. The type of pulse shape makes only marginal differences and is of no real significance. Using degradation of probability of detection error as a measure, two significant results are observed. First, performance for the square pulse is significantly degraded from that of the other two pulses by about a factor of 4 in memory time. The second, and probably more interesting, result is that there is a knee in the performance curves for memory time vs. degradation. Above the knee, increases in memory time bring improvements in equivalent signal to noise ratio of only a few hundredths of a dB. This knee occurs in the vicinity of 6 to 8 symbol periods of memory for the range of input signal to noise ratios of interest.

From the results for the optimum case, some conclusions concerning correlation techniques can be inferred. One proposed approach to self synchronizers suggests that a bank of correlators be used to search for the correct position. This method is somewhat similar to the case of one symbol period of memory for the optimum solution. For low signal to noise ratios, the results there indicate that such a correlator solution will not yield acceptable operation. The degradation in performance is too severe. More than one period of measurement time is necessary for such techniques.

Two different suboptimum synchronizers were tested. These differed in the type of nonlinear operation which was used. One used an even function nonlinearity and the other a hard limiter--differentiator--full wave rectifier (HL-D-FWR) combination. Concerning the role of the

nonlinearity, the following conclusions are made. The form of the even function nonlinearity is not important. Square root, absolute value, and square nonlinearities were tested and it was found that the performance for all three with all other parameters held constant was not significantly different. Apparently the nonlinearity makes no difference in performance. The results for the second type of nonlinear operation show that for half sine and raised cosine pulses, the even function system is better than the HL-D-FWR system. For square pulses the advantage goes to the HL-D-FWR by a slight amount.

The results from the suboptimum system show that, as in the optimum case, the performance is inversely proportional to the square root of the product of the signal to noise ratio and the memory time. However, contrary to the optimum situation, waveshape does effect the performance. Using $|\bar{\epsilon}|$ as the measure, performance for half sine or raised cosine pulses is about a factor of 8 better in the product of signal to noise ratio and memory than for the case of square pulses. Using degradation of signal to noise ratio as the measure, the results indicate even more the superiority of either the half sine or the raised cosine over the square pulse. At signal to noise ratios of 4 and 16, the amount of memory required to achieve a fixed degradation of signal to noise ratio is 15 times greater for the square pulse. The knee effect also applies to the suboptimum results.

7.2 Conclusions

The conclusions that can be drawn from these results are as follows.

Comparing the suboptimum to the optimum system shows that performance for the suboptimum case is only a factor of 2 worse in memory time. This factor is small enough so that there is no real merit in trying to implement and operate the optimum system.

For a practical suboptimum system, there is a significant gain in synchronizer-detector performance when raised cosine or half sine pulses are used instead of square pulses.

If a degradation of .05 db in effective signal to noise ratio can be tolerated, then a relatively short memory or measurement time can be used. This time may be typically as small as 10 or 15 symbol durations. This indicates that a system which uses a phase lock loop for the narrow-band output filter can operate in a nearly asynchronous mode. Certainly no great precautions are necessary for maintaining a stable rate of symbol transmission. Furthermore, in channels with fading characteristics, the fading rate will always be very slow compared to the required measurement time for all but the very slowest symbol rates. In summary, the short required measurement time allows for considerable variability in the phase characteristics in the system.

7.3 Recommendations for Further Study

The results of this research indicate that self synchronization is feasible and can be implemented in a relatively simple way for anti-correlated signaling. The performance for orthogonal system and M-ary alphabets has not been solved. These systems could be attacked using

some of the same techniques. The results will probably be much the same. The most interesting area for further study lies in the phase response of the bandpass filter to random inputs. The model of the suboptimum synchronizer could be carried only to the point of computing the signal to noise ratio at the filter. Exactly how the filter affects the phase distribution at the output of the narrowband filter and what phase characteristic for the filter is desirable is not known.

BIBLIOGRAPHY

1. Wintz, P. A., and Hancock, J. C., "An Adaptive Receiver Approach to the Time Synchronization Problem", IEEE Trans. on Comm. Tech., Vol. Com-13, No. 1, pp. 90-96, March, 1965.

2. VanHorn, J. H., "A Theoretical Synchronization System for Use with Noisy Digital Signals", IEEE Trans. on Comm. Tech., Vol. Com-12, No. 3, pp. 82-90, September, 1964.

3. Stiffler, J. J., "Maximum Likelihood Symbol Synchronization", JPL Space Programs Summary, Vol. IV, No. 37-35, pp. 349-357, October, 1965.

4. Golomb, S. W., Davey, J. R., Reed, I. S., VanTrees, H. L., Stiffler, J. J., "Synchronization", IEEE Trans. on Comm. Syst., Vol. CS-11, No. 4, pp. 481-491, December, 1963.

5. Lindsey, W. C., "Phase-Shift-Keyed Signal Detection with Noisy Reference Signals", IEEE Trans. on Aerospace and Electronic Syst., Vol. AES-2, No. 4, pp. 393-401, July, 1966.

6. Huggins, W. H., "Signal-Flow Graphs and Random Signals", Proc. of the I.R.E., Vol. 45, pp. 74-86, January, 1957.

7. Zadeh, L. A., and Huggins, W. H., "Signal-Flow Graphs and Random Signals", Proc. of the I.R.E., Vol. 45, pp. 1413-1414, October, 1957.

8. Barnard, R. D., "On the Discrete Spectral Densities of Markov Pulse Trains", Bell System Technical Journal, Vol. 43, pp. 233-259, January, 1964.

9. Davenport, W., and Root, W., Random Signals and Noise, McGraw-Hill Book Company, Inc., 1958.

10. Bracewell, R. M., Fourier Transform and its Applications, McGraw-Hill Book Company, Inc., 1965.

11. Boas, R., and Kac, M., "Inequalities for Fourier Transforms of Positive Functions", Duke Mathematical Journal, Vol. 12, pp. 189-206, 1945.

12. Hancock, J. C., and Wintz, P. A., Signal Detection Theory, McGraw-Hill Book Company, Inc., 1966.

13. Rice, S. O., "Statistical Properties of a Sine-wave Plus Random Noise", Bell System Technical Journal, Vol. 27, pp. 109-157, January, 1948.

14. Viterbi, A. J., Principles of Coherent Communication, McGraw-Hill Book Company, Inc., 1966.

APPENDIX A

APPENDIX A

On the following pages is the digital computer program that was used for the simulation of the performance of the optimum synchronizer using square pulse symbols. The programs for half sine and raised cosine symbols differ only in the equations for the waveshape.

```
41      DO 98 KC = 1,LSY
        DO 42 I = 1,JIN
        XN(I) = GAURN(X)
42      X(I) = XN(I) + SGN*SS(I)
        XXX = GAURN(X)
        IF ( XXX .GT. 0. ) GO TO 43
        SGN = -1.
        GO TO 44
43      SGN = +1.
44      DO 45 I = JINY , LS
        XN(I) = GAURN(X)
45      X(I) = XN(I) + SGN*SS(I)
        DO 15 I = 1,LB
        J = NB(I)
        M = J-1
        SM = 0.
        DO 8 N= 1,M
        NN = LS + N - M
8       SM = SM + X(N)*S(NN)
        P(I) = SM
        T(I) = P(I) + Q(I)
        SM = 0.
        IF(J.GT. LS) GO TO 18
        DO 9 N = J,LS
        NN = LS + N - M
9       SM = SM + X(N)*S(NN)
18      Q(I) = SM
        IF( T(I) .GT. 5.) GO TO 10
        CLX = EXP(T(I))
        Y(I) = ALOG(CLX +1./CLX) +Y(I)
        GO TO 11
10      Y(I) = ABS(T(I)) +Y(I)
11      IF(Q(I) .GT. 5.) GO TO 12
        CLX = EXP(Q(I))
        Z(I) = ALOG(CLX +1./CLX) + Y(I)
        GO TO 15
12      Z(I) = ABS(Q(I)) + Y(I)
15      CONTINUE
        ZXZ = Z(1)
        I = 1
        DO 13 J = 2,LB
        IF(Z(J) .LE. ZXZ) GO TO 13
14      ZXZ = Z(J)
        I = J
13      CONTINUE
98      MM ( KBV,KC ) = I
        WRITE(6,200) (MM(KBV,J) , J=1,LSY)
99      CONTINUE
97      CONTINUE
        DO 30 I = 1,LSY
        DO 30 K = 1,LB
        NA(I,K) = 0.
        DO 30 J = 1,KBV
        IF(MM(J,I) .NE. K) GO TO 30
        NA(I,K) = NA(I,K) + 1
30      CONTINUE
```

```
$IBJOB
$IBFTC SQUAR
      DIMENSION NB(20),S(101),SR(51),Q(20),Y(20),X(51),XN(51),
     1  P(20),T(20),Z(20),MM(500,20),NA(10,20),NAB(10,21),
     2  E(10),F(10),SS(51),NNB(20)
      READ(5,100) LS,LB
      READ(5,101) LSY , LR
      READ (5,100) LSH , NPT
      DO 1001 I = 1,NPT
1001  READ(5,104) E(I)
      DO 2 I = 1,LB
2     READ(5,102) NNB(I)
      ALS = LS
      DO 3 I = 1,LS
      AI = I-1
      S(I) = 1.
      III = I + LS
3     S(III) = S(I)
4     READ(5,104) SNR
      WRITE(6,204) SNR
      R = SQRT(SNR/ALS)
      A = SQRT(SNR/2.)
      PE = .5-.5*ERFC(A)
      DO 1002 I = 1,NPT
      AGE = A
      AFE = A*(1.-2.*F(I))
      YY = 1. - .5*ERFC(AFE)
1002  F(I) = YY - .5*ERFC(AGE)
      DO 5 I = 1,LS
5     SR(I) = R*S(I)
      DO 97 KA = 1,LSH
      JIN = KA*(LS/LSH)
      KAV = (50*KA) - 50
      DO 79 I = 1,JIN
      IA = LS - JIN + I
79    SS(I) = SR(IA)
      JINY = JIN + 1
      IF ( JIN .GE. LS ) GO TO 66
      DO 80 I = JINY,LS
      IA = I - JIN
80    SS(I) = SR(IA)
66    DO 81 I = 1,LB
      NB(I) = NNB(I) + JIN
      IF ( NB(I) .LE. LS ) GO TO 81
      NB(I) = NB(I) - LS
81    CONTINUE
      DO 99 KB = 1,LR
      KBV = KAV + KB
      DO 6 I = 1,LB
      Q(I) = 0.
6     Y(I) = 0.
      XXX = GAURN(X)
      IF ( XXX .GT. 0. ) GO TO 40
      SGN = -1.
      GO TO 41
40    SGN = +1.
```

```
      WRITE(6,201)
      DO 51 I = 1,LSY
      WRITE(6,203) I
      NAB(I,1) = NA(I,LB)
      WRITE(6,202) NB(1), NAB(I,1)
      DO 50 K = 2,LP
      KK = K-1
      NAB(I,K) = NA(I,KK)
50    WRITE(6,202) NB(K), NAB(I,K)
      LBB = LB + 1
      SUM1 = 0.
      SUM2 = 0.
      SUM3 = 0.
      NAB(I,LBB) = 0
      XKBV = KBV
      COEF = 1./(2.*XKBV)
      DO 4000 KM = 1,NPT
      KMN = LBB + 1 - KM
      MRP = NAB(I,KM) + NAB(I,KMN)
      XMRP = MRP
      G = COEF*XMRP
      SUM1 = SUM1 + G*F(KM)
      GG = G*F(KM)
      SUM2 = SUM2 + GG
4000  SUM3 = SUM3 + GG*E(KM)
      WRITE(6,105) SUM1
      RATIO = SUM1/PE
      WRITE(6,106) RATIO
      ABVM = 2.*SUM2
      WRITE(6,107) ABVM
      SIGMA = SQRT(2.*SUM3)
      WRITE(6,108) SIGMA
51    WRITE(6,201)
      GO TO 4
100   FORMAT(I5,I5)
101   FORMAT(I5,I5)
102   FORMAT(I5)
104   FORMAT(F10.0)
105   FORMAT(32H PROBABILITY OF DETECTION ERROR=, E15.5)
106   FORMAT(24H RATIO TO PERFECT SYNCH=, E15.5)
107   FORMAT(23H ABSOLUTE VALUE MOMENT=, E15.5)
108   FORMAT(20H STANDARD DEVIATION=, E15.5,//)
200   FORMAT(1X, 20I4)
201   FORMAT(/)
202   FORMAT(1X, 2I5)
203   FORMAT(19H NUM. OF SYMBOLS = , I4)
204   FORMAT(5H SNR=, F5.1, /)
      END
$IBLDR ERF                                          03/19/66   ERF 000
$IBLDR RANDPK                                                  RANDPK0
$DATA
```

APPENDIX B

APPENDIX B

The probability density function for synchronizing error that is used in this work is the one derived by Rice[13] for the case of additive narrowband gaussian noise and a sine wave. This appendix presents some of the pertinent information about this density function and experimental evidence that it may be used to represent the random synchronizing error process that is observed in the suboptimum synchronizer.

This density function is

$$p(\epsilon) = e^{-R}\left\{1+(\sqrt{\pi R})(\cos 2\pi\epsilon)(1+\operatorname{erf}[\sqrt{R}\cos 2\pi\epsilon])e^{(R\cos^2 2\pi\epsilon)}\right\} \qquad \text{B.1}$$

where ϵ is the fractional error defined over the interval $-1/2 < \epsilon \leq +1/2$ and R is the signal to noise ratio. The low order moments of this function are obviously not easily evaluated in closed form. They have been evaluated by numerical integration, and the results for $|\bar{\epsilon}|$ and $\sqrt{\overline{\epsilon^2}}$ are presented in Fig. B.1.

These results for $|\bar{\epsilon}|$ can be compared with an asymptotic result for large R. For large R, B.1 reduces to

$$p(\epsilon) = 2e^{-R}\sqrt{\pi R}\cos 2\pi\epsilon\, e^{R\cos^2 2\pi\epsilon} \qquad \text{B.2}$$

Let $x = 2\pi\epsilon$ so that

$$|\bar{\epsilon}| = \frac{4\sqrt{\pi R}\, e^{-R}}{(2\pi)^2}\int_0^T x(\cos x)e^{R\cos^2 x}\,dx$$

Expanding cos(x) in a power series results in

$$|\bar{\epsilon}| = \frac{4\sqrt{\pi R}\, e^{-R}}{(2\pi)^2} \left\{ \int_0^{\pi} x\, e^{R\cos^2 x}\, dx - \int_0^{\pi} \frac{x^3}{2!}\, e^{R\cos^2 x}\, dx + \ldots \right\}$$

For large R, only the first integral need be retained. Because the value of $\exp(R\cos^2(x))$ drops off very quickly with x, the majority of the contribution to the integral occurs when x is small. Hence, $\cos^2(x)$ can be replaced by $(1 - x^2/2)^2 = 1 - x^2 + \ldots$. Making these substitutions result in

$$|\bar{\epsilon}| = \frac{4\sqrt{\pi R}}{(2\pi)^2} \int_0^{\pi} x\, e^{-Rx^2}\, dx = \frac{4\sqrt{\pi}}{(2\pi)^2 2\sqrt{R}} \left(1 - e^{-R\pi^2}\right) \simeq \frac{.09}{\sqrt{R}}$$

This line is also drawn on Fig. B.1 to show the range over which this approximation is valid. It is virtually exact for R > 10 and is never more than 10% in error for values of R down to .5.

The relationship of the sine wave plus additive gaussian noise density function to the function that results from the analysis of the first order phase lock loop is interesting. For the first order loop[14]

$$p(\epsilon) = \left(e^{(\alpha \cos 2\pi\epsilon)}\right) / I_o(\alpha)$$

where α is a signal to noise ratio parameter. For the case of large α this reduces to

$$p(\epsilon) = \sqrt{2\pi\alpha}\, e^{-\alpha(1-\cos 2\pi\epsilon)}$$

In the range of relatively small values of ϵ,

$$p(\epsilon) = \sqrt{2\pi\alpha}\, e^{\frac{-\alpha(2\pi\epsilon)^2}{2}}$$

Making the same assumptions on ϵ, B.2 reduces to

$$p(\epsilon) = \sqrt{4\pi R}\, e^{-R(2\pi\epsilon)}$$

Thus, if $R = \alpha/2$, the functions are identical. To compare the two functions over their entire range, the moments $|\overline{\epsilon}|$ and $\sqrt{\overline{\epsilon^2}}$ were also numerically computed and are plotted in Fig. B.1. Observe that over the complete range of signal to noise ratios, the value of α for a particular value of $|\overline{\epsilon}|$ is twice the value of R. The same result is true for $\sqrt{\overline{\epsilon^2}}$. It can be concluded that as far as the lower order moments are concerned, the two density functions are equivalent.

A second observation that can be made from these graphs is that $|\overline{\epsilon}|$ and $\sqrt{\overline{\epsilon^2}}$, the RMS error, are related by an approximate constant of 1.25. Since the error, ϵ, has zero mean, RMS error and σ are the same. Hence $|\overline{\epsilon}|$ can be directly related to the more commonly used variance measure.

The results presented in Chapter VI show that the shapes of the curves as computed using the assumed density function matched very well with those of the observed data. Further experimental evidence that the sine wave plus narrowband gaussian noise distribution is a reasonable approximation to the actual distribution function was obtained by measuring the distribution function of the synchronizer error made under several different sets of operating conditions.

The measurements were made in the following way. For positive errors, the output of the error detector is a positive pulse of duration equal to the error. This pulse is applied to an AND circuit along with a short pulse that is delayed by a chosen amount from

the correct synchronizing time. An output occurs at the AND circuit only for errors greater than, or equal to, the chosen delay. By counting the number of output pulses for a fixed number of synchronizing pulses, an estimate $F(\epsilon)$ can be obtained. This estimate was obtained by making 10 runs with 10,000 synchronizing pulses in each run for each delay. The mean of these 10 runs was used as the estimate of $F(\epsilon)$.

Fig. B.2 and B.3 present the results of such measurements for two representative cases. The first graph is for the synchronizer using a half sine pulse and the second for a square pulse. In order to compare the results with the distribution function for the assumed density two curves of the assumed $F(\epsilon)$ are plotted. One is for a signal to noise ratio which produces an $|\overline{\epsilon}|$ of .023 and the other for $|\overline{\epsilon}| = .031$. The measured points are represented by the circles and the dashed lines indicate the range of $\pm 1\sigma$ for the measured points.

It is seen in these graphs that the measured distribution has the same general shape as the assumed one. Furthermore, comparing the measured value of $|\overline{\epsilon}|$ with the location of the measured points shows that the measured moment is consistent with the moment that is predicted by the assumed density function. It is concluded that the assumed density function is a realistic approximation to the actual function.

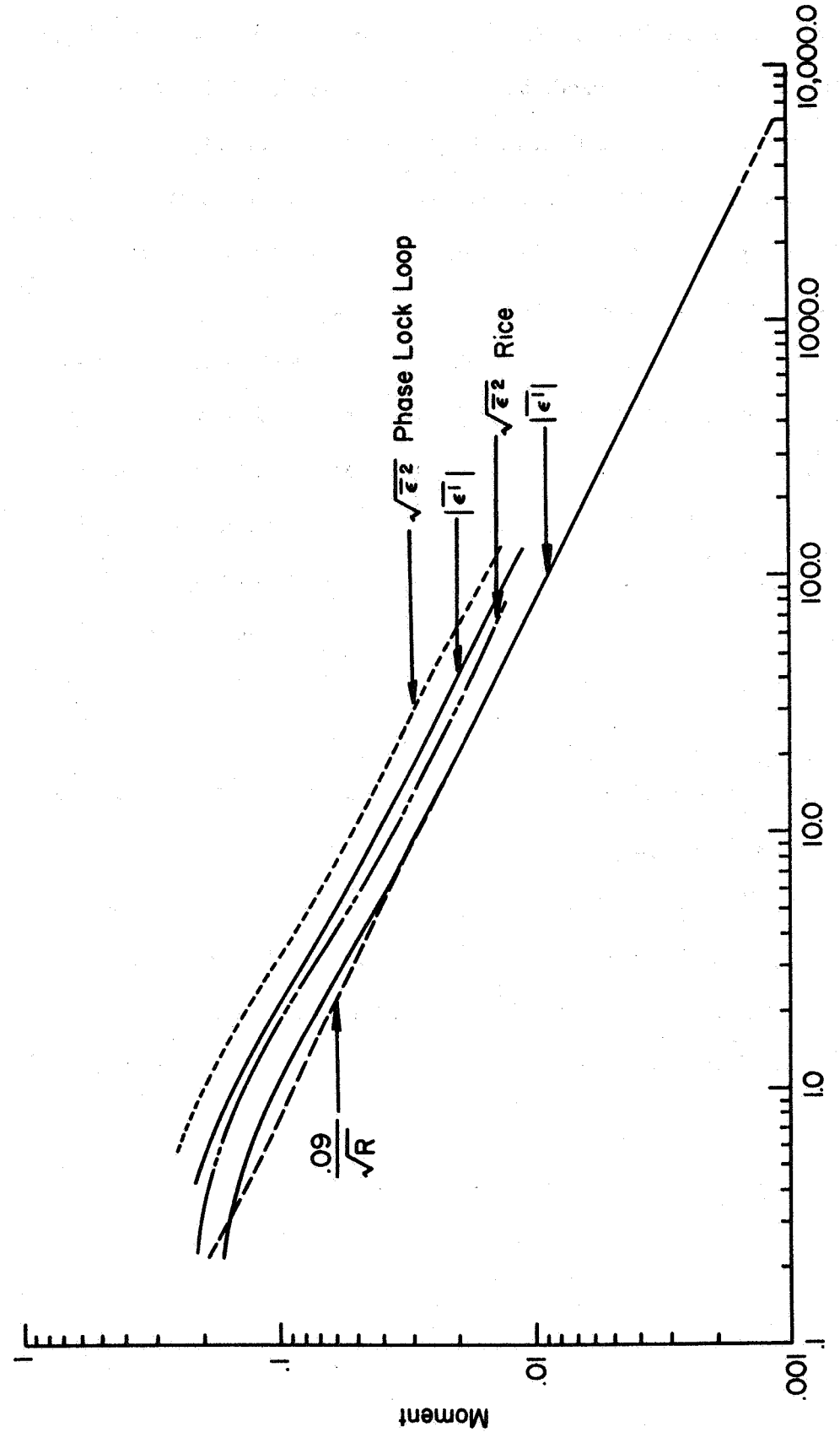

Fig. B.1 Moments of Two Distribution Functions Compared

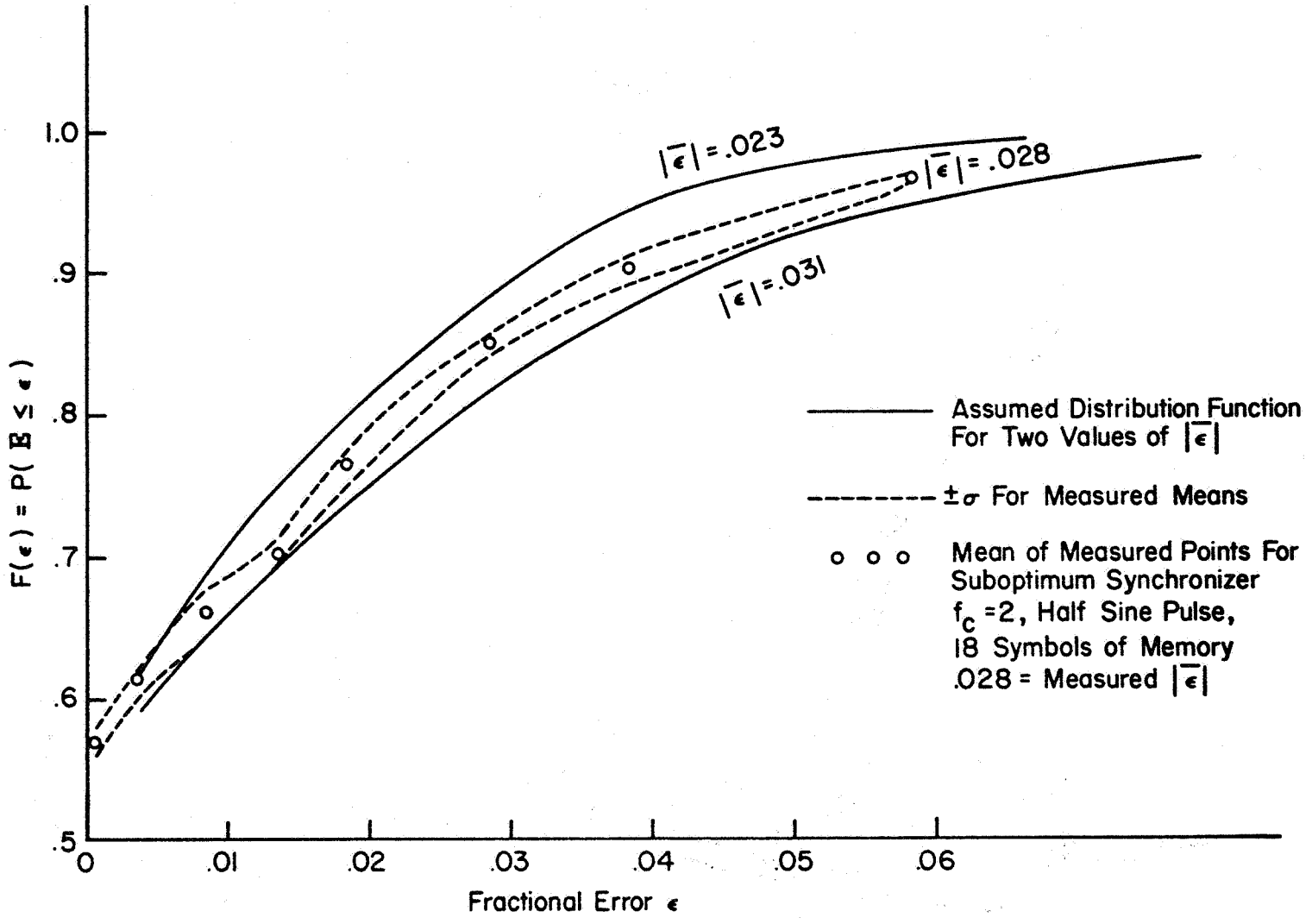

Fig. B.2 Comparison of Assumed and Measured Distribution Functions with Half Sine Symbol Input to System

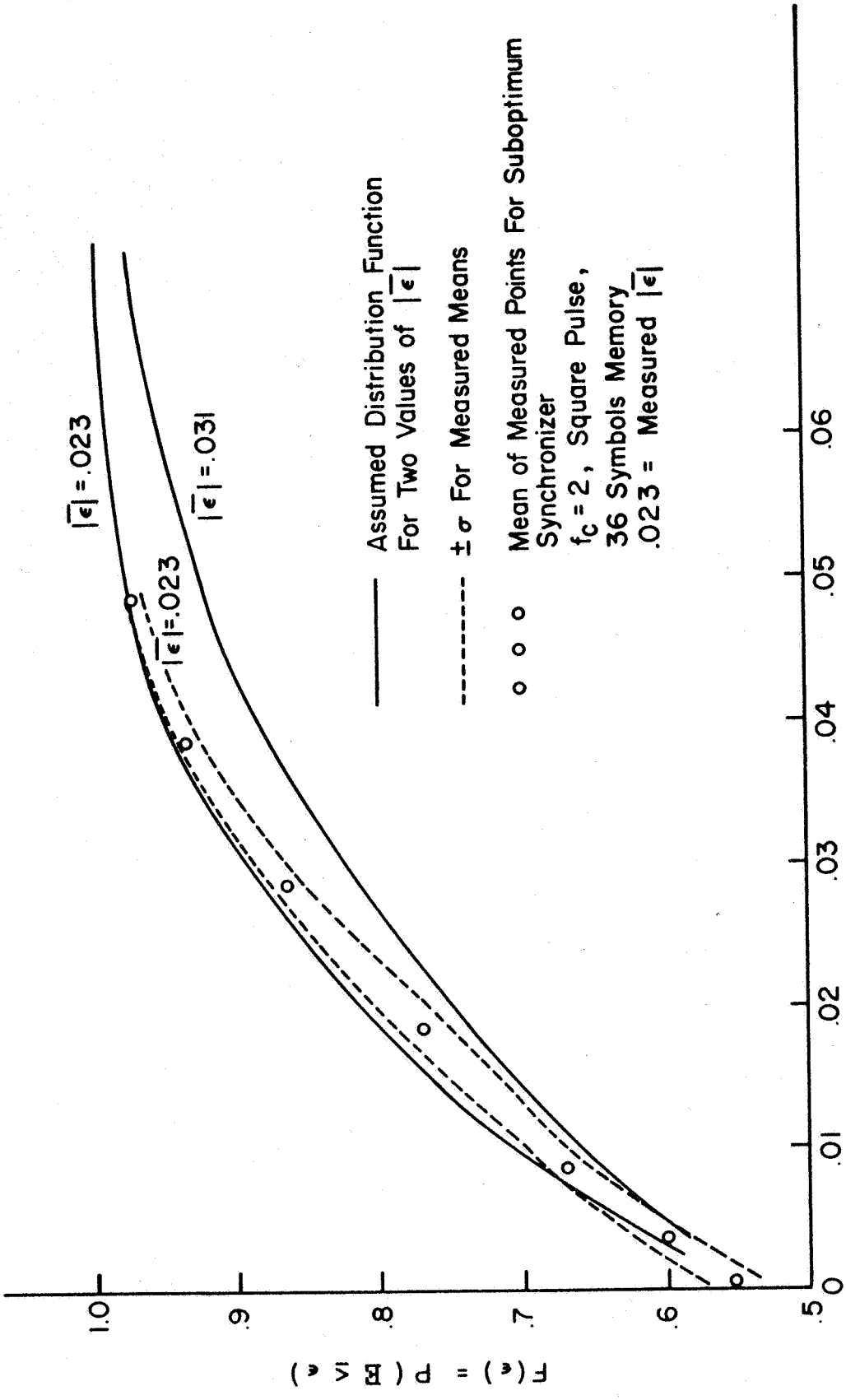

Fig. B.3 Comparison of Assumed and Measured Distribution Functions with Square Symbol Input to System

APPENDIX C

APPENDIX C

In this Appendix, the calculation for the discrete and continuous components of the low pass filtered random anticorrelated digital pulse train is presented. A detailed outline of the calculations for the square pulse case is given and the results for the half sine and raised cosine are presented. Following this, a tabulation is made of the terms necessary for the calculation of 3.39.

In order to compute the discrete and continuous components of the spectrum of the pulse train, as given in 3.25 and 3.27, it is necessary to compute

$$H_1(S) = \mathcal{L}\{(R_h(t))^2 + (R_t(t+T))^2\} \qquad C.1$$

and

$$H_2(S) = \mathcal{L}\{2R_h(t)\, R_t(t+T)\} \qquad C.2$$

$R_h(t)$ is the "head" response of the low pass filter and $R_t(t+T)$ is the "tail" response. The following derivation is for the square pulse. The derivations for the raised cosine or half sine are similar but considerably more involved.

Let $\omega_c = 1/RC = 1/\tau$ be the radian cutoff frequency of the single pole low pass filter. The "head" response to the square pulse is

$$R_h(t) = 1 - e^{-t/\tau} \qquad C.3$$

The "tail" response is, after normalizing the period to T = 1,

$$R_t(t+1) = (1 - e^{-1/\tau})e^{-t/\tau} \qquad C.4$$

Now,

$$H_2(t) = 2R_h(t)R_t(t+1) = 2(1-e^{-1/\tau})(1-e^{-t/\tau})e^{-t/\tau}\{u(t)-u(t-1)\} \qquad C.5$$

Let

$$\theta = e^{-1/\tau}$$

so that

$$H_2(S) = 2(1-\theta)\left\{\frac{1-\theta e^{-s}}{s+1/\tau} - \frac{1-\theta^2 e^{-s}}{s+2/\tau}\right\} \qquad C.6$$

Since only the value of the continuous spectral density is of interest only at the fundamental frequency, f = 1, 3.25 becomes

$$S^c_{sxs}(1) = H_2(j2\pi)\ H_2(-j2\pi) = 4(1-\theta)^2\tau^2\left\{\frac{(1-\theta)^2}{Z}\right.$$
$$\left. + \frac{(1-\theta)^2(1+\theta)^2}{3+Z} - \frac{2(1-\theta)(1-\theta^2)(1+Z)}{Z(3+Z)}\right\} \qquad C.7$$

where $Z = 1 + (2\pi\tau)^2 = 1 + (1/f_c)^2$

For the discrete components, it is necessary to evaluate

$$H_1(S) = \mathcal{L}\{(R_h(t))^2 + (R_t(t+1))^2\} \qquad C.8$$

From C.3 and C.4

$$[R_h(t)]^2 = [1 - 2e^{-t/\tau} + e^{-(2/\tau)t}]\ (u(t) - u(t-1))$$
$$[R_t(t+1)]^2 = (1-\theta)^2 e^{-2/\tau(t)}\ (u(t) - u(t-1)) \qquad C.9$$

Taking the Laplace transform and summing yields

$$H_1(S) = \left[\frac{1-e^{-s}}{s} - \frac{2(1-\theta e^{-s})}{s+1/\tau} + \frac{(1+(1-\theta)^2)(1-\theta^2 e^{-s})}{s+2/\tau}\right] \qquad C.10$$

Evaluating this at $s = j2\pi$ gives

$$S^d_{sxs}(1) = \tau^4 \left|\left(\frac{2(1-\theta^2)(1+[1-\theta]^2)}{3+Z} - \frac{2(1-\theta)}{Z}\right)\right.$$
$$\left. -j2\pi\tau\left(\frac{(1-\theta^2)(1+(1-\theta)^2)}{3+Z} - \frac{2(1-\theta)}{Z}\right)\right|^2 \qquad C.11$$

The corresponding results for the half sine case are

$$S^{c}_{sxs}(1) = \frac{4\pi^4\tau^6(1+\theta)^4}{Y^5}\left[\frac{(1-\theta)^2}{4} + \frac{4(\pi\tau)^2(4-6(1-\theta))}{W}\right] \qquad C.12$$

and

$$S^{d}_{sxs}(1) = \frac{1}{Y^4}\left|\left(-\frac{1}{4} + \frac{(\pi\tau)^2}{4} + \frac{\pi^2\tau^3(1-\theta^2)(1+(1+\theta)^2)}{2Y} - \frac{16\pi^4\tau^5(1+\theta)}{YW}\right.\right. \qquad C.13$$

$$\left.\left. + j\pi\tau\left(\frac{1}{2} - \frac{\pi^2\tau^3(1-\theta^2)(1+(1+\theta)^2)}{2Y} - \frac{2\pi^2\tau^3(1+\theta)(1-3\pi^2\tau^2)}{YW}\right)\right|$$

where $Y = 1+(\pi\tau)^2$ and $W = 1(3\pi\tau)^2$

For the raised cosine pulses

$$S^{c}_{sxs}(1) = \frac{1024\pi^8\tau^{10}(1-\theta)^4[3+Z-4Z(1+\theta)+x(1+\theta)^2]}{Z^4x(3+Z)} \qquad C.14$$

and

$$S^{d}_{sxs}(1) = \frac{1}{Z^2}\left|\left(-1 - \frac{8\pi^2\tau^3(1-\theta)}{Z}\left[1 - \frac{4\pi^2\tau^2(1+\theta)(1+(1-\theta)^2)}{3+Z} - \frac{12\pi^2\tau^2}{X}\right]\right)\right.$$

$$\left. + j2\pi\tau\left(1 + \frac{8\pi^2\tau^3(1-\theta)}{Z}\left[1 - \frac{2\pi^2\tau^2(1+\theta)(1+(1-\theta)^2)}{3+Z} + \frac{1-8\pi^2\tau^2}{x}\right]\right)\right|^2$$

where $x = 1+(4\pi\tau)^2$ C.15

It is also necessary to evaluate the signal-cross-noise and noise-cross-noise components of the continuous spectral density. Since the value of these spectral densities is desired at only one frequency, f = 1, the quantity S'_{nxn} in 3.37 is computed by

$$S'_{nxn} = \int_{-\infty}^{+\infty} \frac{d\lambda}{\left[1-\left(\frac{\lambda}{f_c}\right)^2\right]\left[1-\left[\frac{(1-\lambda)}{f_c}\right]^2\right]} = \int_{-\infty}^{+\infty} G(\lambda)d\lambda \qquad C.16$$

The S'_{sxn} in 3.36 for each of the three waveshapes evaluated at $f = 1$ is

SQUARE PULSE

$$S'_{sxn}(1) = \int_{-\infty}^{+\infty} \frac{\sin[\pi(1-\lambda)]}{\pi(1-\lambda)} G(\lambda)d\lambda$$

HALF SINE

$$S'_{sxn}(1) = \int_{-\infty}^{+\infty} \left[\frac{2\cos\pi(1-\lambda)}{\pi(1-4(1-\lambda)^2}\right]^2 G(\lambda)d\lambda$$

RAISED COSINE

$$S'_{sxn}(1) = \int_{-\infty}^{+\infty} \left[\frac{\sin\pi(1-\lambda)}{\pi(1-\lambda)[1-(1-\lambda)^2]}\right]^2 G(\lambda)d\lambda$$

These integrals were evaluated by numerical integration with the infinite interval being approximated by stopping the integration when the argument of the integral dropped to .001 of its maximum value. The results of these integrations and the evaluation of the equations C.7 and C.11 through C.15 are tabulated below for selected values of low pass cutoff frequencies.

Table C.1

Spectral Densities at Selected Low Pass Cutoffs

For Square Symbol

f_c	S^d_{sxs}	S^c_{sxs}	S'_{sxN}	S'_{NxN}
.1	$3.312 \cdot 10^{-4}$	$1.310 \cdot 10^{-3}$	$2.825 \cdot 10^{-3}$	$5.979 \cdot 10^{-3}$
.2	$1.856 \cdot 10^{-3}$	$2.232 \cdot 10^{-3}$	$1.941 \cdot 10^{-2}$	$4.320 \cdot 10^{-2}$
.5	$9.292 \cdot 10^{-3}$	$7.836 \cdot 10^{-3}$	$1.604 \cdot 10^{-1}$	$3.924 \cdot 10^{-1}$
1.0	$1.009 \cdot 10^{-2}$	$1.002 \cdot 10^{-2}$	$4.365 \cdot 10^{-1}$	1.256
2.0	$4.768 \cdot 10^{-3}$	$4.768 \cdot 10^{-3}$	$7.242 \cdot 10^{-1}$	2.850
5.0	$9.646 \cdot 10^{-4}$	$9.646 \cdot 10^{-4}$	$9.169 \cdot 10^{-1}$	6.849
20.0	$6.313 \cdot 10^{-5}$	$6.313 \cdot 10^{-5}$	$9.822 \cdot 10^{-1}$	$1.610 \cdot 10^{2}$
∞	0	0	$9.900 \cdot 10^{-1}$	$2.000 \cdot 10^{2}$

Table C.2

R_M at Selected Low Pass Cutoffs for Square Symbol

$2E/N_o$	$f_c = .2$	$f_c = .5$	$f_c = 1.0$	$f_c = 2.0$	$f_c = 10.0$
1	$1.16 \cdot 10^{-2}$	$6.47 \cdot 10^{-3}$	$2.36 \cdot 10^{-3}$	$5.54 \cdot 10^{-4}$	$9.31 \cdot 10^{-6}$
2	$2.96 \cdot 10^{-2}$	$1.77 \cdot 10^{-2}$	$6.68 \cdot 10^{-3}$	$1.65 \cdot 10^{-3}$	$3.26 \cdot 10^{-5}$
5	$8.75 \cdot 10^{-2}$	$5.54 \cdot 10^{-2}$	$2.20 \cdot 10^{-2}$	$5.87 \cdot 10^{-3}$	$1.47 \cdot 10^{-4}$
10	$1.71 \cdot 10^{-1}$	$1.16 \cdot 10^{-1}$	$4.81 \cdot 10^{-2}$	$1.35 \cdot 10^{-2}$	$4.06 \cdot 10^{-4}$
20	$2.93 \cdot 10^{-1}$	$2.22 \cdot 10^{-1}$	$9.74 \cdot 10^{-2}$	$2.91 \cdot 10^{-2}$	$9.97 \cdot 10^{-4}$
50	$4.86 \cdot 10^{-1}$	$4.43 \cdot 10^{-1}$	$2.20 \cdot 10^{-1}$	$7.34 \cdot 10^{-2}$	$2.87 \cdot 10^{-3}$
100	$6.15 \cdot 10^{-1}$	$6.48 \cdot 10^{-1}$	$3.64 \cdot 10^{-1}$	$1.39 \cdot 10^{-1}$	$6.08 \cdot 10^{-3}$
200	$7.07 \cdot 10^{-1}$	$8.40 \cdot 10^{-1}$	$5.37 \cdot 10^{-1}$	$2.46 \cdot 10^{-1}$	$1.24 \cdot 10^{-2}$
500	$7.75 \cdot 10^{-1}$	1.02	$7.46 \cdot 10^{-1}$	$4.51 \cdot 10^{-1}$	$3.10 \cdot 10^{-2}$
1000	$8.03 \cdot 10^{-1}$	1.09	$8.58 \cdot 10^{-1}$	$6.22 \cdot 10^{-1}$	$6.05 \cdot 10^{-2}$

Table C.3

Spectral Densities at Selected Low Pass Cutoffs for Raised Cosine Symbol

f_c	S^d_{sxs}	S^c_{sxs}	S'_{sxN}	S'_{NxN}
.1	$3.481 \cdot 10^{-2}$	$4.727 \cdot 10^{-3}$	$3.792 \cdot 10^{-3}$	$5.979 \cdot 10^{-3}$
.2	$1.085 \cdot 10^{-1}$	$1.202 \cdot 10^{-2}$	$2.720 \cdot 10^{-2}$	$4.320 \cdot 10^{-2}$
.5	$3.511 \cdot 10^{-1}$	$5.766 \cdot 10^{-3}$	$2.346 \cdot 10^{-1}$	$3.924 \cdot 10^{-1}$
1.0	$5.857 \cdot 10^{-1}$	$5.038 \cdot 10^{-4}$	$6.484 \cdot 10^{-1}$	1.256
2.0	$8.280 \cdot 10^{-1}$	$5.960 \cdot 10^{-6}$	1.098	2.850
5.0	$9.655 \cdot 10^{-1}$	$1.968 \cdot 10^{-9}$	1.409	6.849
20.0	$9.976 \cdot 10^{-1}$	$2.429 \cdot 10^{-15}$	1.494	$1.610 \cdot 10^{1}$
∞	1.0	0	1.5	$2.000 \cdot 10^{1}$

Table C.4

R_M at Selected Low Pass Cutoffs for Raised Cosine Symbol

$2E/N_o$	$f_c = .2$	$f_c = .5$	$f_c = 1.0$	$f_c = 2.0$	$f_c = 10.0$
1	$5.46 \cdot 10^{-1}$	$1.17 \cdot 10^{-1}$	$6.29 \cdot 10^{-2}$	$4.29 \cdot 10^{-2}$	$1.63 \cdot 10^{-2}$
2	1.42	$3.23 \cdot 10^{-1}$	$1.79 \cdot 10^{-1}$	$1.28 \cdot 10^{-1}$	$5.70 \cdot 10^{-2}$
5	3.85	1.04	$5.97 \cdot 10^{-1}$	$4.55 \cdot 10^{-1}$	$2.58 \cdot 10^{-1}$
10	6.67	2.26	1.35	1.05	$7.06 \cdot 10^{-1}$
20	9.77	4.61	2.87	2.30	1.73
50	$1.31 \cdot 10^{1}$	$1.07 \cdot 10^{1}$	7.45	6.08	5.00
100	$1.48 \cdot 10^{1}$	$1.86 \cdot 10^{1}$	$1.50 \cdot 10^{1}$	$1.24 \cdot 10^{1}$	$1.06 \cdot 10^{1}$
200	$1.57 \cdot 10^{1}$	$2.89 \cdot 10^{1}$	$2.99 \cdot 10^{1}$	$2.50 \cdot 10^{1}$	$2.17 \cdot 10^{1}$
500	$1.64 \cdot 10^{1}$	$4.33 \cdot 10^{1}$	$7.23 \cdot 10^{1}$	$6.29 \cdot 10^{1}$	$5.53 \cdot 10^{1}$
1000	$1.65 \cdot 10^{1}$	$5.18 \cdot 10^{1}$	$1.36 \cdot 10^{2}$	$1.26 \cdot 10^{2}$	$1.11 \cdot 10^{2}$

Table C.5

Spectral Densities at Selected Low Pass Cutoffs for Half Sine Symbols

f_c	S^d_{sxs}	S^c_{sxs}	S'_{sxN}	S'_{NxN}
.1	$1.951 \cdot 10^{-4}$	$5.519 \cdot 10^{-4}$		
.2	$1.432 \cdot 10^{-3}$	$1.292 \cdot 10^{-3}$	$9.638 \cdot 10^{-3}$	$4.320 \cdot 10^{-2}$
.5	$1.425 \cdot 10^{-2}$	$8.218 \cdot 10^{-4}$	$8.246 \cdot 10^{-2}$	$3.924 \cdot 10^{-1}$
1.0	$3.706 \cdot 10^{-2}$	$2.009 \cdot 10^{-4}$	$2.257 \cdot 10^{-1}$	1.256
2.0	$5.405 \cdot 10^{-2}$	$1.242 \cdot 10^{-5}$	$3.757 \cdot 10^{-1}$	2.850
5.0	$6.113 \cdot 10^{-2}$	$8.933 \cdot 10^{-8}$	$4.728 \cdot 10^{-1}$	6.849
20.0	$6.242 \cdot 10^{-2}$	$2.454 \cdot 10^{-11}$	$4.980 \cdot 10^{-1}$	$1.610 \cdot 10^{1}$
∞	$6.250 \cdot 10^{-2}$	0	$5.000 \cdot 10^{-1}$	$2.000 \cdot 10^{1}$

Table C.6

R_M at Selected Low Pass Cutoffs for Half Sine Symbol

$2E/N_o$	$f_c = .2$	$f_c = .5$	$f_c = 1.0$	$f_c = 2.0$	$f_c = 10.0$
1	$5.64 \cdot 10^{-3}$	$2.98 \cdot 10^{-2}$	$3.57 \cdot 10^{-2}$	$2.60 \cdot 10^{-2}$	$1.24 \cdot 10^{-2}$
2	$1.45 \cdot 10^{-2}$	$8.12 \cdot 10^{-2}$	$9.98 \cdot 10^{-2}$	$7.65 \cdot 10^{-2}$	$4.16 \cdot 10^{-2}$
5	$3.92 \cdot 10^{-2}$	$2.56 \cdot 10^{-1}$	$3.28 \cdot 10^{-1}$	$2.66 \cdot 10^{-1}$	$1.74 \cdot 10^{-1}$
10	$6.85 \cdot 10^{-2}$	$5.54 \cdot 10^{-1}$	$7.31 \cdot 10^{-1}$	6.13	$4.48 \cdot 10^{-1}$
20	$1.02 \cdot 10^{-1}$	1.12	1.55	1.33	1.04
50	$1.39 \cdot 10^{-1}$	2.57	3.96	3.49	2.92
100	$1.58 \cdot 10^{-1}$	4.27	7.86	7.09	6.06
200	$1.69 \cdot 10^{-1}$	6.45	$1.52 \cdot 10^{1}$	$1.43 \cdot 10^{1}$	$1.24 \cdot 10^{1}$
500	$1.76 \cdot 10^{-1}$	9.24	$3.39 \cdot 10^{1}$	$3.57 \cdot 10^{1}$	$3.13 \cdot 10^{1}$
1000	$1.79 \cdot 10^{-1}$	$1.08 \cdot 10^{1}$	$5.75 \cdot 10^{1}$	$7.09 \cdot 10^{1}$	$6.28 \cdot 10^{1}$

RECENT RESEARCH PUBLICATIONS
SCHOOL OF ELECTRICAL ENGINEERING
PURDUE UNIVERSITY

TR-EE67-1 **PARAMETER ESTIMATION WITH UNKNOWN SYMBOL SYNCHRONIZATION**
J. C. Hancock and T. L. Stewart, NSF Grant GP-2898, PRF 3955-50-285, January 1967

TR-EE67-2 **NONLINEAR OSCILLATION OF A GYROSCOPE**
Chikaro Sato, PRF 4891, National Science Foundation Grant No. GK-01235

TR-EE67-3 **ON THE DESIGN OF SPECIFIC OPTIMAL CONTROLLERS**
V. B. Haas and S. Murtuza, NASA, NGR 15-005-021

TR-EE67-4 **ON THE ANALYSIS AND SYNTHESIS OF CONTROL SYSTEMS USING A WORST CASE DISTURBANCE APPROACH**
V. B. Haas and A. S. Morse, NASA, NGR 15-005-021

TR-EE67-5 **ANALYSIS AND SYNTHESIS OF MULTI-THRESHOLD THRESHOLD LOGIC**
K. S. Fu and W. C. W. Mow, Contract ONR-N00016-66-C0076,A04 Joint Services Electronic Program

TR-EE67-6 **ESTIMATION OF SONAR TARGET PARAMETERS**
G. R. Cooper and J. U. Kincaid, National Science Foundation Grant GK-189, PRF 4243

TR-EE67-7 **ON GENERALIZATIONS OF ADAPTIVE ALGORITHMS AND APPLICATION OF THE FUZZY SETS CONCEPTS TO PATTERN CLASSIFICATION**
K. S. Fu and W. G. Wee, National Science Foundation Grant GK-696, PRF 4502

TR-EE67-8 **COMPUTER AIDED ANALYSIS AND SYNTHESIS OF MULTIVALUED MEMORYLESS NETWORKS**
L. O. Chua and W. H. Stellhorn, National Science Foundation Grant GK-01235, Joint Services Electronics Program Contract ONR-N00016-66-C0076-A04, PRF 4711

TR-EE67-9 **OPTIMUM FINITE SEQUENTIAL PATTERN RECOGNITION**
K. S. Fu and G. P. Cardillo, National Science Foundation Grant GK-696, PRF 4502

TR-EE67-10 **MINIMUM SENSITIVITY OPTIMAL CONTROL FOR NONLINEAR SYSTEMS**
V. Haas and A. Steinberg, NASA NGR 15-005-021, PRF 4558

TR-EE67-11 **RANDOM SIGNAL RADAR (Final Report)**
G. R. Cooper and C. D. McGillem, NASA, NsG-543

TR-EE67-12 **INTRODUCTION TO THE PERFORMANCE OF DISTRIBUTION FREE, MINIMUM CONDITIONAL RISK LEARNING SYSTEMS**
E. A. Patrick and F. P. Fischer II, Naval Ship Systems Command Contract N00024-67-C-1162 PRF No. 4925-53-2859

TR-EE67-13 **P-I-N THERMO-PHOTO-VOLTAIC DIODE**
R. J. Schwartz and C. W. Kim, Joint Services Electronic Program Contract ONR-N00014-67 A00226-004

TR-EE67-14 **ESTIMATION OF PROBABILITY DENSITY AND DISTRIBUTION FUNCTIONS**
R. L. Kashyap and C. C. Blaydon, National Science Foundation Grant GK-1970, PRF 5181, and Joint Services Electronics Program Contract N00014-67-A0226-0004, PRF 4711.

TR-EE67-15 **OPTIMIZATION OF STOCHASTIC CONTROL PROCESSES WITH RESPECT TO PROBABILITY OF ENTERING A TARGET MANIFOLD**
J. Y. S. Luh and G. E. O'Connor, Jr., Jet Propulsion Laboratory Contract 950670, PRF 3807

TR-EE67-16 **CODES FOR UNSUPERVISED LEARNING OF SOURCE AND BINARY CHANNEL PROBABILITIES**
E. A. Patrick and G. Carayannopoulos, Air Force Avionics Laboratory (AVWC), Wright-Patterson AFB, Dayton, Ohio, AF 33(615)3768, PRF 4575

TR-EE67-17 **DIGITAL COMMUNICATION SYSTEMS SUBJECT TO FREQUENCY SELECTIVE FADING**
J. C. Lindenlaub and C. C. Bailey, National Aeronautics and Space Administration, NsG-553, PRF 5120

TR-EE67-18 **DEMO I--A SUPERVISED OR UNSUPERVISED LEARNING COMPUTER DESIGNED FOR DEMONSTRATION**
E. A. Patrick, F. C. Monds, G. L. Carayannopoulos, J. P. Costello, T. A. Martin, Air Force Avionics Laboratory (AVWC), Wright-Patterson Air Force Base, Dayton, Ohio, AF33(615)3768, PRF 4575

TR-EE67-19 **ANALYSIS AND MINIMIZATION OF MESSAGE ERROR IN PCM TELEMETRY SYSTEMS**
P. A. Wintz and A. J. Kurtenbach, National Aeronautics and Space Administration, NsG-553, PRF 5120.

TR-EE67-20 **ANHYSTERETIC MAGNETIZATION AND FLUX REVERSAL IN TAPE CORES, AND AN ANALOG CORE MEMORY**
F. J. Friedlaender and J. D. McMillen, Joint Services Electronics Program N0014-67A0226-0004, PRF 4711, National Science Foundation, PRF 4959

RECENT RESEARCH PUBLICATIONS
SCHOOL OF ELECTRICAL ENGINEERING
PURDUE UNIVERSITY

TR-EE67-21 **THE RELATIONSHIP OF MAGNETIC MATERIAL PROPERTIES TO THE OPERATION OF A MAGNETIC SENSE AMPLIFIER DEVICE**
F. J. Friedlaender and J. R. Eaton, Jr., Joint Services Electronics Program N0014-76a-0226-0004, PRF 4711, National Science Foundation

TR-EE68-1 **PERFORMANCE OF SELF-BIT SYNCHRONIZATION SYSTEMS**
P. A. Wintz and E. J. Luecke, National Aeronautics and Space Administration, NsG-553, PRF 4695-52-285

TR-EE68-2 **SEQUENTIAL METHODS IN PATTERN RECOGNITION AND MACHINE LEARNING**
K. S. Fu, National Science Foundation Grant GK-1970, PRF 5187